NOTE TO USERS

This reproduction is the best copy available.

FINITE ELEMENT ANALYSIS OF CORROSION AND BOND-SLIP

by

Yan Lan

(B.Eng., Fuzhou University, Fuzhou, P.R.China, 1990)

A project

presented to Ryerson University

in partial fulfillment of the

requirement for the degree of

Master of Engineering

in the Program of

Civil Engineering

Toronto, Ontario, Canada, 2003

Author's Declaration

I hereby declare that I am the sole author of this thesis.

I authorize Ryerson University to lend this thesis to other institutions or individuals for the purpose of scholarly research.

Yan Lan

Department of Civil Engineering

Ryerson University

I further authorize Ryerson University to reproduce this thesis by photocopying or by other means, in total or in part, at the request of other institutions or individuals for the purpose of scholarly research.

Yan Lan

Department of Civil Engineering

Ryerson University

Borrower's Page

Ryerson University requires the signatures of all persons using or photocopying this thesis. Please sign below, and give address and date.

Name of Borrowers	Date	Address	Signature

FINITE ELEMENT ANALYSIS OF CORROSION AND BOND-SLIP

Mast of Engineering, 2003, Yan Lan
Department of Civil Engineering
Ryerson University

ABSTRACT

Although reinforced concrete (RC) has an important advantage that it has virtue durability against an environmental attack, especially the resistance of corrosion of embedded reinforcements, due to the high alkalinity nature of concrete property, unfortunately, the problems of reinforcement corrosion still exist in many reinforced concrete structures. It has brought out many questions on the safety and serviceability of these corroded RC structures. Thus, it needs more effective approach for structural performance evaluation of the corroded structures. The residual capacity of the corroded reinforcement was determined through the evaluation of the volume increase of reinforcing steel and concrete crack propagation. The final determination of the service life of concrete structures was made based on the above evaluation results. Also, the effects of reinforcement corrosion on structural behaviors of RC members are investigated so that the reliable evaluation of structural performances of corroded RC members can be achieved by finite element method (FEM). The corrosion attack penetration has been given as a function of the time as input in the analyses. The load of corrosion applied inside the structural members can be modeled by the displacement around the circumferential surface between the reinforcing bars and concrete. The reduction of capability of the structures is determined from the corrosion level in the service years.

Another complex phenomenon that governs concrete behavior is the transfer of shear force across the interface by bond mechanism between concrete and steel reinforcement. It is a fundamental to most aspects of concrete behavior. The bond mechanism is influenced by multiple parameters, such as the strength of the surrounding structures, the occurrence of splitting cracks in the concrete and the yielding of the reinforcement. However, when RC structures are analyzed using the FEM, it is quite common to assume that the bond stress depends solely on the slip between the bars and concrete. In this research the relationship of bond slip is also studied using FEM.

An analytical study based on fracture mechanics was carried out to investigate the behavior of three different types of specimens. In recent RC research, finite element modeling techniques have been developed to quickly evaluate the physical phenomena associated with cracking and bond. The nonlinear finite element program ATENA with the nonlinear material models for concrete, reinforcement bar and bond-slip is used to analyze cracking propagation and bond failure process. The influence between corrosion and bond slip in RC structure is also studied. Therefore, the understanding of serviceability of RC structure is improved.

It was concluded that with the increase of load and the propagation of the crack, stress redistributed in the steel continues until the specimen is damaged. The nonlinear finite element fracture analysis shows that nonlinear fracture mechanics can be effectively applied to investigate concrete fracture. Also, comparisons between the analyses of crack propagation and stress redistribution obtained using the finite element analysis was in good agreement with tests found in the literature.

ACKNOWLEDGMENTS

I would like to express my deepest gratitude and indebtedness to Dr. Lamya Amleh, for her valuable advices, guidance, suggestion, patience and encouragement throughout the entire period of study at Ryerson University. Dr. Amleh taught me all about research and led me to this research field. No expression of thanks is sufficient in describing my thanks to her. I would like to extend my sincere gratitude to other committee members, Dr. Sennah and Dr. Poh, for their valuable comments and advice.

Grateful acknowledge is given to all Civil Engineering staffs for their teaching and assistance.

Finally, I would like to express my heartfelt thanks to my parents and my family, their love, care, and support encourage me to the completion of this project.

Table of Contents

Abstract.....i

Acknowledgements.....iii

Table of Contents.....iv

List of Figures.....viii

List of Tables.....xii

List of Symbols.....xiii

Chapter 1 Introduction.....1

1.1 Background.....1

1.2 Scope.....4

1.3 Report Layout.....5

Chapter 2 Review of Corrosion of Steel in Concrete.....6

2.1 Introduction.....6

2.2Mechanics of Corrosion of Steel in Concrete.....8

2.2.1 Destroy of Passive Film.....8

2.2.2 Electrochemical Process of Steel Corrosion.....11

2.2.2.1 Electrochemical Process.....12

2.2.2.2 Faraday's Law.....16

2.2.2.3 Nernst Equation.....17

2.2.2.4 Pourbaix Diagrams.....18

2.2.2.5 Polarization.....19

2.2.2.6 Passivity.....22

2.2.2.7 Corrosion Rate.....22

2.2.3 Factors Affecting Steel Corrosion.....24
2.2.3.1 Concrete.....24
2.2.3.2 Other Factors.....30

Chapter 3 Review of Bond Slip.....31
3.1 Mechanism of Bond.....31
3.1.1 Conception of Bond-Slip.....31
3.1.2 The Process of Bond Failure.....33
3.2 Factors Affecting Bond Performance.....36
3.2.1 Reinforcement.....36
3.2.2 Concrete Quality and Stress State.....39
3.2.3 Load History.....40
3.3 Experimental Investigation.....41
3.4 General Bond-Slip Calculation.....44
3.4.1 Bond Modeling.....45
3.4.1.1 Constitutive Equation of Bond Slip.....45
3.4.1.2 Analysis Model.....49
3.4.2 Stress Redistribution after Cracking.....53
3.4.2.1 Transient Cracking.....54
3.4.2.2 Tension Stiffening.....56
3.5 The Relationship between Corrosion and Bond Slip.....58

Chapter 4 Finite Element Analysis.....63
4.1 ATENA Program.....63
4.2 Finite Element Modeling of Crack.....65
4.2.1 Two Basic Modes.....65
4.2.2 Basic Concepts in Crack Modeling.....69

4.2.2.1 Strain Softening.....69
4.2.2.2 Fracture Process Zone (Blunt Front Zone).....70
4.2.2.3 Representative Volume.....72
4.2.2.4 Fracture Energy.....74
4.2.2.5 Element Size Effect and Element Orientation Effect.....75
4.3 Material Modeling-SBETA Material Model.....79
4.3.1 Stress-Strain Relations for Concrete.....80
4.3.1.1 Equivalent Uniaxial Law.....80
4.3.1.2 Stress-Strain Relation in Tension Condition.....81
4.3.1.3 Stress-Strain Relation in Compression Condition.....83
4.3.1.4 Biaxial Stress Failure Criterion of Concrete.....85
4.3.2 Shear Stress and Stiffness in Cracked Concrete.....87
4.3.3 Reinforcement Properties.....91
4.4 Fracture Analysis by Finite Element Method.....99
4.5 Finite Element Analysis of Bond-Slip.....99

Chapter 5 Result of Finite Element Analysis.....103
5.1 Materials Properties.....103
5.2 Corrosion Analysis.....105
5.2.1 Method and Procedures.....105
5.2.2 Volume Increase of Corrosion Products.....106
5.2.3 Mathematical Simulation of Corrosion.....107
5.2.4 Example.....111
5.3 Two-Dimensional Corrosion-Cracking Analysis Example.....112
5.4 Two-Dimensional Bond-Slip Modeling Analysis Example.....122
5.4.1 Example 1 - Tension Test (Specimen II).....122
5.4.2 Example 2 - Simply Supported Beam (Specimen III).....125

Chapter 6 Conclusion and Future Direction.....148

6.1 Conclusion.....148

6.2 Current Needs and Future Directions.....149

References.....151

List of Figures

Figure 2.1 Collapse of the Berlin Congress Hall [Isecke, 1982].....6

Figure 2.2 Collapse of a Salt-Damaged Parking Garage [Heidersbach, 1986].....7

Figure 2.3 Corroded Reinforcing Steel on Bridge Substructure [http://www.corrosionsource.com/corrosioneering/journal/Jul02_Tullmin].....8

Figure 2.4 The Critical Chloride Content According to CEB Recommendations [CEB, 1985].....11

Figure 2.5 Electrochemical Corrosion Cell 12

Figure 2.6 Mechanism of Corrosion of steel in Concrete [Metha, 1993].....14

Figure 2.7 The Relative Volumes of Iron and Its Corrosion Reaction Products [Nielsen, 1985].....16

Figure 2.8 Pourbaix Diagram for Fe-H_2O at 25° C [Pourbaix, 1976].....19

Figure 2.9 A Schematic of Evans Diagram [Evans, 1960].....20

Figure 3.1 Process of Bond Failure.....33

Figure 3.2 Longitudinal tensile Stresses at the Tip of the Rib.....34

Figure 3.3 The Stresses Between Two Ribs of a Deformed Bar.....34

Figure 3.4 Separation Near a Primary Crack Between Reinforcing Bar and Concrete.....35

Figure 3.5 Bond Stress Distribution in Concrete Near a Crack.....36

Figure 3.6 Failure Mechanisms at the Ribs of Deformed Bars.....37

Figure 3.7 Bond Stress Distribution for 25 mm Ribbed Bar.....40

Figure 3.8 Beam Dimensions for Test by Lutz and Gergely (1967).....42

Figure 3.9 (a) Sketch of Pullout Specimen for FE Analytical Studies, (b) Deformed concrete between transverse cracks (macro-scale).....43

Figure 3.10 Tepfers Tensile Stress Ring [Tepfers, 1979].....44

Figure 3.11 Stresses and Strains in the Bar and concrete layer (δ r).....45

Figure 3.12 Analytical Bond Stress-Slip Relationship (Monotonic Loading) [CEB Model Code].....50

Figure 3.13 Bilinear Constitutive Relationship for the Reinforcement.....51

Figure 3.14 Assumed Bond Stress Distribution.....52

Figure 3.15 Chord Tension Model.....53

Figure 3.16 Primary and Secondary Cracks in a Reinforced Concrete Member in Tension [ACI, 1986]....53
Figure 3.17 Experimental and Analytical Bond Stress-Slip Relationship for Tension Test [Russo and Romano, 1992]....54
Figure 3.18 Cracking in a Long-Member....55
Figure 3.19 Steel, Concrete and Bond Stress Variation along the Bar at Different States....56
Figure 3.20 Tension Stiffening: Tensile Stress Versus (Mean) Tensile Strain....58
Figure3.21 Effects of Corrosion in Residual Strength [CEB-FIP, 2000]....59
Figure 4.1 Two Finite Element Models of Crack Analysis....67
Figure 4.2 (a) Linear and (b) Exponential Strain Softening....69
Figure 4.3 The Difference in Fracture Process Zone between Metal and Concrete....70
Figure 4.4 Hillerborg Model and Peterson Fracture Mechanics Model....72
Figure 4.5 (a) Actual Crack Morphology, (b) Actual Stress and Then Smoothing....73
Figure 4.6 Bilinear Stress-Strain Relationships....74
Figure 4.7 Size Effect According to Strength Criteria and Linear or Nonlinear Fracture Mechanics....76
Figure 4.8 Definition of Localization Bands....77
Figure 4.9 Stages of Crack Opening....79
Figure 4.10 Uniaxial Stress-strain Law for Concrete....81
Figure 4.11 Compressive Stress-strain Diagram....83
Figure 4.12 Biaxial Failure Function for Concrete....86
Figure 4.13 Tension-compression Failure Function for Concrete....87
Figure 4.14 Stress and Strain State in Fixed Crack Model....88
Figure 4.15 Stress and Strain in Rotated Crack Model....89
Figure 4.16 Shear Retention Factor....89
Figure 4.17 The Multi-linear Stress strain Law for Reinforcement....92
Figure 4.18 Smeared Reinforcement....93
Figure 4.19 Components of Plane Stress State....94
Figure 4.20 Components of Strain State....94
Figure 4.21 Reinforcement Bar with Slips....100

Figure 5.1 Diagrammatic Representation of the Cracking-Corrosion-Cracking Cycles in Concrete [Metha, 1993]....106
Figure 5.2 Physical Interpretation of the Variables in the Corrosion Model....110
Figure 5.3 Specimen for Corrosion-Crack Analysis (Specimen I)....113
Figure 5.4 Geometry of CCIsoQuad Element....114
Figure 5.5 Corrosion Crack Analysis—Step 1....115
Figure 5.6 Corrosion Crack Analysis—Step 2....116
Figure 5.7 Corrosion Crack Analysis—Step 4....117
Figure 5.8 Corrosion Crack Analysis—Step 6....118
Figure 5.9 Corrosion Crack Analysis—Step 8....119
Figure 5.10 Corrosion Crack Analysis—Step 10....120
Figure 5.11 Corrosion Penetration Verse Max. Crack Width Response....121
Figure 5.12 Dimensions of Tension Specimen (Specimen II)....122
Figure 5.13 Bond Slip-Stress Relationship Used in This Study....124
Figure 5.14 Tension Test-Step 1 (Bond Stress)....126
Figure 5.15 Tension Test-Step 3 (Bond Stress and Crack)....127
Figure 5.16 Tension Test-Step 5 (Bond Stress and Crack)....128
Figure 5.17 Tension Test-Step 7 (Bond Stress and Crack)....129
Figure 5.18 Tension Test-Step 9 (Bond Stress and Crack)....130
Figure 5.19 Tension Test-Step 10 (Bond Stress and Crack)....131
Figure 5.20 Tension Test-Step 1 (Stress Distribution of Reinforcement)....132
Figure 5.21 Dimensions of Simply Supported Beam (Specimen III)....133
Figure 5.22 Simply Supported Beam-Step 1 (Bond Stress and Concrete Stress of Cuts)...136
Figure 5.23 Simply Supported Beam-Step 3 (Bond Stress and Concrete Stress of Cuts)...137
Figure 5.24 Simply Supported Beam-Step 4 (Bond Stress and Concrete Stress of Cuts)...138
Figure 5.25 Simply Supported Beam-Step 6 (Bond Stress and Concrete Stress of Cuts)...139
Figure 5.26 Simply Supported Beam-Step 8 (Bond Stress and Concrete Stress of Cuts)...140
Figure 5.27 Simply Supported Beam-Step 10 (Bond Stress and Concrete Stress of Cuts)..141
Figure 5.28 Simply Supported Beam-Step 1 (Engineering Strain with Cuts)....142
Figure 5.29 Simply Supported Beam-Step 3 (Engineering Strain with Cuts and Cracks)...143
Figure 5.30 Simply Supported Beam-Step 4 (Engineering Strain with Cuts and Cracks)...144

Figure 5.31 Simply Supported Beam-Step 6 (Engineering Strain with Cuts and Cracks)...145
Figure 5.32 Simply Supported Beam-Step 8 (Engineering Strain with Cuts and Cracks)...146
Figure 5.33 Simply Supported Beam-Step 10 (Engineering Strain with Cuts and Cracks).147
Figure 5.34 Load Deflection Curve.....134

List of Tables

Table 3.1 Parameters for Defining the Mean Bond Stress-Slip Relationship.....51

Table 5.1 Properties of Concrete Material.....104

Table 5.2 Properties of Reinforcement Steel.....104

Table 5.3 Corrosion Penetration Calculation Results.....112

Table 5.4 Applied load (Displacement) due to Corrosion and the Crack Width.....114

Table 5.5 Parameters of Bond Stress and Slip Relationship Used in This Study.....123

Table 5.6 The Bond Stress at Two Ends of Tension Specimen.....125

Table 5.7 The Maximum Displacement after Each Load Step.....134

List of Symbols

v	= the Poisson's ratio
ρ_r	= the density of the rust product
ρ_s	= the density of the steel
$\varepsilon_1, \varepsilon_2$	= the principal strain in concrete
ε_c, ε_s	= normal strain in the concrete, in the reinforcement
ε_{cr}	= the crack opening strain of concrete
ε^{eq}	= the equivalent uniaxial strain of concrete
ε_{sh}	= the strain at the strain hardening of reinforcement
σ_{c1}, σ_{c2}	= the principal stress in concrete
σ_c^{ef}	= the effective compressive stress of concrete
σ_s, σ_y	= normal stress in the steel, stress at yielding
$\sigma_s^{'}$	= the steel stress between the cracks
$\sigma_{scr}^{'}$	= the steel stress in crack
γ_m	= the ratio of steel mass and rust mass
η	= the measured polarization
η_a	= anodic overpotential,
η_c	= cathodic overpotential
σ_1	= the maximum principle stress
a	= the Tafel intercept
Ac	= the cross section of cocnrete
A_s	= cross section of steel bar
b	= the Tafel slope

d_a = the maximum aggregate size for the concrete

D = the material stiffness matrix

d_b = the bar diameter

$d_{rb}(t)$ = the reduced bar diameter

E = the measured potential

E_a = the surface potentials for anode

E_c = the surface potentials cathode

E_{corr} = the corrosion potential

E_c = the elastic modulus of concrete

E_s = the Young's modulus of reinforcement

E_{sh} = the strain-hardening modulus

f_c = the concrete ultimate strength

f_c' = the concrete compressive strength

f_{cc} = concrete compressive strength measured on cubes

f_{coh} = cohesive strength at bar-concrete interface

f_{ct} = the concrete tensile strength

f_R = bond index (or relative rib area)

f_y = the yield strength of reinforcement

G_c = the inertial concrete shear modulus:

G_f = the fracture energy

I = the current density

I_a = the applied current

I_o = the exchange current

I_{corr} = the corrosion current density

L_t = the tension failure band as projection of the finite element dimension

L_t = the compression failure band as projection of the finite element dimension

Ms = the mass of iron

r = the corrosion rate

R	= the gas constant
R	= the film resistance in ohms
s	= the slip
s_R	= rib spacing in a deformed bar
t	= the exposure time
Vs	= the volume of iron
w_c	= the crack width of concrete
x	= corrosion penetration depth

Chapter 1
Introduction

1.1 Background

The deterioration of concrete structures due to chloride-induced reinforcement corrosion is recognized as one of the major challenges facing the owners of facilities and infrastructure systems made up of concrete structures. Chloride-induced corrosion of reinforcing steel in concrete bridge decks, parking garage slabs and marine structures has been identified as the primary cause of concrete deterioration. Structures exposed to marine environments or deicing salts are particularly at risk. Despite of the durability of reinforced concrete structures when compared to steel and timber structures, reinforced and prestressed concrete structures are vulnerable to the damaging effects of corrosion induced primarily by chlorides (from deicing slats and seawater) and to a lesser extent to carbonation-induced corrosion. It is estimated that one-third to one-half of the projected bridge rehabilitation costs in North America are related to bridge deck deterioration [Cady and Weyers, 1983; Lounis and Mirza, 2001]. The corrosion of the reinforcement leads to concrete fracture through cracking, delamination and spalling of the concrete cover, reduction of concrete and reinforcement cross sections, loss of bond between the reinforcement and concrete, reduction in strength (flexural, shear, etc.), and ductility. As a result, the safety and serviceability of concrete structures are reduced, and their useful service lives shortened.

Reinforcement corrosion is the main cause of damage and early failure of reinforced concrete structures worldwide with subsequent enormous costs for maintenance, restoration and replacement. According to a 1997 report by Corrosion Doctors Organization, about 101,518 bridges were rated as structurally deficient as a result of corrosion of the 581,862 bridges in and off the U.S.A. federal-aid system. Most of these bridges were not in danger of collapse,

but they were likely to be load posted so that overweight trucks will be required to take a longer alternative route. The estimated cost to eliminate all backlog bridge deficiencies (including structurally and functionally) was approximately $78 billion, and it could increase to as much as $112 billion. The average annual cost, through year 2011, for just maintaining the overall bridge conditions, for example, the total number and the distribution of structurally and functionally deficient bridges in the US alone, was estimated to be $5.2 billions [http://www.corrosion-doctors.org/Bridges/Introduction.htm].

Canada also faces huge infrastructures deterioration because of lack of funding and related political decisions leading to deferred maintenance. The cost of Canada's infrastructure is estimated between three and five trillion dollars and approximately 10% of GDP annually is directed towards civil engineering construction. Furthermore, more than 80% of this investment is used in repair, rehabilitation, and renewal.

Usually concrete provides an ideal protective environment for the reinforcing steel. However, when some harmful salts such as chlorides or sulphates penetrate the concrete and reach the steel bars, corrosion commences. Chloride-induce corrosion of reinforcing steel is a very common phenomenon in concrete bridge decks, parking garage slabs and marine structures as a result of the use of deicing agents in the winter seasons in North America. Corrosion of RC has been identified as the primary cause of deterioration in the infrastructure system.

Two consequences of corrosion can manifest the damage and reduction of the serviceability of reinforced concrete structures. First, corrosion produces expansive products that generate tensile stresses in the concrete surrounding the reinforcing steel, which may cause concrete cracking. Cracks can reduce the overall strength and stiffness of the concrete structure and accelerate the ingress of aggressive ions, leading to other type of concrete deterioration and resulting in further cracking [Metha and Gerwick, 1982]. Second, corrosion products are

highly porous, weak, and often form around reinforcing steel, thus decreasing the bond strength between the reinforcement and concrete [Wang and Monteiro, 1996].

To study these phenomena, some experimental studies have been carried out in the past research. Although it has shown some interesting features from the test results, the limitations still exist, such as difficulties of isolating factors affecting corrosion of the reinforcing steel and the cost and duration of the tests.

In order to overcome these drawbacks, great efforts have been made by using numerical methods to study some these problems. One of the difficulties in such efforts is modeling of cracking which is very specific to reinforced concrete structures. Cracking has a significant influence in the service life of a reinforced concrete structure, hence, the development and propagation of crack must be carefully modeled by the finite element method in the analysis. Some nonlinear analysis models of reinforced concrete structure in the cracking situation have been developed.

Another difficulty in the finite element analysis of reinforced concrete structures is to model bond slip which is the relative displacement between the bar and the concrete. Reinforced concrete depends on the combined action of the concrete and its embedded reinforcement for satisfactory operation as a construction material. This action is produced by the interaction between both of its components, plain concrete and reinforcing bars. The transfer of forces across the interface between these two materials is completed by the bond, so bond plays a very important role in most aspects of reinforced concrete behavior. It is dependent on cohesion and adhesion at the steel concrete interface and the mechanical interlocking between the lugs or deformations of the reinforcing bar and the surrounding concrete.

Considerable research has been directed toward the study of bond-slip between the steel reinforcing bar and the surrounding concrete, and many attempts have been made to model bond-slip behavior using finite element analysis. Several laws to describe the behavior have been developed on experimental ground, and constitutive laws between the bond-slip on the interface have been formulated for theoretical analysis purposes. The fracture mechanics theory is applied to investigate the bond-slip problem in the present finite element analysis. In this research the software ATENA was carried out to achieve this objective.

The corrosion of reinforcement affects bond stress significantly in the reinforced concrete structures. In the past research it was mostly studied on the basis of experiment work, and some empirical formulas have been formulated such as those in the CEB-FIP, 2000. Basically, there are two effects between the corrosion of the reinforcement and the bond mechanism. 1) One is the increase volume of the steel reinforcing bar due to the corrosion of reinforcement, which leads to splitting stresses in the concrete; 2) Also corrosion is known to influence friction between the reinforcement and the concrete. Although many models are set up to analyze the bond stress problem, however, no general analytical model with respect to the corrosion of bars affecting bond mechanism is available, which has aroused many researchers' interest and great efforts have been made on it.

1.2 Scope and Objectives

The purpose of this project is to study the effect of corrosion and bond slip in the reinforced concrete structures. The analysis is based on the fracture mechanics and carried out by the finite element method. There are two major concerns in this research. They are:

(1) Cause and propagation of cracks due to the corrosion of reinforcing bar in the reinforced concrete structures.

(2) Mechanisms of cracking and bond stress-slip behavior in the reinforced concrete structures.

The first problem is studied by the stress analysis of concrete specimen in which the volume has increased around the reinforcing bar caused by the corrosion. Also, the propagation of cracks in the concrete specimen during its service life is studied. The second problem is studied using finite element analysis of a tension specimen and a simply supported beam. In summary, it presents some new developments in the corrosion and bond slip problems. It is anticipated that the findings of this research program and its application will result in a better understanding of the behavior of reinforced concrete structures in the complex conditions such as corrosion and cracking, and its influence on the bond between the steel and concrete.

1.3 Report Layout

The report comprises six chapters. This chapter, Chapter 1, addresses the background and scope of this project. Chapter 2 presents an overview of the state-of-the-art of the mechanisms of corrosion in reinforced concrete structures, and several factors affecting the corrosion are also discussed. The corrosion is analyzed by the volume expansion of corroded reinforcement, and a new lifetime analysis of the reinforced concrete structures is presented. Chapter 3 describes the background to the bond between the concrete and reinforcing bars. The chapter includes the factors affecting bond behavior and bond failure. Some analysis models and calculation methods are also studied. The relationship between bond and corrosion in the reinforced concrete members are presented. Chapter 4 discusses the finite element analysis used in this research, which is based on the fracture mechanics. Two basic models and analysis procedures are described. The material model used in software ATNEA is introduced. Chapter 5 reports and discusses the results obtained the calculation of corrosion and bond-slip problems. Finally the conclusions are presented in Chapter 6, and recommendations for further research and development of the influence of corrosion on bond behaviour at the steel-concrete interface are included.

Chapter 2
Corrosion of Steel in Concrete

This chapter presents some of the latest literature review of the mechanisms of reinforcement corrosion, which have been the subject of intensive research over the past few decades. It discusses how the concrete environment protects the embedded steel. Also, it discusses the characteristics of the concrete of relevance to the corrosion of the reinforcing steel and presents the basic principles of corrosion. The emphasis is placed on the electrochemical process which is fundamental in the corrosion process, and two major factors affecting the corrosion are also discussed.

2.1 Introduction

Corrosion of steel in concrete has received increasing attention in recent years. The corrosion of steel reinforcement was first observed in marine structures and chemical manufacturing plants. More recently, numerous reports of its occurrence in bridge decks, parking structures, and other structures exposed to chlorides has made the problem particularly prominent.

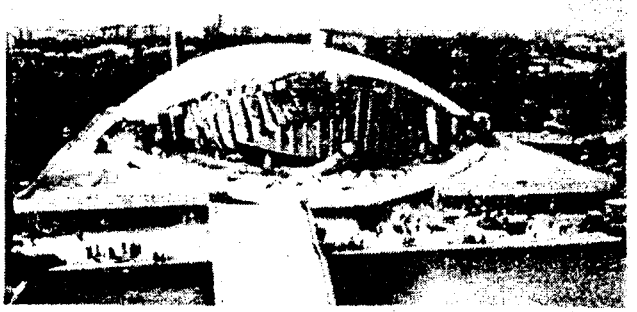

Figure 2.1 Collapse of the Berlin Congress Hall [Isecke, 1982]

The corrosion of reinforcement in concrete structures is a very serious problem in North America. It may occur in all types of infrastructure such as parking garages, industrial

facilities, bridges and any other auxiliaries. Corrosion of steel reinforcement may lead to a catastrophic failure, such as Berlin Congress Hall (Figure. 2.1) [Isecke, 1982] and the parking garage in Minnesota (Figure 2.2) [Heidersbach, 1986]. In Canada this damage is also very heavy as a result of using deicing agents during winter seasons. One of the frequent corrosion phenomena in Canada is the corrosion of reinforcing steel in bridges. Figure 2.3 shows the corroded reinforcing steel in one bridge abutment.

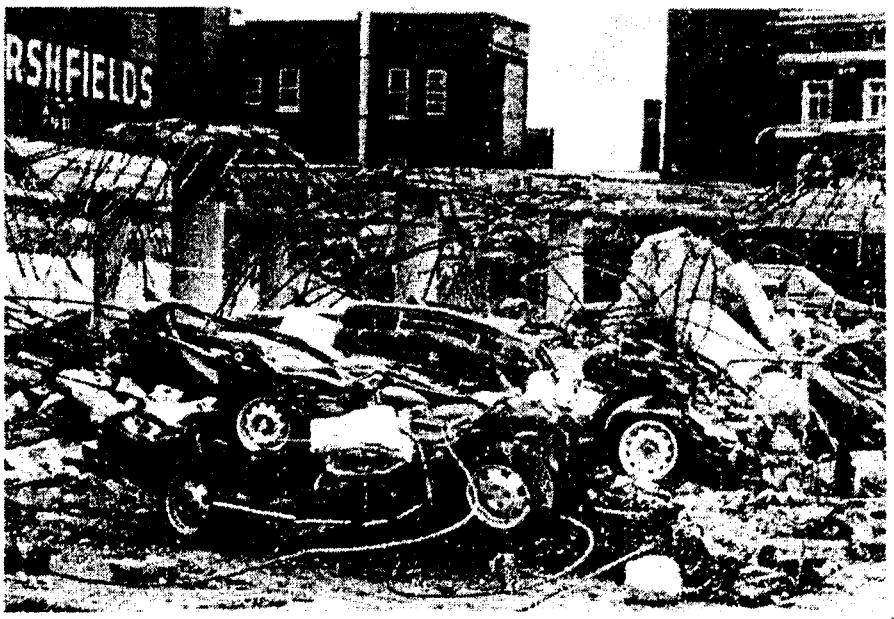

Figure 2.2 Collapse of a Salt-Damaged Parking Garage [Heidersbach, 1986]

The consequence of corrosion may not be limited to engineering failure, but it can also deteriorate our economy. The corrosion damage is costing us billions of dollars annually on repair, rehabilitation, and maintenance of reinforced concrete structures. For example, in 1986 the Ontario Ministry of Housing estimated the cost for repair in the approximately 3000 existing parking structures was a $1 billion plus [Ministry of Housing, 1986], where most of the damage was due to reinforcement corrosion. This was only one province and refers to one type of structure only. In United States, the annual direct cost of corrosion for highway bridges is estimated to be $6.43 to $10.15 billion. In Europe these costs are also very significant, for example, in the U.K. the Department of Transportation estimated a total

repair cost of 1 billion EURO due to corrosion damage on motorway bridges. These bridges only represent about 10% of the total inventory in the U.K. In addition, from life-cycle analysis it was estimated that the indirect costs due to traffic delays and lost productivity to the user may be more than 10 times the direct cost of corrosion damage [www.corrosioncost.com]. Therefore, the total costs due to corrosion damage may be far beyond the current estimation.

Figure 2.3 Corroded Reinforcing Steel on Bridge Substructure [http://www.corrosionsource.com/corrosioneering/journal/Jul02_Tullmin]

2.2 Mechanisms of Corrosion of Steel in Concrete

2.2.1 Destroy of Passive Film

It is well known that pure metals, such as iron and aluminum, exist in nature in the oxide forms. Iron is produced from iron ore through a process of iron oxide reduction. A lot of energy is involved in this process, and as a result the iron has higher energy level than the iron oxide. Since the most stable form of the material is always associated with the lowest energy level, the energy acquires by iron during its production is ready to be released and provides the driving force for corroding iron into an iron oxide form.

Steel reinforced concrete structures are a combination of materials that includes concrete and reinforcing steel, the corrosion of steel in concrete is different with the corrosion of steel in

atmosphere. The concrete cover surrounding the steel forms a physical barrier that protects the steel bars from the corrosive environments. The concrete pore solution has a high pH value (usually 12.5-13.5), this alkaline condition can chemically interact with the surface of reinforcing steel leading to a passive layer forming on the steel surface. It is a dense, impenetrable film which, if fully established and maintained, prevents further corrosion of the steel. The layer formed on steel in concrete is probably part metal oxide/hydroxide and part mineral from the cement. A true passive layer is a very dense, thin layer of oxide that leads to a very slow rate of oxidation (corrosion). Unfortunately, the physical barrier of the cover concrete is not perfect, because the porous structure of concrete and existing microcracks allow the ingress of aggressive species which cause the breakdown of the passive film. The most commonly encountered cause for reinforcing corrosion is associated with neutralization of the pore solution by atmospheric carbonation (CO_2) and chloride ions that penetrate into concrete.

Carbonation

Carbon dioxide (CO_2), which is present in the air in proportions of around 0.3 percent by volume, dissolves in water to form a mildly acidic solution. Unlike other acids that may chemically attack and etch the surface of the concrete, this acid forms within the pores of the concrete itself where the carbon dioxide dissolves in any moisture present. Here it reacts with the alkaline calcium hydroxide and calcium silicate hydrate (C-S-H).

$$Ca(OH)_2 + CO_2 \rightarrow CaCO_3 + H_2O \quad (2.1)$$

$$2NaOH + CO_2 \rightarrow Na_2CO_3 + H_2O \quad (2.2)$$

The carbonation process reduces pH value and destroys the passive film around the steel, but it seems to density the concrete surface and reduce the chloride ion penetration, by reducing the surface porosity and hence sorptivity in the concrete [Verbeck, 1958; Leber and Blakey, 1956; Dias, 2000]. Carbonation could have both positive and negative effects on concrete durability. Glass et al. (1991) pointed out that the presence of even a small amount of chloride in carbonated concrete enhances the corrosion rate resulted from carbonation of the concrete.

The basic factor influencing carbonation is the diffusivity of the hardened cement paste. Carbonation rate is controlled by the ingress of CO_2 into concrete pore system by diffusion with a concentration gradient of CO_2 acting as the driving force. Factors affecting diffusion rate include the type and amount of cement, porosity of the material, time of curing, type and quantity of pozzolanic additions [Roper and Baweja, 1991; V'eleva, 1998]. Moreover, several mechanical properties of concrete such as compressive strength, surface hardness and resistance to aggressive agents may change due to carbonation [Verbeck, 1958].

Chloride Attack

The chloride-induced corrosion is the most prevalent and damaging cause of corrosion of steel in concrete. The role of the chloride ion in inducing reinforcement corrosion is well documented among them [Page and Treadaway, 1982; Mehta, 1993; Tuutti, 1982; Bazant, 1979].

Chlorides can be introduced when seawater or water with a high chloride concentration is used as mixing water, when chloride contaminated coarse or fine aggregates are used, or when chloride containing admixtures such as calcium chloride are used. In addition, chloride ions can enter into the concrete from deicing salts that are applied to the concrete surface, or from seawater in marine environment and chloride-contaminated soils.

While it has been determined that chloride ions act as catalysts for the loss of the protection offered by the passive film, the exact mechanisms of this process are not well understood. However, attack on the passive film by chloride ions is generally accepted to be a localized phenomenon. This form of attack causes microgalvanic cells to form on the reinforcing steel. In regions where the depassivation has occurred become anodic sites and iron will be lost by oxidation, and the areas that remain protected by the passive film will become cathodic and, thus, sites of oxygen reduction.

To initiate corrosion, a chloride threshold (the amount of chloride required to initiate steel corrosion in reinforced concrete under a given set of exposure condition; commonly expressed in percent of chloride ion by mass of cement) is required. Chloride ions exist in

concrete in two forms, which are bound and free. It is generally believed that only the free chloride ions-those dissolved in the pore solution-participate in the corrosion process. This threshold concentration of chloride ions is dependent on so many factors including quality of concrete (water/cement ratio, mixture proportions, type of cement), relative humidity and temperature of the concrete, the pH of the pore solution and sulfate content [Schiessl and Raupach, 1990; Berman, 1975]. Figure 2.4 illustrates the relation between some factors and the threshold of chloride concentration given by CEB [CEB, 1985].

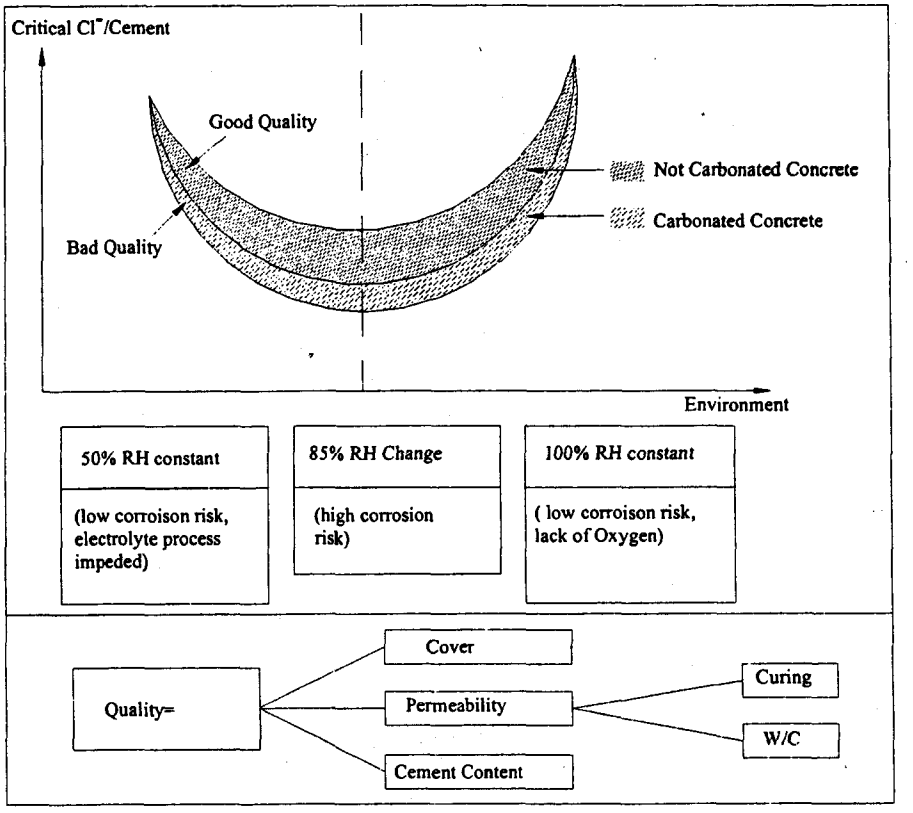

Figure 2.4 The Critical Chloride Content According to CEB Recommendations [CEB, 1985]

2.2.2 Electrochemical Process of Corrosion

After the passive film is destroyed, an electrochemical process begins in the corrosion of reinforcement bars. The electrochemical process and some electrochemical nature of corrosion are discussed in this part.

2.2.2.1 Electrochemical Processing

The electrochemical process requires a flow of electric current and several chemical reactions in the corrosion of steel reinforcing bars. In order to achieve this process, four essential components of a galvanic corrosion cell are needed. They are:

1-Anode;

2-Cathode;

3-Electrolyte.

4- Electrical conductor

The general relationship between the components of a corrosion cell is illustrated in Figure 2.5 [Hime, 1987].

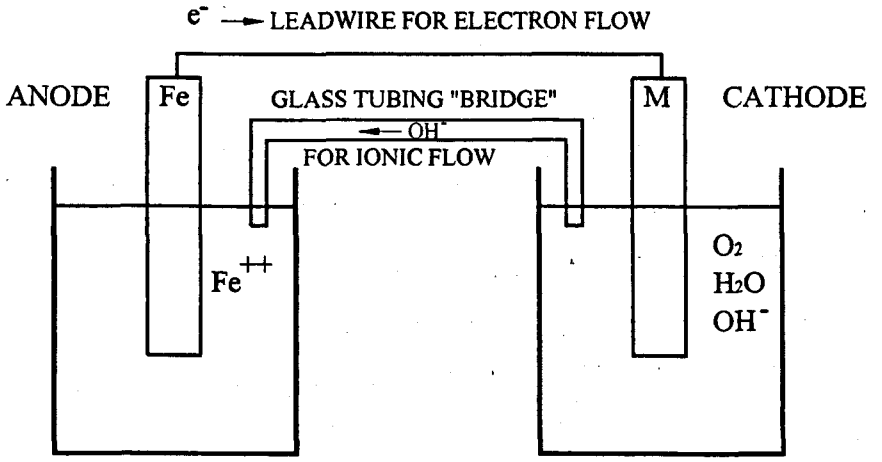

Figure 2.5 Electrochemical Corrosion Cell

a. The anode. The anode usually corrodes by loss of electrons from electrically neutral metal atoms to form discrete ions. These ions may remain in solution or react to form insoluble corrosion products. The corrosion reaction of a metal M is usually expressed by the simplified equation:

$$M \rightarrow M^{z+} + ze^{-} \qquad (2.3)$$

In which the number of electrons taken from each atom is governed by the agency of the metal. For iron, z equals two.

b. The cathode. The cathode reaction must consume the electrons produced by the anode process. There are two basic reactions which occur at the cathode depending on the pH of the solution:

(1) pH<7: $2H + 2e^- \rightarrow H_2$ (2.4)

(2) pH>7: $2H_2O + O_2 + 4e^- \rightarrow OH^-$ (2.5)

c. An electrolyte. This is the name given to the solution, which must, of necessity, conduct electricity. In the solution, the reactions can move from anodic to cathodic regions and anions move in opposite direction.

d. Electrical connection. The anode and cathode must be in electrical contact for a current to flow in the corrosion cell.

The removal of any one of the four components of the simple corrosion cell will stop the corrosion reaction.

If the steel in concrete in the presence of oxygen, but without chloride, the corrosion will take place in the following several steps:

1. At the anode, iron is oxidized to the ferrous state and release electrons.

$$Fe \rightarrow Fe^{2+} + 2e^- \quad (2.6)$$

2. The electrons released at the anode flow through the steel to the cathodic area, as illustrated in Figure 2.6 [Metha, 1993]. These electrons migrate to the cathode where they combine with water and oxygen to form hydroxyl ions.

$$2e^- + H_2O + \frac{1}{2}O_2 \rightarrow 2OH^- \quad (2.7)$$

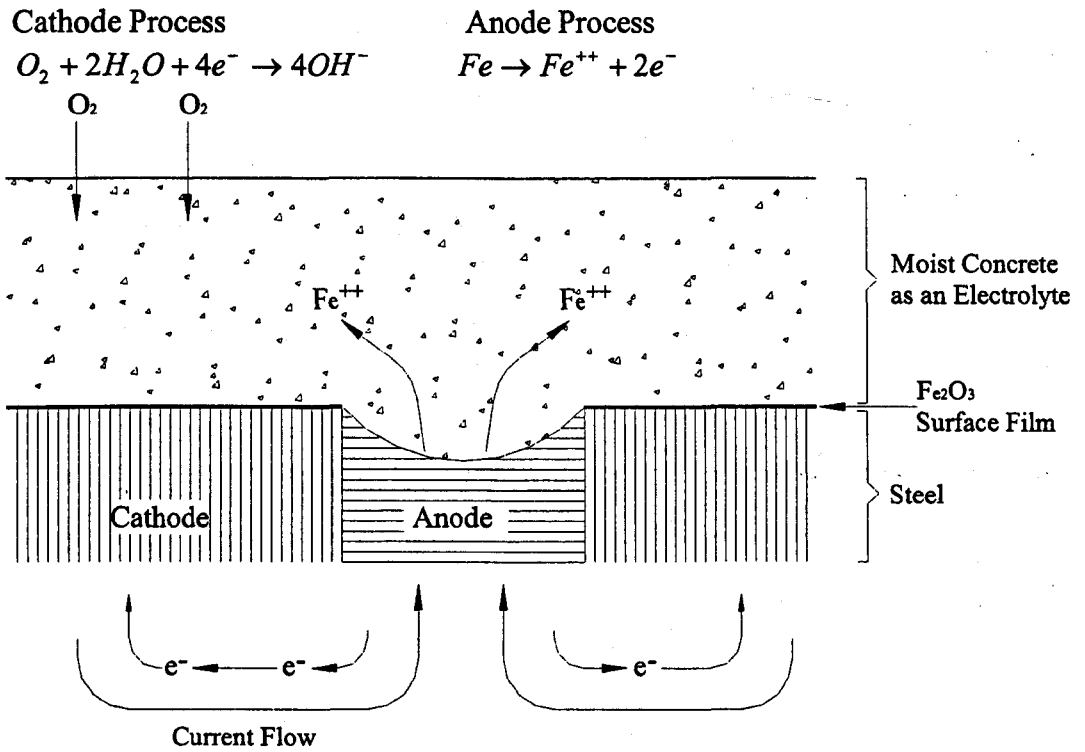

Figure 2.6 Mechanism of Corrosion of steel in Concrete [Metha, 1993]

3. The hydroxyl ions combine with the ferrous ions to form ferrous hydroxide.

$$Fe^{2+} + 2OH^- \rightarrow Fe(OH)_2 \tag{2.8}$$

4. The Fe(OH)2 can be further converted to hydrated ferric oxide ($Fe_2O_3.H_2O$), also known as ordinary red-brown rust, and black magnetite Fe_3O_4 preceded by the formation of green hydrated magnetite ($Fe_3O_4.H_2O$):

$$\begin{aligned} 4Fe(OH)_2 + O_2 &\rightarrow Fe_2O_3 \cdot H_2O + 2H_2O \\ 6Fe(OH)_2 + O_2 &\rightarrow 2Fe_3O_4 \cdot H_2O + 4H_2O \\ Fe_3O_4.H_2O &\rightarrow Fe_3O_4 + H_2O \end{aligned} \tag{2.9}$$

In contrast, if the steel in concrete in the presence of chlorides, but with no oxygen (at the anode), the following steps may occur in the electrochemical process:

1. At the anode, iron reacts with chloride ions to form an intermediate soluble iron-chloride complex.

$$Fe + 2Cl^- \rightarrow (Fe^{++} + 2Cl^-) + 2e^- \quad (2.10)$$

2. When the iron-chloride complex diffuses away from the bar to an area with a higher pH and concentration of oxygen, it reacts with hydroxyl ions to form $Fe(OH)_2$. this complex reacts with water to form ferrous hydroxide.

$$(Fe^{++} + 2Cl^-) + 2H_2O + 2e^- \rightarrow Fe(OH)_2 + 2H^+ + 2Cl^- \quad (2.11)$$

3. The hydrogen ions then combine with electrons to form hydrogen gas.

$$2H^+ + 2e^- \rightarrow H_2 \uparrow \quad (2.12)$$

4. As in the case of the corrosion of steel without chlorides, the ferrous hydroxide, in the presence of water and oxygen, is further oxidized to form Fe_2O_3.

$$4Fe(OH)_2 + O_2 + H_2O \rightarrow 4Fe(OH)_3 \quad (2.13)$$

$$2Fe(OH)_3 \rightarrow Fe_2O_3 \cdot 2H_2O \quad (2.14)$$

The corrosion rate can also be increased by the presence of other ions in the concrete. According to Hime and Erlin (1987), the reaction of ferrous ions and hydroxyl ions in the presence of chloride ions can also result in the formation of the corrosion product $Fe(OH)_2$.

The corrosion products are ferrous hydroxide [$Fe(OH)_2$], ferric hydroxide [$Fe(OH)_3$], and hydrated ferric oxide (rust) [$Fe_2O_3.H_2O$] etc. The relative volumes of iron and its corrosion reaction products are shown in Figure 2.7 [Nielsen, 1985]. The corrosion products will occupy a volume equal to three to six times that of the original steel. This increase in volume induces stresses in the concrete that result in cracking, delaminating, and spalling of the

cover concrete when expansive stress exceeds the tensile strength of the concrete. However, the true crossing section of reinforcing bars is reduced, which may lead to failure of the structural element in concrete structures. The detailed calculation of volume expansion due to corrosion is presented in Chapter 5.

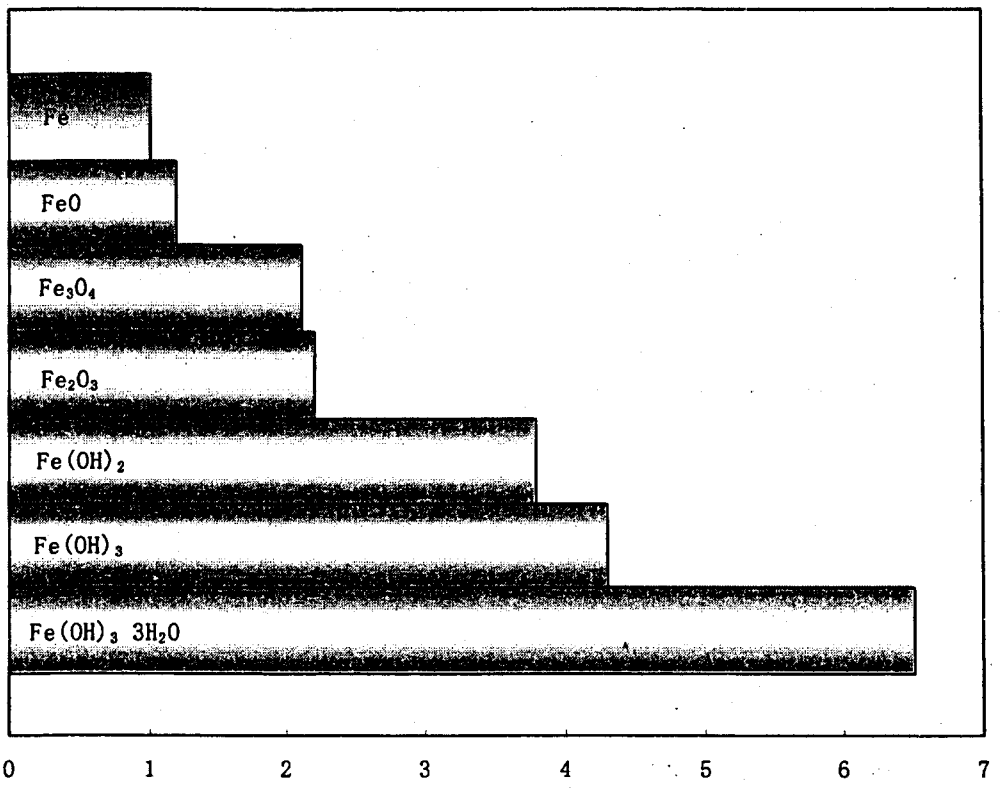

Figure 2.7 The Relative Volumes of Iron and Its Corrosion Reaction Products [Nielsen, 1985]

2.2.2.2 Faraday's Law

The free energy change of the corrosion process in terms of the potential difference and the charge transported is known as Faraday's Law:

$$\Delta G = (-zF)E \tag{2.15}$$

where E is the measured potential (volts), z is the number of electrons transferred in the corrosion reaction, and F represents the charge transported by one mole of electrons and has the value of 96,494 coulombs per mole.

2.2.2.3 Nernst Equation

For any chemical reaction, occurring under conditions of constant temperature and pressure, the driving force is measured by the decrease in free energy which accompanies the transformation of molar quantities of the reactants to the products. In the case of the hypothetical reaction:

$$n_a A + n_b B = n_c C + n_d D$$

in which n_a represents the number of moles of component A etc.

$$\Delta G = \Delta G^o + RT \ln \frac{[C]^{n_c}[D]^{n_d}}{[A]^{n_a}[B]^{n_b}} \qquad (2.16)$$

where R is the gas constant, T is the absolute temperature, and effective concentrations (activities) of the various components are denoted by square brackets. The superscript (^{O}) represents standard condition parameters at 298K and 1 atmosphere pressure. From this reaction of change in free energy, equation 2.15 can be,

$$E = Eo - \frac{RT}{zF} \ln \frac{[products]}{[reactants]} \qquad (2.17)$$

Equation 2.17 is known as the Nernst equation and it has great theoretical and practical significance. As a consequence, it is common to introduce the numerical values into the equation. Using the standard temperature, 298K, and $R = 8.3143 Jmol^{-1}K^{-1}$, together with conversion into logarithms to the base 10, equation 2.16 becomes

$$E = Eo - \frac{0.059}{z} \lg \frac{[products]}{[reactants]} \qquad (2.18)$$

where E is the non-equilibrium potential generated by the reaction, [reactants] is the reactant concentration and [products] is the product concentration. If these concentrations were chosen to be the equilibrium values, there would be no driving force ($\Delta G = 0$) and E would be zero.

2.2.2.4 Pourbaix Diagrams

Thermodynamic data (ΔG^o and E^o values) for chemical and electrochemical reactions that may influence the corrosion of metals in aqueous environments at 25°C have been collected by Pourbaix and co-workers [Pourbaix, 1976]. They provide the means for deciding which set of reactions are thermodynamically favored and for predicting the most stable reaction products under specified conditions of electrode potential and solution composition.

A convenient form of representation of such information is the Equilibrium Potential/ pH diagram (or Pourbaix diagram) in which the axes are the electrode potential and solution pH value. The domains of stability of the various substances considered are bounded by lines that represent conditions of equilibrium for the following classes of reaction:

-chemical reactions involving H^+ or OH^- (vertical lines)

-electrochemical reactions involving H^+ of OH^- (sloping lines)

-electrochemical reactions without participation of H^+ or OH^- (horizontal lines).

An important example of an equilibrium potential /pH diagram is that for the system Fe-H_2O at 25°C, shown in Figure 2.8, in which the concentration of dissolved ions, other than H^+ and OH^-, are taken to be 1 μ mol l^{-1} and solid phases are assumed to be pure.

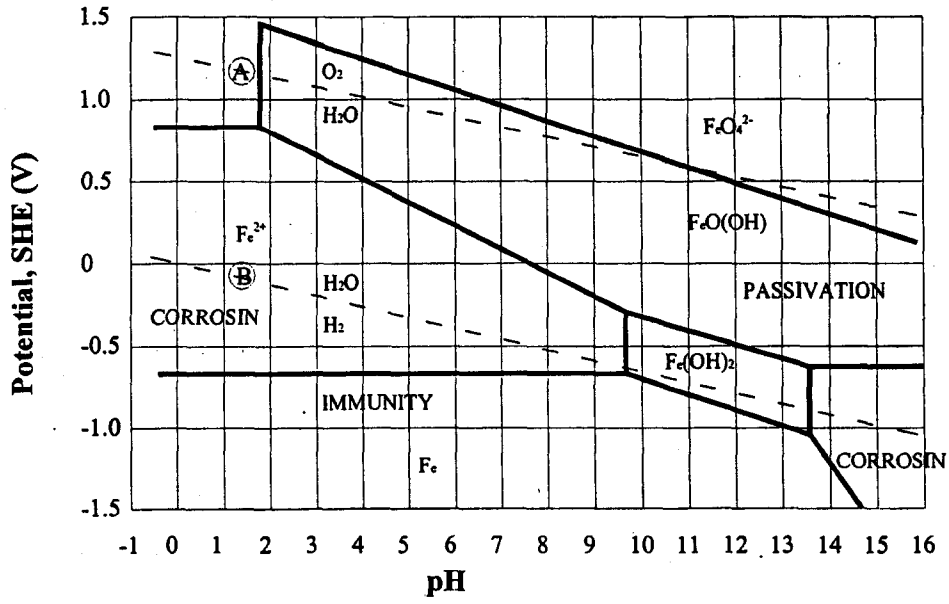

Figure 2.8 Pourbaix Diagram for F e-H2o at 25o C [Pourbaix, 1976]

2.2.2.5 Polarization

In an electrochemical reaction cell, the anode releases electrons while the cathode consumes electrons. The anodic and cathodic reactions are in balance if the production and the consumption of electrons proceed at the same rate.

This does not always happen in nature. If reaction rate at the anode is slower than the reaction rate at the cathode, a deficiency of electrons occurs at the surface of anode because electrons are consumed at the cathode at a faster rate than the anode can supply them. This deficiency of electrons produces a positive potential change at the anode (anodic overpotential, η_a), this potential change is called anodic polarization. When the positive potential change at the anode increases, the tendency for anodic dissolution also increases. On account of this, anodic polarization represents the driving force for corrosion reaction at the anode.

On the other hand, if the amount of electrons supplied by anode is greater than the amount that can be consumed at the cathode, extra electrons will accumulate at the surface of cathode waiting for reaction. Since the electrons are negatively charged, the potential of the cathode

will become more negative, this potential change is called cathodic polarization (cathodic overpotential, η_c).

This polarization can be defined as:

$$\eta_a = E_{corr} - E_a \tag{2.19}$$

$$\eta_c = E_c - E_{corr} \tag{2.20}$$

where E_a and E_c are the surface potentials for anode and cathode, respectively. E_{corr} is the steady state potential .

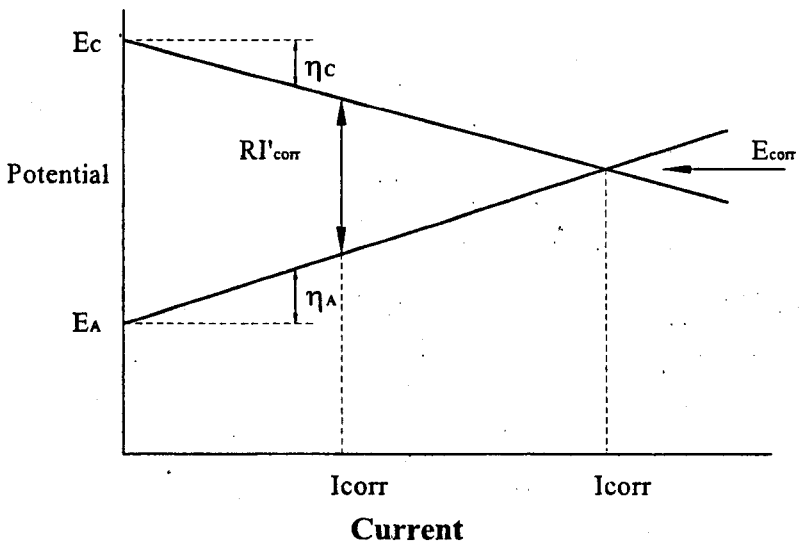

Figure 2.9 A Schematic of Evans Diagram [Evans, 1960]

Evans (1960) introduced a simplified graphic method of representing the relationship between current I and potential E. Figure 2.9 illustrates the simplest example of an Evans diagram. The abscissa may represent the total current or its logarithm. The intersection of two curves represents the conditions at which the anodic and cathodic currents are equal and no net external current flows and, thus, defines the corrosion potential, E_{corr} ,and corrosion current, I_{corr} .

There are three kinds of polarizations which may act separately or simultaneously, namely concentration, resistance (Ohmic) and activation polarization.

1. Concentration Polarization. Concentration polarization is caused by the concentration on the electrode surface from that of the bulk solution. An example of this would be depletion of oxygen at the cathode. The rate of oxygen diffusion through the concrete to the reinforcement determines the rate of corrosion.
2. Resistance (Ohmic) Polarization. An ohmic resistance gradient occurs through the electrolyte between working electrode and auxiliary electrode when the current, I, is passed in any polarization cell [Jones, 1992]. Resistance polarization is due to an ohmic resistance in a film, e.g. an oxide film on the electrode surface, causing an ohmic potential drop, which may be written as:

$$\eta_R = RI \tag{2.21}$$

where R is the film resistance for all the electrode surface.

3. Activation Polarization. When some step in the half-cell reaction controls the rate of charge (electron) flow, the reaction is said to be under activation of charge-transfer control, and activation polarization results. A logarithmic relationship is obtained based on the well-known Tafel's equation [Tafel, 1904] (for $I_a > 10I_o$):

$$\eta_A = b\log\frac{I_a}{I_o} = a + b\log I_a \tag{2.22}$$

where a and b are constants known as the Tafel intercept and Tafel slope parameters, respectively, and can be determined empirically I_a is applied current, and I_o exchange current. The parameter is related to the exchange current I_o, which is the equilibrium current flowing back and forth through the electrode-electrolyte interface at equilibrium and is measured by the reversibility of the reaction. The parameter b, on the other hand, gives an insight into mechanism of the electrode reaction [Steam, 1957]. The activation polarization is strongly

dependent on the composition of the solution, particularly its content and inhibitors.

2.2.2.6 Passivity

Passivity of a metal is generally characterized by a thin and tightly adherent oxide film on the metal surface, which tends to protect the metal against further corrosion. The exact composition of the thin and normally invisible film has been difficult to determine. It seems clear, however, that it is made up of chemical combinations of oxygen and is simply called an oxide film. Passivity is of two kinds: chemical and mechanical passivity.

Chemical passivity: This type of passivity is due to an invisible thin but dense and semiconducting oxide film on the metal surface, displacing the electrode potential of the metal strongly in the positive direction.

Mechanical passivity: Mechanical passivity is due to the precipitation of solid salts on the metal surface. The cause of strongly reduced corrosion rate in this case is a thick but more or less porous salt layer, usually non-conducting in itself.

When a potential is applied to an iron electrode, the rate of current flow depends on the state of passivity. Iron in concrete is generally passive, such that little current flows when a potential is progressively increased, eventually the current will flow. This is because, at this point, oxygen is evolved and the electrode reaction involves the electrolysis of water.

2.2.2.7 Corrosion Rate

Corrosion process involves production and consumption of electrons. The higher the rate of corrosion reaction, the higher the rate at which electrons are released from the anode and consumed at the cathode. Thus, a quantitative description of corrosion propagation is usually given in terms of the corrosion rate. Corrosion rate can be measured as the weight loss of metal per unit of surface area per unit of time ($mass/area \cdot time$) or depth of penetration (given as depth of penetration per unit of time).

Electron flow is represented by the current I, which is typically reported in units of amperes. The relationship between the current, I, and mass reacted, m, in a corrosion reaction is given by Faraday's Law:

$$m = \frac{Ita}{nF} \tag{2.23}$$

where a is the atomic weight, t is the time in which the measurement is carried out, F is Faraday constant (96500 $A \cdot s / mol$), and n is the number of electrons lost (valence change).

Most non-destructive techniques currently used for monitoring the corrosion are based on electrochemical measurements, with the corrosion rate estimated in terms of a corrosion current density, I_{corr} [Andrade, 1996]. Dividing the previous equation by time, t, and the surface area of the electrode, A, one gets the corrosion rate, r, as:

$$r = \frac{m}{tA} = \frac{I_{corr} a}{nF} \tag{2.24}$$

where I_{corr} is the current density in amperes per square meter (A/m^2) and n equals 2 for steel. If iron corrodes as a corrosion current density of 1 μ A/m^2, the

$$\text{Corrosion rate} = \frac{I_{corr}}{nF} = \frac{1\times10^{-6} A(55.85g/molFe)(86400s/d)}{(10^{-2})^2 m^2 \frac{2mole^-}{molFe}(96500A \cdot s/mole^-)} = 0.25\ g/m^2 \cdot d \tag{2.25}$$

And also can convert the weight loss to depth of penetration, divided by the metal density, which is 7.86 g/cm^3 for Fe.

$$\text{Corrosion rate} = (0.25\ g/m^2 \cdot d)(1m^3/7.85x10^6\ g\ of\ Fe)(365d/y) = 0.012\ mm/y \tag{2.26}$$

The effects of the concrete pore solution (electrolyte conductivity) and the conductivity of other phases, such as corrosion product and interfacial transition, is reflected in changes in the corrosion current density.

2.2.3 Factors affecting Corrosion

2.2.3.1 Concrete

Concrete normally provides reinforcing steel with excellent corrosion protection. The high alkaline environment in concrete results in the formation of a tightly adhering film which passivates the steel and protects it from corrosion. In addition, concrete can be proportioned to have a low permeability which minimizes the penetration of corrosion-inducing substances. Low permeability also increases the electrical resistivity of concrete which impedes the flow of electrochemical corrosion currents. However, corrosion of steel can occur if the concrete is not of adequate quality, the structure was not properly designed for the service environment, or the environment was not as anticipated or changes during the service life of the concrete structure. On the one hand, Portland cement forms an alkaline environment to protect the embedded steel; meanwhile, the concrete quality and thickness of concrete cover influence this protection. On the other hand, concrete acts as an electrolyte which makes corrosion may occur in it. In order to understand the concrete's properties as an electrolyte, some relative bases of concrete will be introduced.

1. Bases of Concrete

Hydration of Portland Cement

The mineral components of cement are mainly tricalcium silicate (C_3S), dicalcium silicate (C_2S), tricaalcium aluminate (C_3A), and tetracalcium ferroaluminate (C_4AF). The hydration products of cement paste are calcium silicate hydrate (C-S-H), calcium hydroxide (CH), and calcium sulfoaluminate. Unhydrated cement particles may also exist in the paste.

Calcium silicate hydrate. The calcium silicate hydrate (C-S-H) phase makes up 50 to 60 percent of the volume of solids in a completely hydrated Portland cement paste and is the most important in determining the properties of the paste. The morphology of C-S-H varies from poorly crystalline fibers to reticular network. The internal crystal structure of C-S-H also remains unresolved.

Calcium hydroxide. Calcium hydroxide crystals constitute 20 to 25 percent of the volume of solids in the hydrated paste. In contrast to the C-S-H, the calcium hydroxide $Ca(OH)_2$ is a

compound with a definite stoichiometry,. It tends to form large crystals with distinctive hexagonal-prism morphology. Also, calcium hydroxide in hydrated Portland cement has an adverse effect on chemical durability to acidic solutions because of the higher solubility of calcium hydroxide than C-S-H.

Calcium sulfoaluminates. Calcium sulfoaluminate compounds occupy 15 to 20 percent of the solids volume in the hydrated paste and therefore play only a minor role in the structure-property relationships.

Voids of Hydrated Cement Past

In addition to the solids components, hydrated cement paste (*hcp*) contains several types of voids which have an important influence on its properties.

Interlayer space in C-S-H. It accounts for 28 percent porosity in solid C-S-H and is too small to have an adverse affect on the strength and permeability of the *hcp*.

Capillary voids. Capillary voids represent the space not filled by the solid components of the *hcp*. The volume and the size of the capillary voids are determined by the original distance between the anhydrous cement particles in the freshly mixed cement paste (i.e. water/cement ratio) and the degree of cement hydration.

Air voids. Air can be entrapped in the fresh cement paste during the mixing operation. Both the entrapped and entrained air voids in the *hcp* are much bigger than the capillary voids, and are capable of adversely affecting its strength and impermeability.

Cement Paste Pore Solution

The composition of the pore solution is the decisive factor in determine whether embedded steel will be passivated or whether it will be actively corroded. Researchers on the influence of a number of factors on the composition of pore solution have shown that the presence of sodium and potassium oxides in the cement, as well as calcium hydroxide produced in the

hydration reactions of cement components can give the pore solution of ordinary Portland cement a pH of about 13 while the pH of blended cement is somewhat lower. The range of high pH values of typical concrete is within the pH domain in which insoluble oxides of irons are thermodynamically stable to maintain a passive film on steel surface. Unfortunately, the pH value of concrete can be reduced by carbonation and by leaching.

The structure and Distribution of Pores

The structure, pore size distribution and pore connectivity in the cement phase determine the availability of oxygen and moisture at the steel surface, both of which are necessary for the maintenance of a passive film. They also determine the penetration or diffusion rate of chloride ions and carbon dioxide which, as mentioned above, are the two most common causes in the corrosion of embedded steel in concrete

Pore size distributions are mainly affected by the water/cement ratio, and the degree of hydration. The size of interlayer space (gel pore) is too small to have an adverse affect on the permeability of the hydrated cement paste, and water in these small voids are held by hydrogen bonding. It is the capillary pore system which is responsible for diffusion and permeation and, therefore, of importance for corrosion

Interfacial Transition Zone

The microstructure of the paste near the aggregate appears to differ from that within the bulk [Taylor, 1992]. In fact, an interfacial transition zone (ITZ) has been identified by some writers [Metha and Montiero, 1992] as a distinct phase to which separate properties are given. The significant of the interfacial region is evident from the fact that the particles of aggregate are separated by rather small distances, implying that a large fraction of the interparticle volume may be composed of microstructural gradients.

Among the solid constituents of concrete, it is the transition zone which is the weakest link of the chain that has the greatest influence on concrete strength, elastic modulus, and permeability. At early age, ettringite and calcium hydroxide in the transition zone make this layer weak and porous. If mineral admixtures are incorporated into concrete, calcium

hydroxide further reacts with the supplementary materials and forms calcium silicate hydrate (C-S-H), which reduces zone thickness, makes it denser, and thus less permeable.

As mentioned earlier, the permeation of air and water is a necessary prerequisite to corrosion of steel in concrete. The characteristics of transition zone influence the durability of concrete. The existence of microcracks in the transition zone at the interface with steel and coarse aggregate is the primary reason that concrete is more permeable than corresponding *hcp* or mortar.

Water in Concrete

The concrete pore system filled with pore water and air provides a path for corrosion elements and the electrolyte.

Water may accumulate in concrete pores and capillaries. The amount of water depends on the pore size distribution and the humidity of the environment. This pore water solution can be classified into different types depending on how difficult it is to remove it from concrete. Water in the hardened cement paste, it can exist in the following forms:

1. Capillary water. This is the water present in voids larger than about 50 °A.
2. Adsorbed water. This is the water that is close to the solid surface; that is, under the influence of attractive forces, water molecules are physically adsorbed onto the surface of solids in the *hcp*. A major portion of the adsorbed water can be lost by drying the *hcp* to 30 percent relative humidity.
3. Interlayer water. This water is associated with C-S-H structure. It has been suggested that a monomolecular water layer between the layers of C-S-H is strongly held by hydrogen bonding. The interlayer water is lost only on strong drying (i.e. below 11 percent relative humidity).
4. Chemically combined water. This is the water that is an integral part of the structure of various cement hydration products. This water is not lost on drying; it is evolved when the hydrates decompose on heating.

2. Effects of Concrete Environment on Corrosion

Portland cement. When Portland cement hydrates, the silicates react with water to produce C-S-H and calcium hydroxide. The following simplified equations give the main reactions of Portland cement with water

$$2(3CaO \cdot SiO_2) + 6H_2O \rightarrow 3CaO \cdot 2SiO_2 \cdot 3H_2O + 3Ca(OH)_2 \quad (2.27)$$

$$2(3CaO \cdot SiO_2) + 4H_2O \rightarrow 3CaO \cdot 2SiO_2 \cdot 3H_2O + Ca(OH)_2 \quad (2.28)$$

As previously mentioned, the high alkalinity of the chemical environment normally present in concrete protects the embedded steel because of the formation of a protective oxide film on the steel. The integrity and protective quality of this film depends on the alkalinity (pH) of the environment.

Calcium hydroxide crystals may be 15 to 30 percent of the weight of the original cement in a well-hydrated Portland cement . This is usually sufficient to maintain a solution at a pH 13 in the concrete independent of moisture content.

The silicates are the major components in Portland cement imparting strength to the matrix. No reactions have been detected between chloride ions and silicates. Calcium chloride seems to act as an accelerator in the hydration of tricalcium silicate as well as to promote the corrosion of steel.

The chemical combining of C_3A with chlorides is frequently referred to as a beneficial effect in that it will reduce the rate of chloride penetration into concrete. According to Mehta (1993), a chemical binding of penetrating chlorides cannot be expected unless the C_3A content is higher than about 8 percent. However, recent studies have found more corrosion-induced distress associated with high C_3A content.

Concrete Quality. Concrete will offer more protection against corrosion of embedded steel if it is of a high quality. A low water/cement ratio will slow the diffusion of chloride, carbon

oxide, and oxygen and also the increase in strength of the concrete, which may extend the time before corrosion-induced stresses cause cracking of the concrete. The pore volume and permeability can be reduced by lowering the water/cement ratio. The type of cement or use of superplasticizers and mineral admixtures may also be an important factor in controlling the permeability and the ingress of chlorides [Gjorv and Vennesland, 1979].

Thickness of Concrete Cover over Steel. The amount of concrete cover over the steel should be as large as possible, consistent with good structural design, the severity of the service environment, and cost. The effect of cover thickness is more than a simple linear relationship. Considering the normal diffusion of an electrolyte into a porous solid without chemical reaction, a relationship would be anticipated. However, in the case of cement paste, the diffusion of chloride ions into the paste is accompanied by both physical adsorption and chemical binding. These effects reduce the concentration of chloride ion at any particular site and hence the tendency for inward diffusion is further reduced.

Concrete as an Electrolyt. The concrete pore system as mentioned above filled with air and pore water solution provides an excellent path for deleterious substance and acts as an electrolyte. In mature concrete water movement is controlled by cracking and the *hcp* properties. Furthermore, the movement of water in *hcp* depends on changes in pore structure due to continued hydration, as well as changing the solubility of its constituents.

All properties of concrete as an electrolyte will influence the character of the electrochemical reactions significantly by changing the conditions required for cathodic and anodic processes. The most fundamental characteristic of electrochemical reactions is the difference in mechanism and the rate of oxygen supply under different corrosion conditions: through the liquid electrolyte (corrosion of metal in solution), through a thin film of electrolyte (such as atmospheric corrosion), or through a solid microporpus electrolyte (such as steel corrosion in concrete). In solution, access of oxygen to the corroding surface of the metal is dependent primarily on diffusion, and in concrete, on its structure (pore size distribution, porosity and pore connecticity), degree of saturation and cover depth. The corrosion process (or rate of corrosion) in concrete also is dependent on the conductivity of concrete electrolyte system.

Permeability in Hydrated Cement Paste. Permeability is defined as the ease with which a fluid can flow through a solid. It should be obvious that the size and continuity of the pores in the structure of the solid determine its permeability. Strength and permeability of the *hcp* are two sides of the same coin in the sense that both are closely related to the capillary porosity or the solid/space ratio. As hydration proceeds, the void space between the originally discrete cement particles gradually begins to fill up with hydration products. It has been shown that the water/cement ratio and the degree of hydration determine the total capillary porosity, which decreases with the decreasing water/cement ratio and/or increasing degree of hydration.

2.2.3.2 Other Effects

Moisture. The rate of electrochemical reaction in a corrosion cell depends upon the moisture content in the vicinity of reinforcement in concrete. The moisture content in hardened concrete depends upon the water/cement ratio used for mixing the ingredients, and circulation of free water absorbed from the surrounding environment. The water content in fresh concrete must be just sufficient for hydration of cement. However, for easy workability more water is added. Evaporation of this excess water makes concrete more permeable. Therefore, the water/cement ratio and the impermeability of concrete play an important role in the corrosion process in concrete structures.

Oxygen Availability. All of the corrosion processes described above requires oxygen. In the absence of oxygen, the corrosion rate is appreciably reduced even with chloride concentration above the threshold level, except in acid solution. So, the availability of oxygen is one of the main controlling factors for corrosion of steel. The penetration of oxygen in different concentrations at different places causes the formation of differential aeration cells which in turn produce the potential difference and flow of current. The corrosion which is quantitatively measured in grams of steel per year depends upon the oxygen flow rate to the reinforcement through the concrete cover.

Chapter 3

Review of Bond Slip

In this Chapter the mechanisms of bond are discussed, first by introducing the conception of bond slip and the process of bond failure. The factors, which can affect the bond behavior significantly, are described. Two types of experiments that are frequently used in the study of bond slip behavior are presented, and the general calculation in terms of bond slip is reviewed. The stress redistribution and deformations in concrete associated with bond are also presented. Finally the relationship between bond slip and corrosion is investigated.

3.1 Mechanism of Bond

3.1.1 Conception of Bond-Slip

The capability of reinforced concrete member in resisting the external loads depend on the compatibility of the concrete materials and reinforcing bars in the tension area. In order to maintain composite action, some stress transformation between the concrete and steel bars is necessary, this transformation behavior is called bond. Usually it is assumed perfect bond in the analysis of reinforced concrete (RC) structures, which implies full compatibility between concrete and reinforcement strains. This assumption is valid only in regions where there is no slip between the concrete and reinforcing bars [Keuser and Mehlhorn, 1987], this behavior takes place at early loading stages and at low strain levels. The reinforcing bars have to undergo the same strain or deformation as the surrounding concrete in order to prevent the discontinuity or separation of the two materials under loads. As the load increases, cracks will appear, and a certain amount of bond stresses in terms of relative displacement between concrete and reinforcement, usually called bond-slip, takes place. All of them will in turn affect the stress distribution in both steel and concrete. The stress and relative displacement between concrete and the reinforcement steel are extremely higher near the cracks. It results

in different strains in the steel rebars and in the surrounding concrete.

According to Lutz and Gergely (1967), bond can be conceived as compromising three components, chemical adhesion, friction, and mechanical interaction between concrete and steel.

Bond of plain bar depends primarily on the first two of these mechanisms, although there is some mechanical interlocking due to the roughness of bar surface. The effect of the chemical adhesion in bond is normally considered very small. Once slip occurs, the bond of plain bar is only developed by means of friction between the bar and the surrounding concrete.

Deformed bars primarily depend on the interlocking of the ribs with the surrounding concrete. This does not mean that friction and chemical adhesion are negligible in the case of deformed bar, but they are secondary. This investigation will focus on the study of bond behavior in the deformed bars

According to ACI Committee 408 (1966), bond stress can be defined as the unit shear force acting parallel to the bar on the interface between bar and concrete. In transferring from concrete to bar, this shear stress – bond stress modifies the steel stress in the bar, either increasing or decreasing it. The bond stress is usually measured by the stress per unit area of bar surface, using the nominal surface of the deformed bar which ignores the extra surface created by the lugs and ribs. Bond stress can also be measured by the rate of change of steel stress in the bar. Attention must be paid to that unless the bar stress changes, there is no bond stress existing between the concrete and reinforced bars. The principle is also correct in contra verse.

3.1.2 The Process of Bond Failure

The process of bond failure can be divided into several stages according to the phenomenon of failure of chemical cohesion, the appearance of cracks and crushed concrete in front of ribs (Figure 3.1).

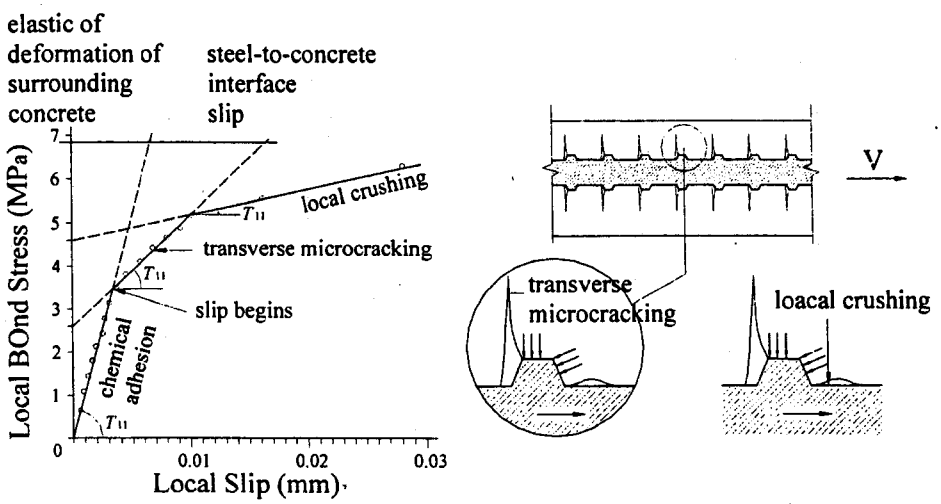

(a) Local Bond Stress-Slip Law [Tassios, 1979]

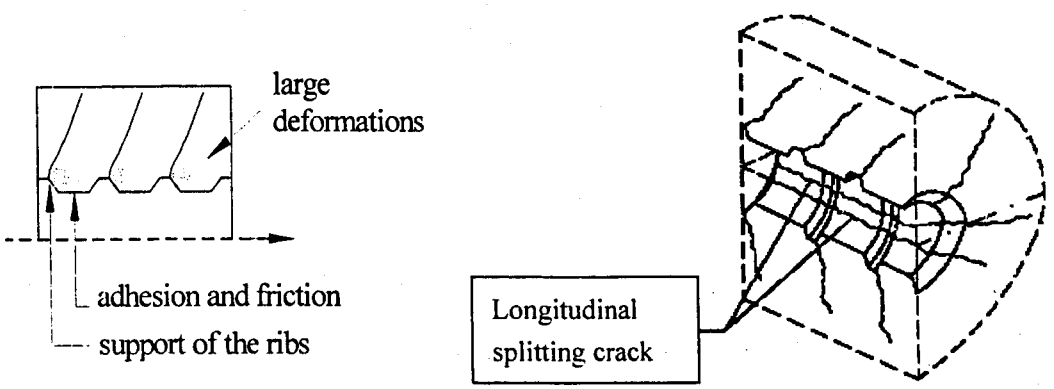

(b) Chemical Adhesion, Friction and Bearing Action (Not All Active at the Same Time)

Figure 3.1 Process of Bond Failure

At the early stage of bond slip process, the only resisting mechanism is chemical adhesion which is very small value of the average bond stress (τ). It enables concrete to follow steel

deformations with no relative slip, or with negligible slip, but highly localized stresses arise close to rib tips.

After increasing the values of average bond stress with the increasing of loads, interaction between the ribs and concrete occurs. This interaction induces large bearing stresses under the ribs. Also the highly localized tensile stresses at the tip of the ribs result in opening transverse cracks in the concrete (Figure 3.2).

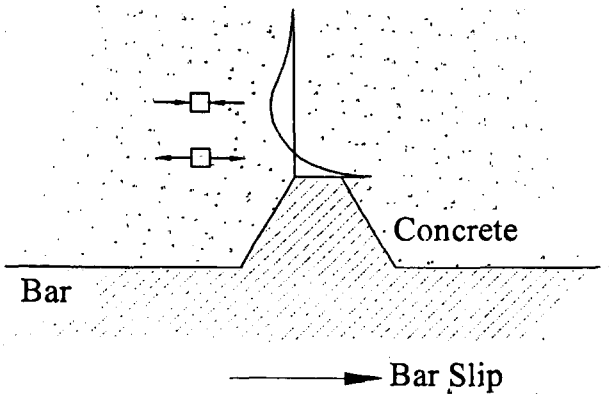

Figure 3.2 Longitudinal tensile Stresses at the Tip of the Rib

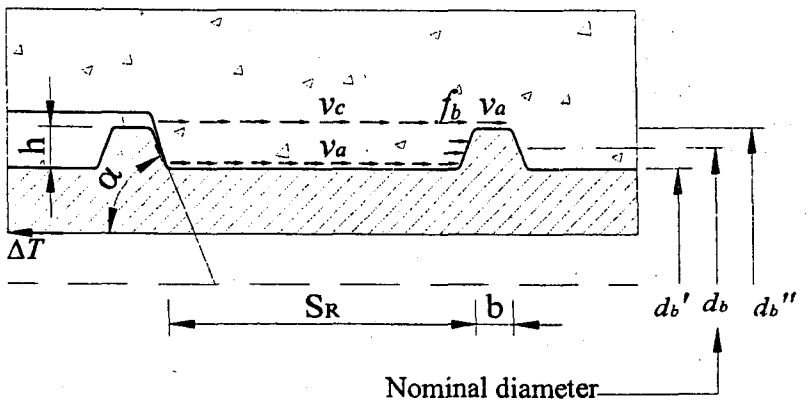

Figure 3.3 The Stresses Between Two Ribs of a Deformed Bar

Figure 3.3 shows the stresses developed between two ribs of a deformed bars, they include:

(a) Shear stresses v_a, developed through adhesion along the surface of the bar.

(b) Bearing stresses f_b, against the face of the rib.

(c) Shear stresses v_c, acting on the cylindrical concrete surface between adjacent ribs.

As soon as transverse cracking occurs, the transverse cracks decrease concrete stiffness and countenance bar slip. The concrete will be crushed in front of the ribs and form a crushed concrete wedge which enhances the wedging action of the bars against the surrounding concrete. Also large hoop stresses will arise in the concrete layer close to the bar, which may cause localized longitudinal cracks lying in plane passing through the bar axis which cause splitting cracking. The concrete keys will also deform in such a way that they tend to move away from the bar surface. As the chemical adhesion is destroyed, the wedging action of the ribs will push the concrete away and separate the concrete from steel as shown in Figure 3.4.

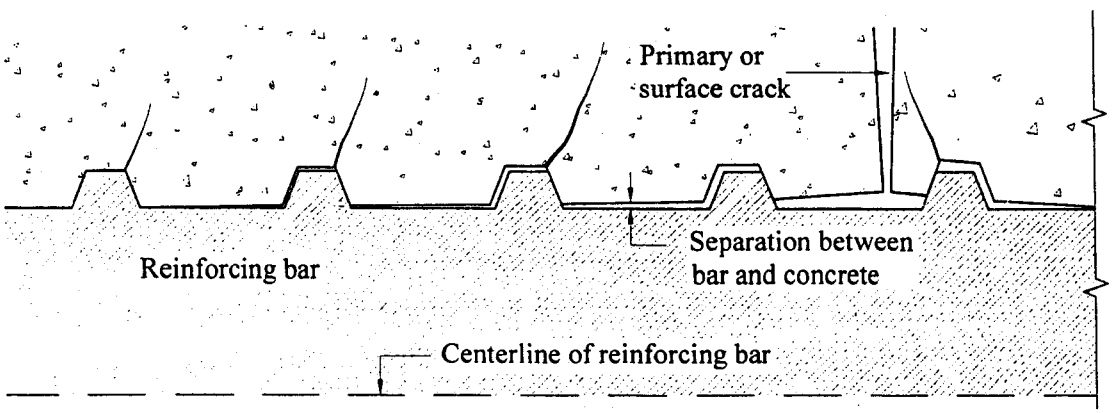

Figure 3.4 Separation Near a Primary Crack Between Reinforcing Bar and Concrete

The stress condition in the vicinity of the crack is very complex. For an example, Figure 3.5 shows bond stress distribution in the area subjected to the pure moment in the simply supported beam test. It can be found that even when shear is zero and moment is constant, the bond stress is so variable that the average bond stress seems more significant than the

local value at any particular point, especially in the place where flexural cracking exists. Each such cracks, creates points of bond stress concentration which influences the average usable stress.

As the load continue to increase, both transverse and longitudinal cracks spread; and the splitting tend to outbreak through the whole cover. In the case of deformed bars confined by an adequate amount of transverse reinforcement, bond failure would be pullout. On the contrary, in the case of the cover or confinement is insufficient, bond failure would occur in the form of splitting which means the splitting cracks spread across the whole cover of the bars.

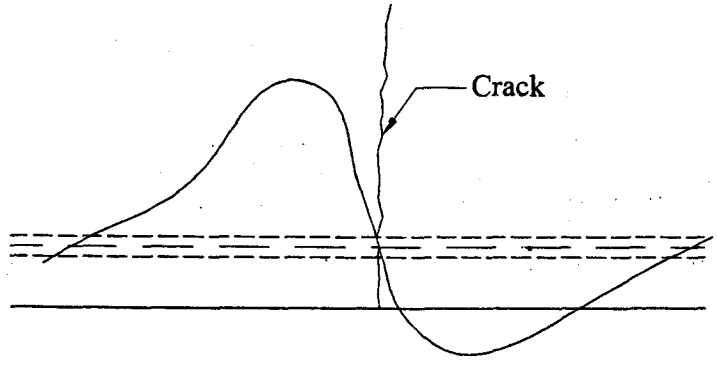

Figure 3.5 Bond Stress Distribution in Concrete Near a Crack

3.2 Factors Affecting Bond Performance

3.2.1 Reinforcement Rusting

The bar rusting, which consists of a thin coating of iron oxide, is a result of the exposure of the steel bar to the environment. It may result from cooling down from rolling temperature. Such type of rusting can improve the bond behavior because it increases the surface roughness and hence the frictional force. But if corrosion happens and continues to rust, it will reduce bond stress between the reinforced bars and concrete.

The Rib Height Space Ratio h/S_R

Rehm (1968) revealed the aspect of the geometric parameter h/S_R to the bond problem. He found the most satisfactory performance of a bar embedded in concrete over the short length c is when h/S_R is in the vicinity of 0.065. When the ribs are higher and spaced too closely, the shear stress, v_c, will govern the behavior and the failure of bond which is pullout failure. When the rib spacing is larger than approximately 10 times the rib's height, the partly crushed concrete may form a wedge in front of the rib, and failure is normally considered as a result of splitting of the surrounding concrete. The two types of failure associated with the rib are illustrated in Figure 3.6.

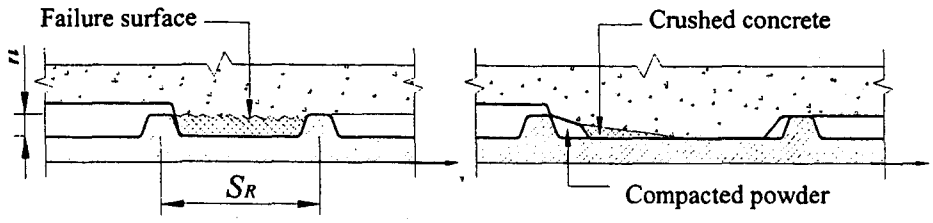

(a) h/S_R>0.15 (b) h/S_R <0.10

Figure 3.6 Failure Mechanisms at the Ribs of Deformed Bars

Deformation Patterns of Steel Bars

It has been proved by many researchers that the deformation pattern of a reinforcing bar can affect bond response. It is characterized by the rib spacing (S_R), rib height (h), bar diameter (d_b), rib face angle and pattern. Furthermore, we can use the relative rib area (f_R) of the reinforcing bar can be used to represent these parameters in the analysis. The relative rib area is defined as the rib area perpendicular to the bar axis normalized by the bar surface area between ribs.

$$f_R = \frac{A_R}{\pi \cdot d_b \cdot S_R} \tag{3.1}$$

where A_R is the area of the projection of a single rib on the cross-section of a bar. The generally accepted values 0.05-0.10 represent a good compromise for f_R in terms of ultimate bond strength, splitting ability, industrial requirement, good service-load performances (limited crack opening and cover splitting). Results of study conducted by Darwin and Graham (1993) indicate that increased relative rib area results in increased bond stiffness and increased strength for specimens that do not exhibit a splitting-type bond failure. A study conducted by Hamad (1995) shows similar results through increased bond strength is observed for specimens that exhibit a splitting-type bond failure as well as for those that exhibit a pullout failure. Hamad concludes that specimens with rib face angles in excess of 45 degrees exhibit increased strength over bars with face angle less than 45 degrees. However, the importance of the confinement should be always kept in mind.

Steel Stress Level

The non-linear behavior of bond-slip depends on the steel stress level in the concrete. In the pullout tests, the steel stress is kept relatively small and cannot play any significant role. However, in long anchorages the reinforcement stresses are higher, but still their role can be neglected as long as rib bearing is the force transferring mechanism (with concrete crushing in front of the ribs and/or cover splitting). In fact, the transverse deformation coupled with the longitudinal steel stress is small in comparison with rib height (Poissons' effect). However, when the force transfer mechanism is based mostly on friction (as in smooth bars and pretensioned strands) the local transverse deformation of the bar cannot be disregarded, since the surface roughness and the transverse reduction of bar diameter may have the same magnitude. This transverse contraction may considerably reduce the radial compressive stress and, hence, the frictional bond stress.

For ribbed bars the influence of steel stress is small as long as the steel is in the elastic range. However, experimental results show that yielding has a drastic negative effect on the bond

mechanism resulting in a non-linear descending branch in the bond-slip relationship at the very onset of yielding [Shima et al., 1987]. Hence, the bond stress-slip relationship can be influenced not only by the softening of surrounding concrete, but also by the softening of the steel at yielding. The effect on the bond-stress development similar to the effect of splitting cracks through the concrete cover. The influence of steel yielding is yet not well understood.

3.2.2 Concrete Quality and Stress State

Since bond action results from the localized pressure underneath the ribs and is directly related to the shear component of the interface forces, bond performances depend on both concrete multiaxial behavior in compression f_c and on concrete tensile strength f_{ct}. Mirza and Houde (1979) examined the influence of concrete strength and the thickness of the concrete cover, they found that the slip increases linearly with the increase in the concrete strength and the specimen dimension up to a certain size.

The stress state in the concrete surrounding a bar also has a significant effect on bond action. Transverse tensile forces worsen the behavior of both splitting-prone anchorages and splices, and may even turn a pullout failure into a splitting failure. In both cases, the situation is even worse if further tensile stresses are present, owing to temperature and shrinkage effects.

Transverse compressive forces favor bond action, depending on their nature (active or passive confinement). Active confinement is always favorable, particularly in a splitting–prone situation, but becomes almost irrelevant in a friction-type situation with large cover values. Passive confinement requires a certain amount of crack slip and opening to be activated, and is helpful after cover splitting. Finally, it should be noted that the state of tension within the concrete that is parallel to the reinforcement impairs the efficiency of bond markedly [CEB-FIP, 2000].

3.2.3 Load History

Bond behavior is also influenced by load history. Since the load repetition, rate, frequency and long-term action have a remarkable influence on concrete strength and deformability, they can affect bond performance significantly. As a result, not only the bond-stress relationship, but also the failure model, either splitting or pullout, are affected by the load history. The loading rate has a strong influence on bond stiffness and resistance. The higher the loading rate and the higher the concrete strength, the greater the mechanical properties of the bond in deformed bars.

The data provided by Eligehausen et al. (1983) contributes to characterization of the bond-slip response for deformed reinforcement subjected to monotonic load history. Figure 3.7 shows bond stress distribution curves corresponding to a number of load increments. As the tensile load increased, the form of the distribution curve generally changes slightly. Nevertheless, it was impossible to describe the curves by any simple consistent form. In general, with increasing load, there was a consistent increase in the bond stress at almost all points.

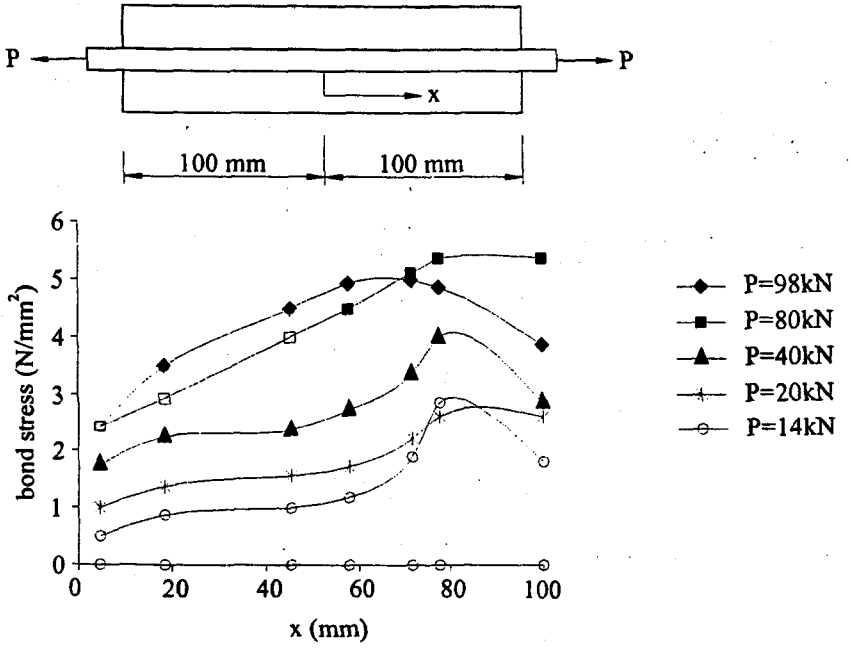

Figure 3.7 Bond Stress Distribution for 25 mm Ribbed Bar

For the cyclic load condition, the reverse cycling at low bond stress deteriorates bond behavior during cycling, but not at ultimate. On the contrary, reverse cycling (above 80% of bond static strength) leads to sort of shake down [ACI Committee 408, 1966].

3.3 Experimental Investigation

There are many types of experiments are available in the study of bond behavior shown from the past research. One of them is pullout test which was first introduced by Rehm in 1958. The test is carried out by anchoring one deformed bar in a plain concrete block, then it is subjected to monotonically increasing tensile load till failure. It is noted that sufficient concrete cover must be provided in order to guarantee the failure in the form of pullout.

Rehm (1958) did series of pullout tests with the face angle of ribs on the reinforcing bar varied from 30 to 105 degrees. He concluded that the response of specimens with rib face angles greater than 40 degrees was approximately in the same bond stress value and thus apparently is independent of rib face angle.

Later Lutz et al. (1966) convinced the Rehm's test results, they pointed out that the concrete in the vicinity of the bar and extending in front of the ribs a distance equal to 5 to 7 times of the height of the ribs is crushed under moderate bond demand and that a zone of crushed concrete extending in front of the ribs a distance of at most twice the height of the ribs, moves with the reinforcing bar as slip occurs.

Lutz and Gergeley (1967) carried out another investigation of bond response, they presented a comprehensive evaluation of the mechanisms of bond response for systems with deformed reinforcement. It shows that the bond of deformed bars is developed mainly by bearing pressure of the bar ribs against the concrete. According to Lutz and Gergeley, slip of deformed bars can occur in two ways: (1) the ribs can push the concrete away from the bar

(wedging action), and (2) the ribs can crush the concrete.

Lutz and Gergely (1967) also investigated the effect of cracking on the bond stress and the stress distribution in the concrete beam. One simply supported beam is used in their experiment as shown in Figure 3.8.

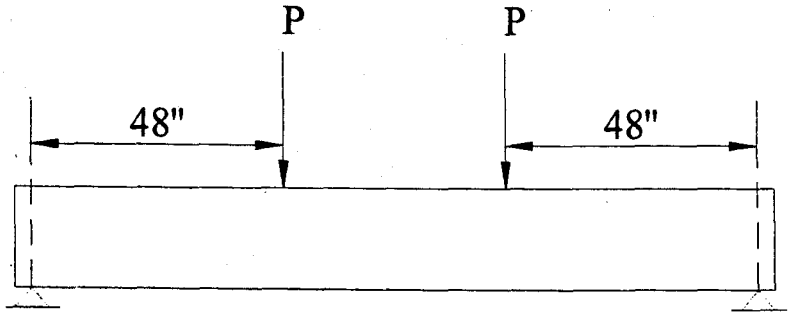

Figure 3.8 Beam Dimensions for Test by Lutz and Gergely (1967)

The test results show that the circumferential tensile stresses in the concrete around the bar are very small prior to flexural cracking. However, near transverse cracks bonding forces cause large circumferential tensile stress. Also, radial tensile stresses, acting normal to the concrete-steel interface, destroy contact near the crack and allow separation and slip of the bar (Figure 3.4). Due to the large longitudinal concrete tensile stresses, internal transverse cracks form, and radial (splitting) cracks can start at transverse cracks due to the large circumferential stresses. They also used elastic finite element method to analyze a cylinder of concrete with a concentrically embedded reinforcing bar. The results of the finite element analysis are quite close to the situation existing between two flexural cracks near a reinforcing bar in a reinforced concrete as shown in Figure 3.9.

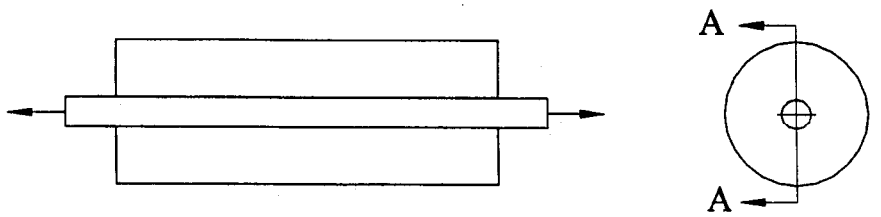

(a) Sketch of Pullout Specimen for FE Analytical Studies

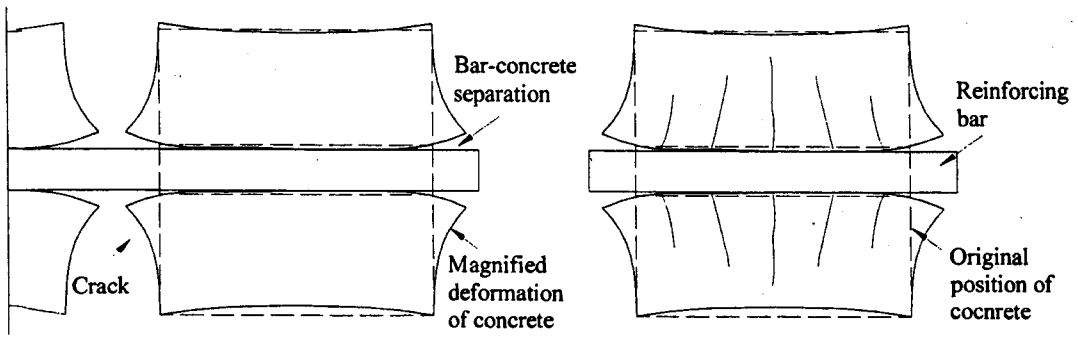

Section A-A (without internal cracks) Section A-A (with internal cracks)

Figure 3.9 (b) Deformed concrete between transverse cracks (macro-scale)

Goto (1971) conducted tension test and provided additional understanding of the wedging action of reinforcing ribs acting against concrete. This experimental investigation focused on characterizing the concrete damage associated with tensile bond stress. The prototype specimen consists of a single, deformed reinforcing bar embedded in a plain concrete prism. The tension was loaded through the exposed ends of the bar. Cracks in the concrete were penetrated by ink from special injection holes. Afterwards the prisms were cut axially and the cracks colored by the ink became visible. The slopes of the internal cracks, from 45 to 80 degrees, indicate the trajectories along which the compressive forces leave the ribs of the deformed bar and spread out into the concrete. Their slope also depends on whether the ribs are lateral, diagonal or staggered about the axis of the bar. The slopes of the internal cracks would be different and have different values on each side of the bar if the test specimen constituted an anchorage zone in a beam. The dimensions of the surrounding concrete will

also influence the slope.

A study presented by Tepfers (1979) was one of the first investigations to focus on predication of bond strength for deformed reinforcement. Tepfer studied theoretically the circumferential stress distribution over the thick-walled cylinder confining the reinforcing bar. These circumferential tensile stresses are caused by the outward stresses from the action of the deformed bar on the concrete cylinder as shown in Figure 3.10. Tepfers proposed that bond strength is determined by the capacity of the concrete surrounding the reinforcing bars to carry the hoop stresses. Three modes of system failure were proposed: elastic, partially cracked-elastic and plastic. The data presented by Tepfers supported the proposition that bond strength is determined by the hoop stresses developed in the surrounding concrete. The data also supported the conclusion that the partially cracked elastic model proposed by Tepfers results in a lower bound bond strength.

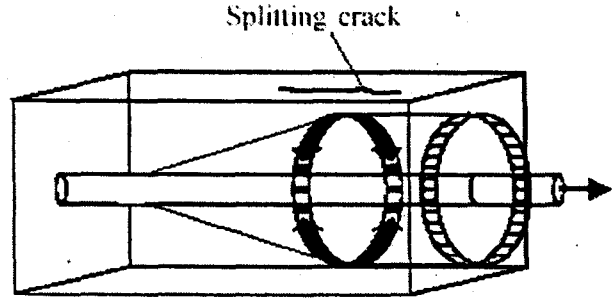

Figure 3.10 Tepfers Tensile Stress Ring [Tepfers, 1979]

3.4 General Bond-Slip Calculations

In the analysis of bond slip the following aspects of bond must be considered [Yener and Li, 1991; Baldwin and Clark, 1995; Mo and Chan, 1996]:

1) Geometry of the reinforcement (relative rib area);
2) Type of collapse (pull-out and splitting bond failure);

3) Type of loading;

4) The confining action (active/passive confinement);

5) The size effect;

6) The concrete type (HSC, NSC, FEC);

7) The environment and the effect on bond (bar corrosion; high/low temperature);

8) The boundary conditions.

As it is very difficulty to include all of the above aspects in the calculation, only some parts of effects are considered in the analysis approach. In this investigation, the bond slip in the macroscopic level was considered.

3.4.1 Bond Modeling

3.4.1.1 Constitutive Equation of Bond Slip

For the bond-slip relationship the equilibrium and compatibility must be satisfied. Considering equilibrium of the section shown in Figure 3.11, we have:

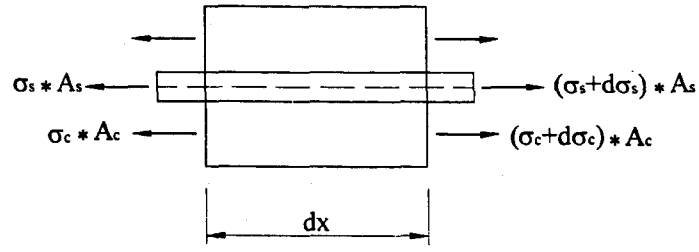

(a) Element Length dx with Steel and Concrete Stresses

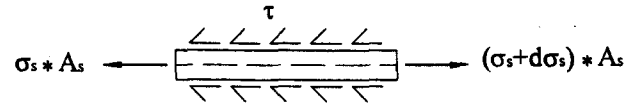

(b) Free-body Diagram of the Steel Bar of Length dx

Figure 3.11 Stresses in an Element

$$d\sigma_c \cdot A_c + d\sigma_s \cdot A_s = 0 \tag{3.2}$$

$$\therefore \quad d\sigma_s = \frac{-A_c \cdot d\sigma_c}{A_s}$$

$$\text{or} \quad d\sigma_c = \frac{-d\sigma_s \cdot A_s}{A_c}$$

$$\tau = \frac{A_s \cdot d\sigma_s}{d_b \cdot \pi \cdot dx} \tag{3.3}$$

$$\frac{d\sigma_s}{dx} = \frac{4\tau}{d_b} \tag{3.4}$$

where d_b is the bar's diameter, Ac and As are the area of the concrete and steel bar, σ_c and σ_s are the stresses in the concrete and the steel, respectively and $d\sigma_c$ and $d\sigma_s$ are the change in the concrete and steel stresses, respectively.

The increment of the local slip, S_x, within an infinitesimal bar length dx at the location x can be defined as the difference between the extension of the bar, S_s, and the concrete extension, S_c, at x.

In addition, since the change in length with respect of the original length is equal to strain, it follows that the difference between the bar strain, ε_s, and the concrete strain, ε_c, is

$$S_x = S_s - S_c \tag{3.5}$$

$$\frac{dS_x}{dx} = \varepsilon_s - \varepsilon_c \tag{3.6}$$

The value of strain can be related to stress by assuming that concrete and steel behave elastically. Therefore, Hook's law can be used and the stress is a linear function of the strain.

$$\sigma_s = E_s \cdot \varepsilon_s \quad \text{and} \quad \sigma_c = E_c \cdot \varepsilon_c \tag{3.7}$$

where *Ec* and *Es* are the elastic modulus of the concrete and the steel respectively.

Submitting Eq. (3.9) into Eq. (3.8), we have:

$$\frac{dS_x}{dx} = \frac{\sigma_s}{E_s} - \frac{\sigma_c}{E_c} \tag{3.8}$$

The differentiation of the Eq. (3.10) with respect to x gives:

$$\frac{d^2 S_x}{dx^2} = \frac{d\sigma_s}{E_s \cdot dx} - \frac{d\sigma_c}{E_c \cdot dx} = \frac{d\sigma_s}{E_s \cdot dx}\left(1 + \frac{A_s \cdot E_s}{A_c \cdot E_c}\right) \tag{3.9}$$

Substituting for $\frac{d\sigma_s}{dx} = \frac{4\tau}{d_b}$, results in

$$\frac{d^2 S_x}{dx^2} = \frac{1}{Es} \cdot \frac{4\tau}{d_b}\left(1 + \frac{A_s \cdot E_s}{A_c \cdot E_c}\right) \tag{3.10}$$

Let $k = \frac{4}{E_s \cdot \phi}\left(1 + \frac{A_s \cdot E_s}{A_c \cdot E_c}\right)$, then

$$\frac{d^2 S_x}{dx^2} = k \cdot \tau \tag{3.11}$$

As the bond stress is calculated by $\tau = \frac{A_s \cdot d\sigma_s}{d_b \cdot \pi \cdot dx}$, which means that it varies with the change of axial stress and the axial stress resulting from the steel strain. In this case, the bond stress

includes two zones, one in the elastic zone and the other in the non-elastic zone.

If we consider a constant stress along the total bar length, $\tau = b_1$, where b_1 is constant, resulting in:

$$\frac{d^2 S_x}{dx^2} = kb_1 \tag{3.12}$$

Alternatively, τ can also be directly proportioned to the slip S_x, i.e.: $\tau = b_2 \cdot S_x$, now the equation is:

$$\frac{d^2 S_x}{dx^2} = k \cdot b_2 \cdot S_x \tag{3.13}$$

and in general

$$\frac{d^2 S_x}{dx^2} = k \cdot b_2 \cdot S_x^{\,N} \tag{3.14}$$

$\tau = b_3 \cdot S_x^{\,N}$, which means that τ is found to be as a nonlinear function.

If it is constant, recall $\frac{d^2 S_x}{dx^2} = kb_1$, and by integrating it, we have,

$$\frac{dS_x}{dx} - A_1 x + A_2 = 0 \tag{3.15}$$

$$S_x = \frac{A1x^2}{2} + A_2 x + A_3 \tag{3.16}$$

A_1, A_2, and A_3 can be found by defining the boundary conditions.

What is being done in the above formulations is a trial for a combination between the slip and the bond stress at any x.

Many other studies have been made in order to get a best-fit curve for bond-slip phenomena, but all those studies were based in one way or another on initial assumptions between the bond stress and the slip.

3.4.1.2 Analysis Model

(1) Rehm model (1961)

$$\tau = f_{c,cub} \cdot (\varphi \cdot s^{\alpha} \pm \psi \cdot s) \tag{3.17}$$

where $f_{c,cub}$ is the cube concrete strength; and φ, ψ and α are theoretical or experimental constants.

(2) Martin Model (1973) [FIB, 2000]

$$\tau = \tau_0 + c \cdot s^b \tag{3.18}$$

where τ_0 is the adhesion bond-stress; and c and b are experimental constants.

(3) Mirza-Houde model (1979)

$$\tau = 539.8 \cdot s - 256.1 \cdot 10^2 \cdot s^2 + 592.2 \cdot 10^3 \cdot s^3 - 557.4 \cdot 10^4 \cdot s^4 \tag{3.19}$$

(4) The Comité Euro-International du Béton (CEB) Code Model (1990)

This model was proposed by Ciampi at al. (1990), in this model the primary zone is nonlinear and it is modeled by(Figure 3.14):

$$\tau = \tau_{max} \cdot \left(\frac{S}{S_1}\right)^{\alpha} \qquad \text{for } 0 \le S \le S_1 \tag{3.20}$$

$$\tau = \tau_{max} \qquad \text{for } S_1 < S \le S_2 \qquad (3.21)$$

$$\tau = \tau_{max} - (\tau_{max} - \tau_f)\left(\frac{S - S_2}{S_3 - S_2}\right) \qquad \text{for } S_2 < S \le S_3 \qquad (3.22)$$

$$\tau = \tau_f \qquad \text{for } S_3 < S \qquad (3.23)$$

where α is an empirical constant ($0 \le \alpha \le 1$) that describes the shape of the bond-stress-slip curve, starting from a bond characteristic with a constant stress ($\alpha = 0$) up to a bond stress-slip relationship with linear increasing bond ($\alpha = 1$).

The CEB Model Code states that the bond stress-slip curve, presented in Figure 3.12 can be considered as a statistical mean curve, applicable as an average formulation for a broad range of cases. The first curved part refers to the stage in which the ribs penetrate into the mortar matrix, characterized by local crushing and micro-cracking. The horizontal level occurs only for confined concrete, referring to advanced crushing and shearing off the concrete between the ribs. The decreasing branch refers to the reduction of bond resistance due to the occurrence of splitting cracks along the bars. The horizontal part represents a residual bond capacity, which is maintained by virtue of a minimum transverse reinforcement, keeping a certain degree of integrity intact.

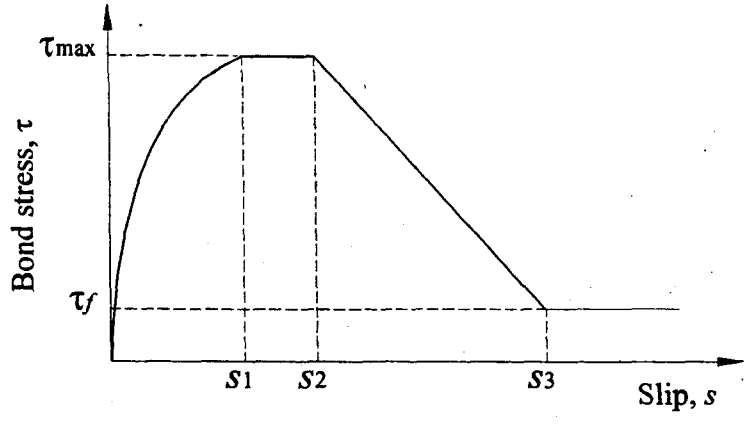

Figure 3.12 Analytical Bond Stress-Slip Relationship (Monotonic Loading) [CEB Model Code]

The model includes a plateau at the peak stress (τ_{max}), follow by a linear degradation zone. The bond stress due to the secondary bond mechanism is assumed constant. According to CEB Model Code MC90, the parameters in Eq. (3.20) to (3.23) are given in Table 3.1.

Table 3.1 Parameters for Defining the Mean Bond Stress-Slip Relationship

	Unconfined Concrete		Confined Concrete	
	Good bond condition	All other bond condition	Good bond condition	All other bond condition
S_1	0.6mm	0.6mm	1.0mm	1.0mm
S_2	0.6mm	0.6mm	3.0mm	3.0mm
S_3	1.0mm	2.5mm	Clear rib spacing	Clear rib spacing
α	0.4	0.4	0.4	0.4
τ_{max}	$2.0\sqrt{f_{ck}}$	$1.0\sqrt{f_{ck}}$	$2.5\sqrt{f_{ck}}$	$1.25\sqrt{f_{ck}}$
τ_f	$0.15\tau_{max}$	$0.15\tau_{max}$	$0.4\tau_{max}$	$0.4\tau_{max}$

(5) Marti's Model (1998)

Marti's approach is based on one main simplified assumption. His rigid-plastic assumption is that the bond stress is constant with respect to the variation of the slip.

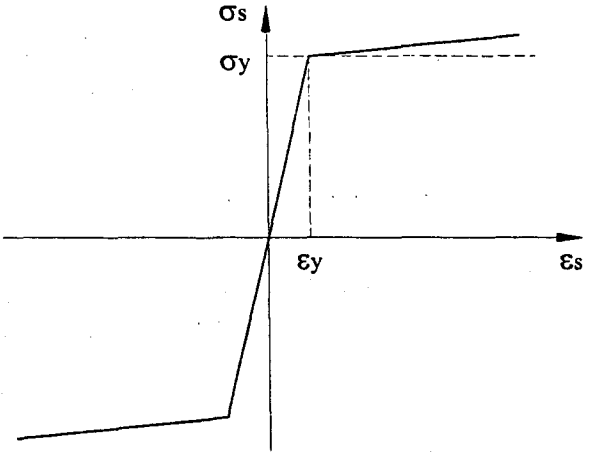

Figure 3.13 Bilinear Constitutive Rela tionship for the Reinforcement

Since the Young modulus of elasticity of steel varies between the elastic and the non-elastic region (Figure 3.13), Marti's assumption was based on the change of the Young modulus of elasticity of steel, and he conceded that the bond stress will have two constant values one before yielding and one after it.

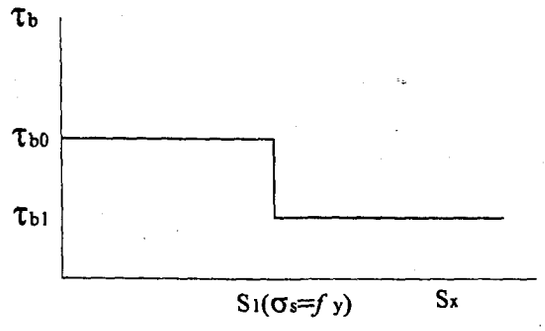

Figure 3.14 Assumed Bond Stress Distribution

Figure 3.14 shows the rigid plastic assumption that have been made, in order to have a bond slip before yielding the force that should be applied must create a stress= $\tau_{b0}=2.0f_{ct}$. But as $\sigma_s = f_y$ we will have a yielding steel and in this case a smaller force is required to create a bond stress $\tau_{b1}=f_{ct}$.

Based on these assumptions (bilinear stress-strain diagram for the reinforcement and a stepped, rigid-perfectly plastic bond stress-slip relationship) and especially on the one before yielding Marti was able to get standard crack spacing at a fully developed crack in which no more crack can occur.

$$s_{rm} = \frac{\phi \cdot f_{ct} \cdot (1-\rho)}{2 \cdot \tau_{b0}} \qquad (3.24)$$

Also based on his assumption the following stress and strain distributions (shown in Figure 3.15) were obtained for steel bars beyond yield at cracks.

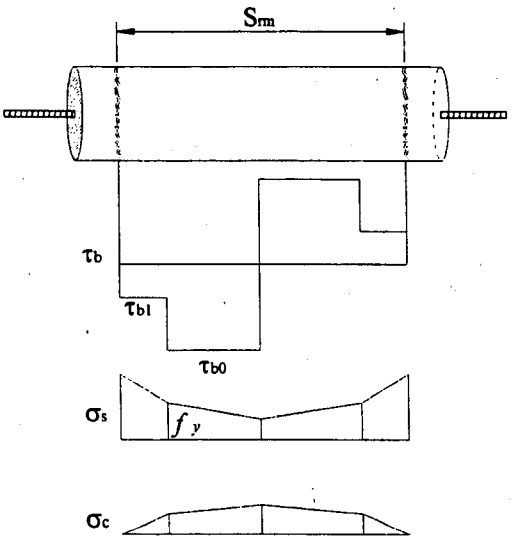

Figure 3.15 Chord Tension Model

3.4.2 Stress Redistribution After Cracking

Concrete is a type of material that is very weak in tension, so whenever it is subjected to tensile force greater than its tensile strength, primary cracks (Figure 3.16), which are at roughly right angles to element axis (transverse cracking), start to form.

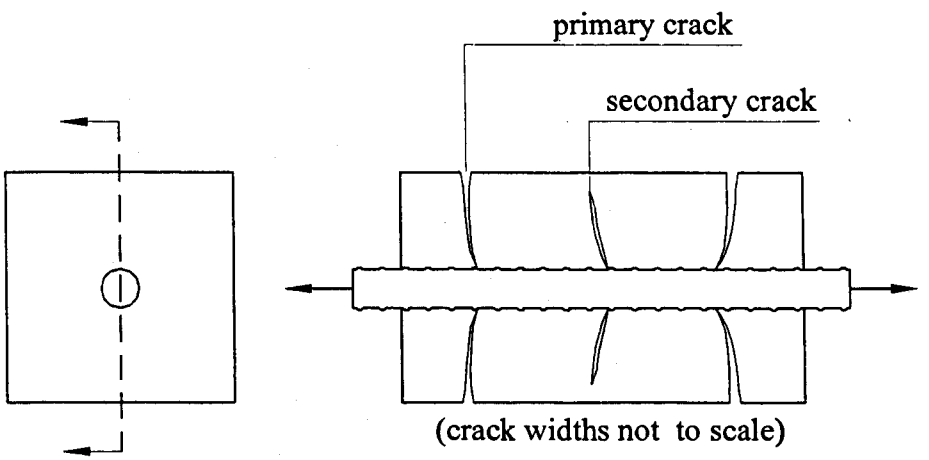

Figure 3.16 Primary and Secondary Cracks in a Reinforced Concrete Member in Tension [ACI, 1986]

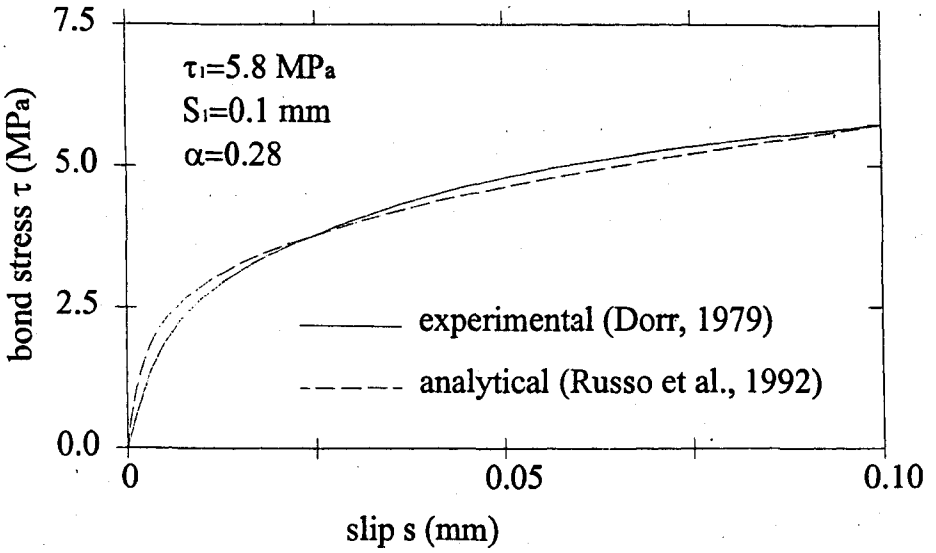

Figure 3.17 Experimental and Analytical Bond Stress-Slip Relationship for Tension Test [Russo and Romano, 1992]

The analysis of transverse cracking should be based on bond modeling since concrete strain mainly depends on steel strain. So in this case, a nonlinear relationship should be used (Figure 3.17) [Russo and Romano, 1992].

Once the elastic behavior of concrete ends a transverse crack starts to appear but since cracking is not controlled, the fracture process spreads abruptly across the whole section.

3.4.2.1 Transient Cracking

In case of a member that is subjected to tension from both sides (Figure 3.15), for a low value of load and steel strain at the loaded end, the slip vanishes before reaching the symmetry axis (as in long members). The element will not crack as long as there is no enough length for which the steel will transmit enough strain to concrete in order to crack. In this case, any further load increase may produce a different member response [Ouyan and Shah, 1994]:

(a) It may occur that the concrete strain attains the cracking value at a point R (shown in Figure 3.18) with $x_R \leq \frac{l}{2}$. In this case $x_R = x_{Rcrack}$ where x_{Rcrack} is the distance of the crack from the loaded end. The first primary crack forms and the member is divided into m smaller parts (Figure 3.18), with m being the first integer number not lower than $\frac{l}{x_{Rcrack}}$.

(b) On the contrary, it may occur that the point R reaches the symmetry axis $x_R = \frac{l}{2}$ with the concrete strain still smaller than ε_{ct}. So any increase in the applied load will lead to an increase in concrete strain at the symmetrical axis. In this way if there is going to be a crack it will be at the symmetrical axis because the length of x_{Rcrack} cannot exceed $\frac{l}{2}$.

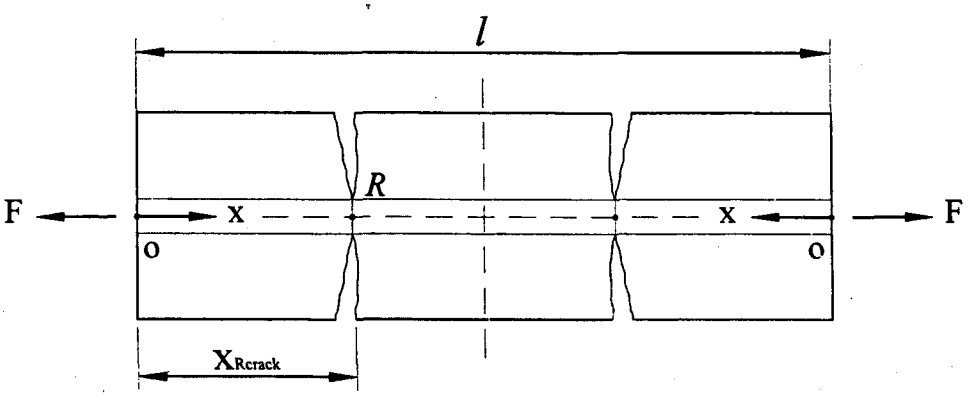

Figure 3.18 Cracking in a Long-Member

After the formation of the first primary crack, a second-generation of primary cracks occur, for a somewhat higher load levels. Before this second generation each part is in a load situation similar to the one of the original (uncracked) member but with a smaller length. A crack pattern reaches to a stabilized state when the length of a single part is no more sufficient to allow the concrete strain to reach the failure value in tension.

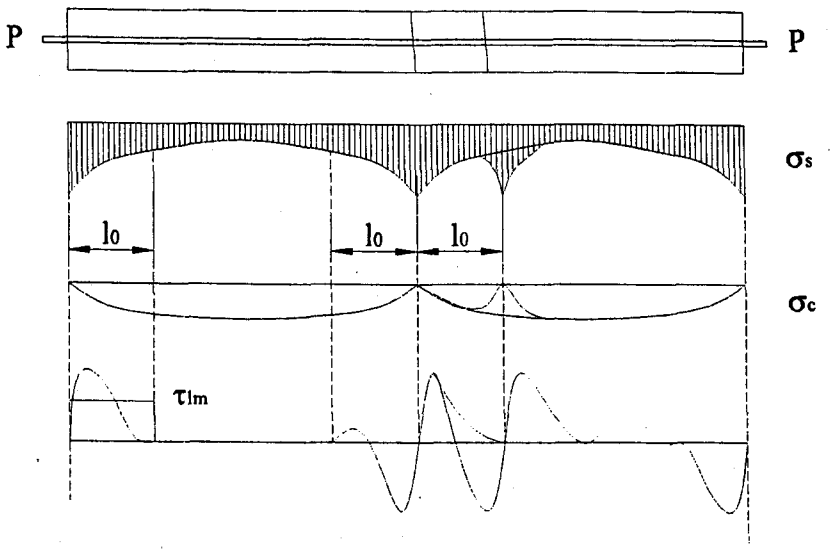

Figure 3.19 Steel, Concrete and Bond Stress Variation along the Bar at Different States

As a result for the transient cracking bond property will be affected and it will start to fluctuate each time a new crack take place. The bond variation comes as compatibility requirement as both concrete and steel stress varies drastically at crack location. Hence, theoretically stresses distribution for all variable will have the shapes proposed by Leonhardt [1964] (Figure 3.19).

3.4.2.2 Tension Stiffening

In a reinforced concrete member that is subjected to tension, its tensile force is resisted by both the reinforcing steel and surrounding concrete. Only across a crack is the load carried entirely by the reinforcement. Consequently the strains in a bar embedded in concrete are smaller than those in a naked one. So, the decrease in steel strain due to the concrete may be considered as a stiffness increase of the reinforcement compared to the naked bar. This bond-related phenomenon is known as "tension-stiffening" [Giuriani, 1982].

The overall elongation of a bar embedded in concrete subjected to uniaxial tension is:

$$\Delta l = 2\int_0^{1/2} \varepsilon_s dx \tag{3.25}$$

The overall elongation of a naked bar is:

$$\Delta l = \varepsilon_{s0} \cdot l \tag{3.26}$$

The overall equivalent shortening of the bar due to concrete restraining action (Δl_c) is:

$$\Delta l_c = \Delta l_0 - \Delta l \tag{3.27}$$

Hence, the relative contribution of the concrete to the overall stiffness of the member can be defined [Bresler and Bertero, 1968] as follows:

$$\lambda = \frac{\Delta l_c}{\Delta l_0} \tag{3.28}$$

The parameter λ is an index of tension-stiffening effectiveness. The greater the value of λ, the more effective the stiffness contribution of the concrete becomes [ASCE, 1982].

Once a crack happens, the stiffening effect will be affected, and this can be explained by considering the relationship between the load and the average strain in both cracked and uncracked section. A typical stress verses strain is shown in Figure 3.20, both primary cracks and slip are introduced indirectly through smearing the subsequent nonlinear branch starts from point *A*.

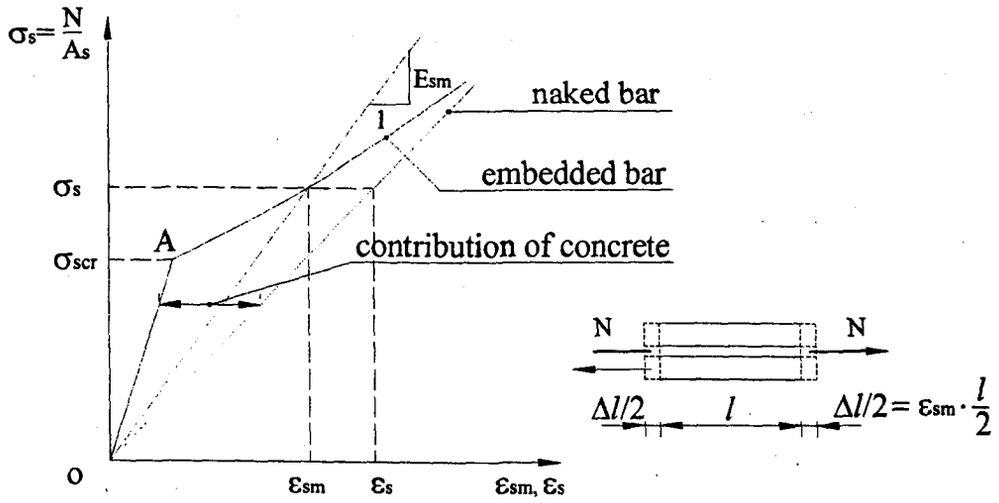

Figure 3.20 Tension Stiffening: Tensile Stress Versus (Mean) Tensile Strain

The increase of stiffness in the regions between adjacent cracks (tension stiffening) can be included by either considering the tensile resistance of concrete or by increasing the tensile stiffness and strength of the steel bar. Tension stiffening mostly affects the member response under serviceability conditions, because the effect of bond is completely lost when member failure occurs.

3.5 Relationship between Corrosion and Bond Slip

Corrosion can affect bond behavior significantly in the reinforced concrete members. The loss of bond strength may also result from the opening of longitudinal cracks along the reinforcement due to radial tensile stresses induced at the steel/concrete interface by the expansive products of corrosion. This strength loss can even cause serviceability failure in reinforced concrete members, if it reaches a certain extent. So it is very important to study the relationship between corrosion and bond slip.

Corrosion can affect bond strength in several ways. The relationship between bond slip and corrosion is shown in Figure 3.21:

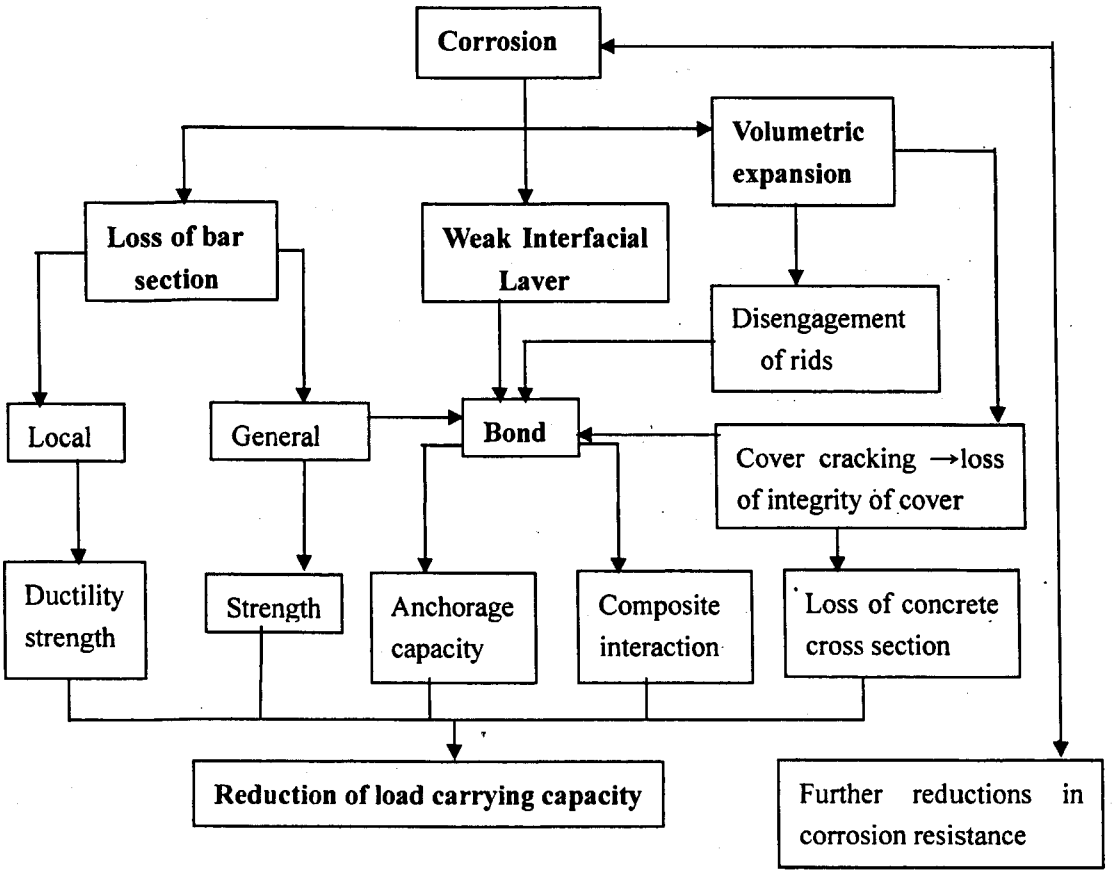

Figure 3.21 Effects of Corrosion in Residual Strength [CEB-FIP, 2000]

- Increase in the diameter of a corroding bar at first leads to an increase in radial stress between bar and concrete and hence increase the friction component of bond. However, further corrosion will lead to development of longitudinal cracking and a reduction in the resistance to the bursting forces generated by bond action.
- Corrosion products at the bar/concrete interface will affect friction at the interface. A firmly adherent layer of rust may contribute to an enhancement in bond strength at early stages of corrosion [Al-Sulaimani et al., 1990; Amleh and Mirza, 1999]. At more advanced stages of corrosion, weak and friable material between bar and

concrete will certainly be at least partially responsible for reductions in bond strength [Cabrera and Ghodussi, 1992].

- Corrosion may reduce the height of the ribs of a deformed bar. However, this is unlikely to be significant except at advanced stages of corrosion.
- Disengagement of ribs and concrete. The layer of corrosion products formed by oxidation of the steel may force the concrete away from the bar and reduce the effective bearing area of the ribs.

Many researchers have carried out experimental work to investigate the relationship between bond and corrosion [Al-Sulaimani et al., 1990; Andrade et al., 1993; Almusallam et al., 1996; Amleh and Mirza, 1999; Amleh, 2000]. From their test, we can conclude that:

(a) Effects of corrosion on the slip and ultimate bond strength

For a small degree of corrosion in the precracking stage (0-4%), the ultimate load increases with the degree of corrosion increasing, whereas the corresponding slip at the ultimate load decreases. It has been observed that for a small degree of corrosion of the reinforcing bar, significant mechanical pressure is exerted on the surrounding concrete before cracking occurs. This pressure is caused by the development of expansive corrosion products which increase the reactionary confinement and the mechanical interlocking of concrete around the bar. Secondly, in the initial stages of corrosion, the roughness of the bar is also increased, thereby enhancing the friction between the bar and the surrounding concrete. Both of these effects increase the bond resistance and decrease the slip of the bar. In this precracking stage, the bond failure of the specimen resulted from the crushing of concrete keys adjacent to the lugs without any splitting of the specimen.

In the cracking stage (4-6%), the specimens with a relative low level of corrosion (4-5%), exhibited a linear relationship between load and slip up to almost ultimate bond strength;

thereafter, a sudden drop occurs which continues to show increasing slip at decreasing loads. The reason for the sudden drop in load-slip curve at ultimate load can be attributed to the sudden splitting of the concrete cover over the bar.

In the post-cracking corrosion (8% or more), considerable slip occurred at ultimate load stage, before failure was observed. Also, the value of the ultimate bond strength remains more or less the same. The reason for this behavior can be explained as follows:

(1) With an increased level of reinforcement corrosion, a significant degradation of the ribs occurs and the deformed steel bar starts acting more and more like a plain bar. The horizontal component of the bearing force produced as a result of mechanical interlocking of the ribs is therefore significantly reduced. The pullout action is therefore facilitated and occurs at a lower load.

(2) Accumulation of a heavy layer of the flaky corroded material around the bar acts as a lubricant and reduces the friction component of the bond strength.

(3) The third important factor in the post-cracking stage is the width of the crack corresponding to a particular level of corrosion. The formation of cracks around the reinforcing bar reduces its confinement in the concrete to the extent that practically any cumulative negative effect of the above mentioned two parameters (1) and (2) do not affect the ultimate bond strength..

(b) Effect of crack width on the bond strength

From the test results done by other researchers [Stanish, 1997; Alonso et al., 1998; Amleh and Mirza, 1999; Amleh, 2000], it is shown that the ultimate bond load is reduced abruptly at the initial stages of the formation of cracks and the associated resulting reduction in the confinement. After a certain degree of corrosion, the effect of crack width on the bond strength decreases, and beyond a certain level, it does not affect the bond strength significantly. The reason for this is that, because of sufficiently wide cracks, the reinforcing

bar has already lost much of its confinement, and a further increase in crack width does not cause any further reduction in the confining force.

The loss in the rib profile also affects the ultimate bond strength. Initially an increase in the bond strength was noted with a loss of rib profile. However, sharp reduction in the ultimate bond strength for rib degradation was recorded. After about 43% loss in the rib profile, the bond strength does not vary significantly right up to 100% rib degradation. The cause for such a change in the ultimate bond strength with rib profile degradation can be explained as follows:

(1) Initially, in the precracking stage, the increase in the bond strength, in spite of some loss in the rib profile, can be attributed to the increase both in the reactionary confinement and the roughness of the bar in contact with concrete. The increase in bond strength, as a result of both of these factors, overshadows the reduction in the bond strength due to rib degradation.

(2) A sharp reduction in the ultimate bond strength for a reduction in the rib profile may be attributed to the formation of small corrosion cracks around the reinforcing bars and a significant reduction in the rib profile with resulting reduction in the interlocking action between ribs and concrete.

(3) The significant change in the bond strength due to the reduction in the rib profile in the range 43-100% indicates that the ribs are degraded to the extent that their interlocking action with the concrete becomes negligible. The confinement of the bar with the concrete is therefore significantly reduced. Thus, beyond this level of corrosion, further degradation of the ribs does not affect the bond strength to any noticeable extent.

Chapter 4
Finite Element Modeling

As discussed in Chapter 2, one of the phenomena as result of corrosion of steel bars in the concrete structures is cracking. In this chapter, an introduction to ATENA software is first presented. The progress of cracking due to corrosion is analyzed by the finite element method. Two finite element models, smeared crack model and discrete crack model, are introduced. The advantages and disadvantages of each model are discussed. The software ATENA is used in this research. It is based on the smeared crack model. Some basic concepts of smeared crack model are described. The formulation and analysis procedure of fracture analysis of concrete are studied. The SBETA material model is adopted in the research.

4.1 ATENA Program

Nonlinear finite element analysis of concrete and reinforced concrete structures has developed steadily in recent decades. The worldwide research effort led to the formulation of sound constitutive models as well as numerical techniques for their implementation in computer software. ATENA is such new generation software established on the basis of finite element (FE) software SBETA. It is targeted for the simulation of the real behavior of concrete and reinforced concrete structures.

The advantage of ATENA is that it can apply nonlinear finite element analysis in the practical engineering design. This program featuring nonlinear material models provides the analysis of entire structures, or structural members with very realistic material behavior, and a simulation of structural performance under real loading conditions and reflects current practice codes and standards.

Nonlinear finite element analysis can eliminate the inconsistency, which exists in the currently used design procedures between the internal force distributions determined from a linear elastic analysis and the section proportioning based on a nonlinear material behavior. The redistribution of internal forces due to a nonlinear material behavior is taken fully into account and a resulting stress and deformation state satisfies all three requirements of mechanics: equilibrium of forces, compatibility of deformations and material laws.

The constitutive model in SBETA covers all important features of concrete and reinforced concrete behavior. It is based on the concept of smeared cracks, damage and fracture mechanics discussed in Chapter 4. The smeared concept allows using the standard FE technique, known well from the linear elastic analysis. Furthermore, it extends to the nonlinear behavior in the pre-failure range including both material and geometrical nonlinearities. For this state prior to failure, SBETA uses a diffused damage concept.

The band crack theory is implemented in the software. The concrete failure in both, tension (cracking) and compression (crushing) causes discontinuities in the displacement fields, which are in basic disagreement with the assumptions of continuum mechanics. On the macro level concrete failure exhibits itself in the form of strain softening, and is of strongly localized nature. Therefore, the special techniques based on localization limiters in form of crack bands are used in order to handle properly the post-peak behavior of concrete within the finite element model.

Besides, the reinforcement is modeled in two ways, either as smeared one, or as discrete bar elements. The software provides efficient solution techniques, pre- and post-processing routines make it possible to monitor the structural behavior with all details. Large deformations, effects of temperature, shrinkage and prestressing can also be considered.

Although it can also deal with the three-dimensional material behavior, it is limited to the two-dimensional plane stress state in this research.

In summary, the ATENA program, which is determined for nonlinear finite element analysis of structures, provides all tools necessary for this investigation especially for computer simulation of concrete and reinforced concrete structure behavior.

4.2 Finite Element Modeling of Crack

The Finite Element Method has been proved to be an efficient method in structural analysis and broadly used in the current engineering practice and research work. One of application is to study the propagation of crack in the concrete structures. Due to the difference in the material properties between the concrete and steel, the finite element modeling for the fracture of concrete is more complex than that for metal.

4.2.1 Two Basic Models

Although there are lots of models available in the research paper, traditionally, the description of cracking and failure within finite element analysis of concrete has led to two fundamental different approaches: smeared crack model and discrete inter-element crack model. They represent two distinct viewpoints on the problem of modeling damage in quasi-brittle materials. In this section, two models are introduced and the advantages and disadvantages of each model are discussed. As more convenient in application, the smeared crack model is more popular than discrete crack model in the fracture analysis of concrete.

The discrete crack approach is the direct application of the type of material models. It uses discrete cracks that form between the elements shown in Figure 4.1 (a). Methods pertaining to discrete crack approach account for each crack individually in an explicit way in the FE mesh. After pioneering works in which cracks would be allowed to open between existing continuum elements according to a maximum stress criterion [Ngo and Scordelis, 1967;

Nilson, 1968], procedures for general crack propagation with remeshing based on linear elastic fracture mechanics (LEFM) were developed for concrete structures [Ingraffea, 1977; Saouma, 1981]. In this approach, elastic behavior is assumed everywhere in the structure except at the crack tip, where a stress singularity develops and energy is dissipated to propagate the crack. Soon, though, it was recognized that for quasi-brittle materials, a fracture process zone (FPZ) with dimensions related to the size of microstructural heterogeneities exists ahead of the crack tip, where material behavior is nonlinear and energy is dissipated. Except for very large structures where the size of the FPZ is negligible and LEFM is applicable, consideration of the FPZ turns out to be very important in quasi-brittle materials. In the fictitious crack model (FCM) [Hillerborg et al., 1976], the FPZ is represented by a fictitious extension of the crack beyond the tip, with normal opening related to the normal stress by a softening law enclosing an area G_f^I (fracture energy under Mode I). Although not strictly required [Carpinteri, 1989; Gopalaratnam and Ye, 1991], the most flexible implementation of the FCM in an FE context is achieved by using zero-thickness interface elements along the crack path [Bittencourt et al., 1992]. This in general requires remeshing when the crack propagates, although in some cases that can be avoided if crack path is known in advance (e.g., a three-point bending beam) or by introducing interface elements along all conceivable paths from the beginning of the analysis.

The counterpart of the discrete crack concept is the smeared crack concept, in which a cracked solid is imagined to be a continuum with the notion of stress and strain. It characterizes cracking as systems of parallel cracks continuously distributed over finite element as shown in Figure 4.1 (b). The behavior of cracked concrete can then be described in terms of stress-strain relations and it is sufficient to switch from the initial isotropic stress-strain relation to an orthotropic stress-strain relation upon cracking. As a consequence, the topology of the original finite element mesh remains preserved which is computationally convenient.

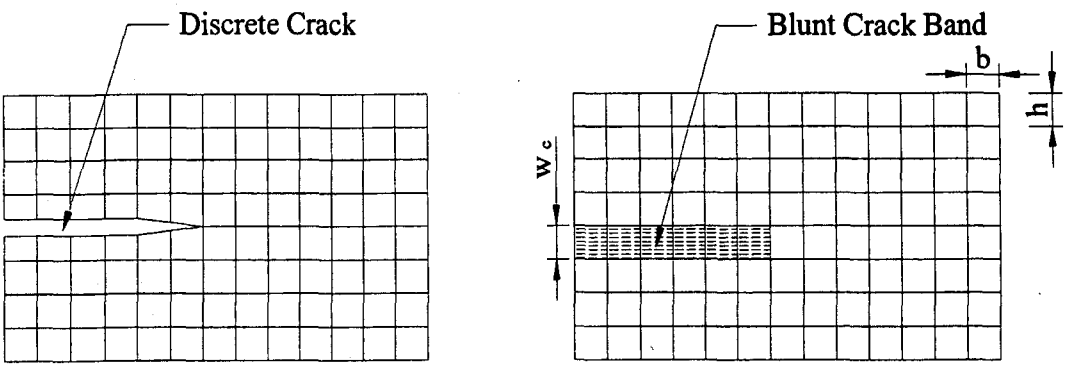

(a) (b)

Figure 4.1 Two Finite Element Models of Crack Analysis

The smeared crack approach, introduced by Rashid (1968), has become the most widely used approach in practice. The reasons may be given for adopting this approach:

1. The procedure is computationally convenient.
2. Distributed damage in general and densely distributed parallel cracks in particular are often observed in structures (measurements of the locations of sound emission sources provide evidence of a zone of distributed damage in front of a fracture).
3. At many size scales, a crack in concrete is not straight but highly tortuous, and such a crack may be adequately represented by a smeared crack bond.

However, there are serious problems with the classical smeared crack models. They are in principle nonobjective, since they can exhibit spurious mesh sensitivity [Bazant, 1976], i.e., the results may depend significantly on the choice of the mesh size (element size) by the analyst. Bazant (1983) modified this method, he proposed blunt cracked band model whose distinguishing characteristic is that no finite element is allowed to become smaller than a certain characteristic length w_c which is material property and is related to the size of inhomogeneity in the material. The cracked band theory solved the problems encountered in the previous application of smeared crack model such as exhibiting spurious mesh sensitivity

and convergence to an incorrect failure mode with zero energy dissipation in the stability analysis of strain softening and no size effect in the geometrically similar meshes, while test results for brittle failures of concrete structures as well as fracture specimens show a pronounced size effect. Extended to describe progressive cracking characterized by gradual strain softening, the crack band model was shown to agree with all of the basic experiment data from concrete or rock fracture testing.

Theoretically the discrete crack model is more suitable to capture the failure localization as it is directly based on the principles of fracture mechanics or the fractious crack concepts. However, since an adaptive re-meshing technique is required to account for phenomena such as progressive failure, the smeared crack model is more acceptable for engineering practice. In smeared crack model the cracking can be analyzed by modification of the material properties of the cracked elements. That means it is more easily incorporated in the current structural analysis software and no special software packages are needed.

The geometry of finite element is very important factor in the modeling of structures by finite element method. In the discrete crack model a node must be separated into two nodes to allow the crack to form, thus increasing the number of nodes, changing the topological connectivity of the mesh, and destroying the band structure of the structural stiffness matrix. Furthermore the discrete crack model is not easy in computation of no bias for the direction and unknown crack direction, since this may need re-mesh or refine the original mesh when the new crack direction does not closely coincides with existing element lines. Also it might be less realistic to achieve required objective, since no condition on minimum admissible crack spacing is used in this model.

As mentioned before, basically two models are equivalent for the reason that fracture propagation depends essentially on the flux of energy into the fracture process zone at the

crack front, and this flux is global characteristic of the entire structure, depending little on the detail stress and strain distributions near the fracture front. But since the smeared crack model is more efficient for computation in the finite element method, now the smeared crack model seems to retain the dominant role in the fracture analysis of concrete. In this research smeared crack model is used by the application of software ATENA.

4.2.2 Basic Concepts in Crack Modeling

4.2.2.1 Strain Softening

Strain softening is a phenomenon that within the fracture zone, stress decreases with increasing tensile strain. A widely used assumption is a triangular stress-strain diagram for uniaxial loading. Figure 4.2a shows a linear strain softening. ε_p is the strain at the peak stress (cracking initiation); and ε_o is the strain when the stress is reduced to zero (full cracking). Later various experimental evidences indicate that it is more realistic to assume a strain-softening curve with a steep initial decline followed by an extended tail. Figure 4.2b shows such exponential strain softening.

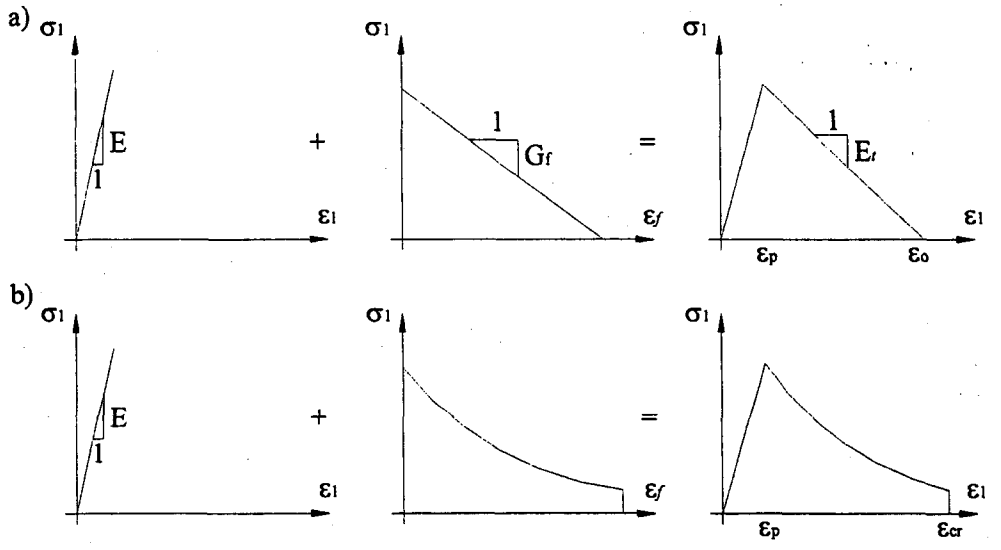

Figure 4.2 (a) Linear and (b) Exponential Strain Softening

4.2.2.2 Fracture Process Zone (Blunt Front Zone)

The fracture process zone representing that part of nonlinear zone in which the material undergoes progressive microcracking manifested by strain softening. It is usually small in ductile fracture of metals, but in concrete it is often very large (compared to the cross section of the structure), due to the large size of aggregate. In addition, since the plastic deformation of concrete in tension is negligible and a horizontal plateau does not precede strain softening in tensile test, the boundary of the fracture process zone may be considered to be nearly identical to the boundary of the nonlinear zone, whereas in metals these boundaries are far apart as demonstrated in Figure 4.3. Consequently, compared to fracture analysis of metals by J-integral, the energy of the crack band can be directly use in analysis the fracture. Thus the analysis can be carried out following the hypothesis that fracture in a heterogeneous material can be modeled as a band of parallel, density distributed microcracks within this blunt front zone.

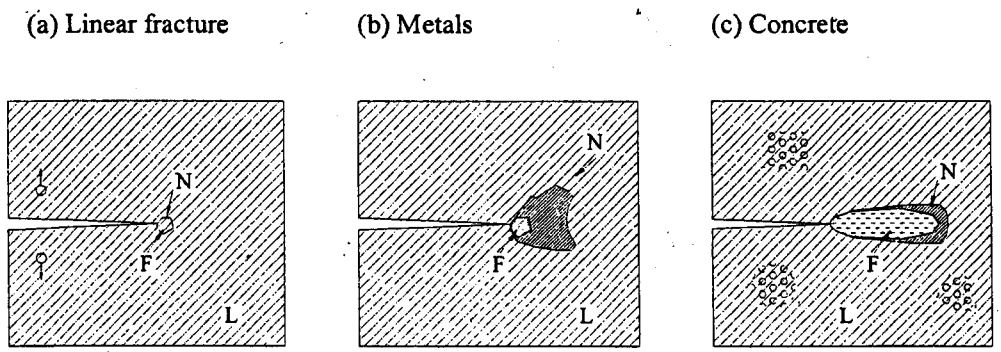

where F: Relative Sizes of Fracture Process Zone; N: Nonlinear Hardening Zone (N); L: Linear Zone (L)

Figure 4.3 The Difference in Fracture Process Zone between Metal and Concrete

Hillerborg, Modder and Peterson fracture mechanics model is one of the widely accepted fracture models as shown in Figure 4.4. It can be divided into three parts. The first part, the true crack, consists of an area which no stresses can be transmitted cross it. This area

experiences both displacement and stress discontinuity. The second part, the fracture process zone, is an area of microcracking. Stresses may still be transferred across the fracture process zone. This area experiences the displacement discontinuity but stress continuity. The last part is the intact material. This area extends from the tip of fracture process zone into concrete and is an undamaged area. The concrete tensile stress is equal to f_t' at the tip of the fracture process zone and decreases through the fracture process zone to become zero at the beginning of the true crack. The crack is assumed to propagate when stress at the tip of the fracture process zone equals f_t'.

The softening behavior of concrete and its relation to the fictitious crack model is also shown in Figure 4.4. Point W_2 begins zero stress area on the graph, and this corresponds to the tip of the true crack of the Hillerborg model. Since there is nothing bridging the true crack, stress can be transmitted across it, as shown by the zero stress value at point W_2 on the graph. The area between W_2 and W_1 corresponds to an area of cracking the fracture process zone where the crack is bridged by aggregate. Because of the aggregate bridging stresses may be transmitted cross the crack. This is shown by the slope between point W_2 and W_1 on the graph. For a given crack opening in the fracture process zone, there will be some stress transmitted. Above point W_1 on the graph, the slope of the line increases, this corresponds to the area of the fracture process zone where microcracking occurs. Since there is no true crack or any aggregate bridging in this area, the stresses can be transmitted across the area better than in the area of the fracture process zone with aggregate bridging. At the crack tip, the stress reaches f_t' and the crack opening is zero, which is the zero point on the graph and the beginning of intact material on the Hillerborg model. The area under the graph is equal to G_F, which is the fracture energy.

It should be note that the boundary of the fracture process zone should not be defined as the boundary of the visible microcracks but as the boundary of the strain-softening region. Since

the strain softening is caused not only by microcracking but also by any bond ruptures, the fracture process zone could be much wider (as well as longer) than the region of visible microcracks. The scatter for the microcracks relative to a smooth line for the macrocraks approximated by homogeneous continuum can be characterized as a microcrack band.

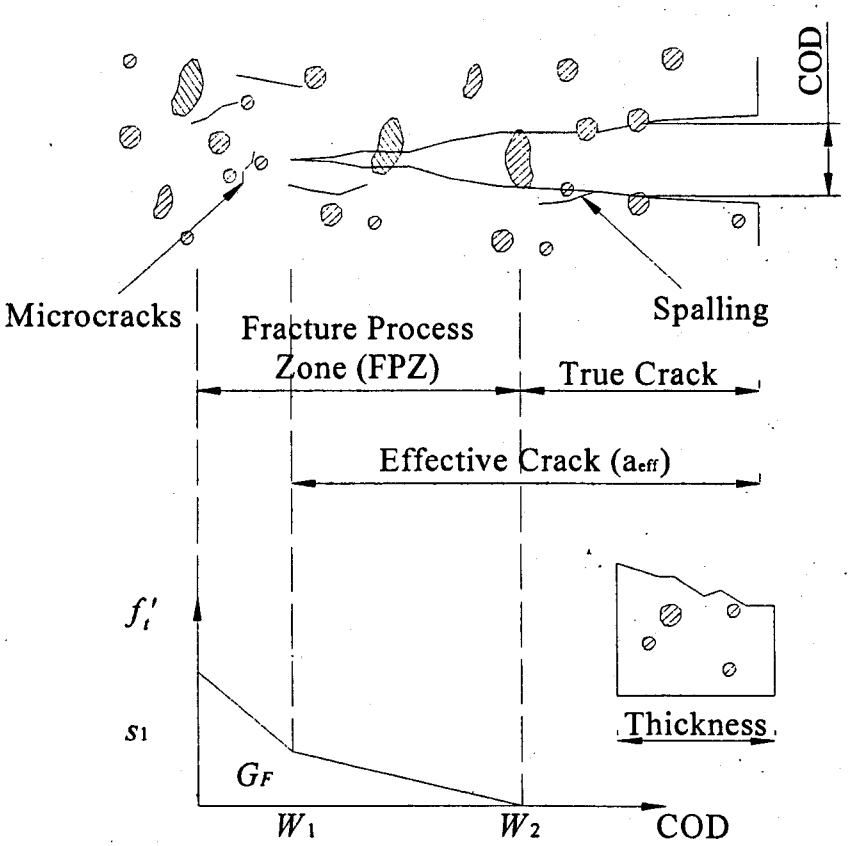

Figure 4.4 Hillerborg Model and Peterson Fracture Mechanics Model

4.2.2.3 Representative Volume

Concrete is a heterogeneous material, but when we analyze the concrete structure, it is approximated as an equivalent homogeneous continuum. The continuum stresses and strains called macrostresses and macrostrains are different with the actual stresses and strains in the microstructure called microstresses and microstrains. In the theory of randomly

inhomogeneous materials, the equivalent continuum stresses and strains are defined as the averages of the microstresses and microstrains over a certain representative volume. The cross section of this volume should be idealized to be much larger than the size of the in homogeneities, usually several times the maximum aggregate size for the concrete. That means the analysis result only reflect the average stress and accumulated strain over the cross section of the representative volume in the usual analysis (see Figure 4.5).

This criterion can also be applied in the finite element modeling. As the actual crack path is not smooth but highly tortuous that it passes around the hard aggregate pieces and randomly sways to the side of the straight path by distances roughly equal to the aggregate size and the actual stress (microstress) variation over such distances, we must try to control the width of the crack band to get the stresses and strains result for the homogeneous contiuum (macrostresses and macrostrains). Other effects such as the instability of strain-softening continuum and local strains also result in that the width of crack band or the minimum size of the finite element must be equal to several times the maximum aggregate size for the concrete in finite element analysis. Generally it is possible to assume $w_c \cong 3d_a$.

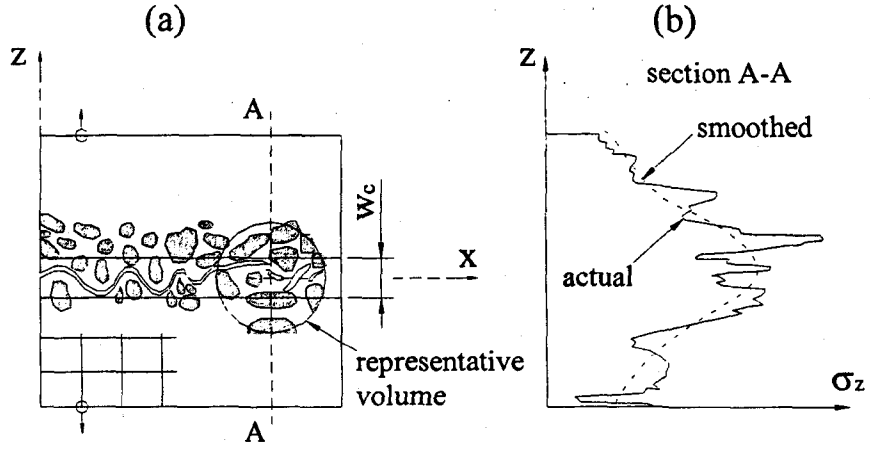

Figure 4.5 (a) Actual Crack Morphology, (b) Actual Stress and Then Smoothing

4.2.2.4 Fracture Energy

The fracture energy, G_f is the energy consumed in the formation and opening of all microcracks per unite area of plane (x, y). The progressive microcracking in the fracture process zone may be described by a triaxial stress-strain relation that exhibits strain softening with gradual reduction of the maximum principle stress σ_z to 0. The uniaxial special form of this stress-strain relation may be simply considered as a bilinear stress-strain diagram shown in Figure 4.6.

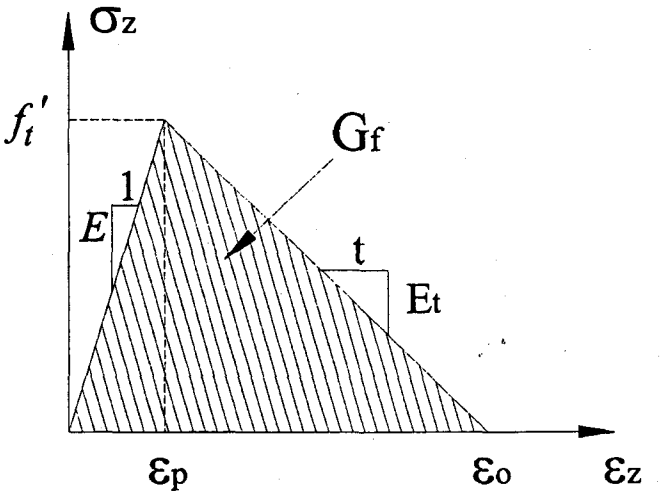

Figure 4.6 Bilinear Stress-Strain Relationships

Characterized by elastic modulus E_c, strength (peak stress) f_t', and strain softening modulus E_t, which is negative. Thus the fracture energy may be simply expressed as:

$$G_f = w_c\left(1-\frac{E_c}{E_t}\right)\frac{f_t'^2}{2E_c} \tag{4.1}$$

By analyzing numerous test data, it was shown that G_f may be predicted (with a coefficient of variation about 16%) from the empirical formula:

$$G_f = 0.0214(f_t'+127)f_t'^2 d_a / E_c \tag{4.2}$$

with E_c, f_t' in pounds per square inch. Substituting this formula into Eq. (4.1), E_t can be solved as a function of f_t', d_a, E_c, and w_c. Note that G_f is not the same as the apparent fracture energy determined on the basis of linear elastic fracture mechanics.

4.2.2.5 Element Size Effect and Element Orientation Effect

One of the fundamental problems in the prediction of fracture is structural size effect. As fracture theories are based on the tests which are normally conducted on relatively small specimens in the laboratory, while in practice the structures are often far larger than those specimens, so structural size effect must be considered to extrapolate the information of real structure.

In terms of the size effect, basically two types of theories may be distinguished:

(1) Strength theory (or the concept of failure surfaces), in which the failure criterions is expressed in terms of stresses (or strains), calculated according to theories of elasticity, plasticity or viscoplasticity.

(2) Linear or nonlinear fracture mechanics, in which failure criterion is expressed in terms of energy consumed per unit crack length increment.

The elastic finite element analysis is based on the strength criterion. But after the crack is formed, the stress is infinite at the tip of the crack and that causes incorrect prediction of crack extension at an infinitely small load even if refining the mesh has be done. For the

geometrically similar specimen or structural of various sizes, the strength criteria will result in same nominal failure stress indicated by a horizontal line in Figure 4.7 which doesn't agree with test results that nominal failure stress decreases with an increase in size.

In fracture mechanics, the basic criterion is that the released energy is needed to create the crack surface. According to the classical linear fracture mechanics, the nominal failure stress is proportion to $(size)^{-1/2}$, shown by the inclined line in Figure 4.7. However, with the exception of very large structures, this slope appears to be too steep in comparison with most existing data.

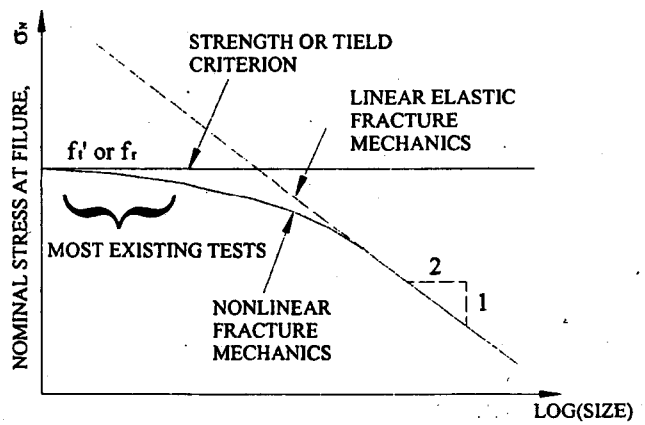

Figure 4.7 Size Effect According to Strength Criteria and Linear or Nonlinear Fracture Mechanics

Bazant and Oh (1983) proposed the crack band theory to remedy this deficiency in original smeared crack model for the size effect. He assumed the fracture process zone or crack band at the front of crack in the concrete has certain characteristic width, w_c. Usually it is about several times the maximum aggregate size for the concrete.

In the original smeared crack model, it may also meet element orientation problems such as: (1) In the case of zig-zag crack band propagation through the mesh, one needs to introduce

some mathematics artifices to prevent spurious locking of the rugged opposite sides of the crack band

(2) The mesh, typically a square mesh, inevitably introduces a certain degree of direction bias for the crack propagation, favoring propagation along the mesh lines or along the diagonals of the mesh, and suppressing propagation directions of small inclination with regard to the mesh line.

The element orientation effect problems can be solved by nonlocal continuum approach which is called localization limiter in ATENA. The nonlocal continuum is a continuum for which at least some variables are defined by spatial averaging. For the fracture analysis of concrete, nonlocal treatment should be applied only to those variables which cause strain softening, while the other variables, especially the elastic strain should be local. It means that the damage ω, which represents what is known in continuum damage mechanics as damage and may be regarded as the cracked area fraction, should be modeled nonlocal from the equation. This is accomplished by specifying it as a function of the average (nonlocal) strain, which is defined by spatial averaging. It can succeed in overcoming element orientation effect and also element size effect in the finite element analysis.

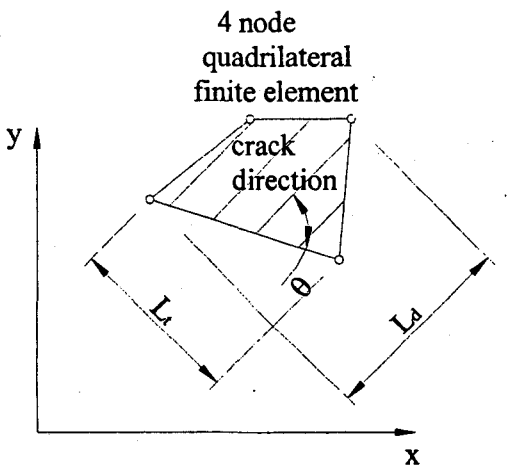

Figure 4.8 Definition of Localization Bands

For ATENA, Figure 4.8 shows the definition of localization bands. The direction of failure plane is assumed to be normal to the principle stresses in tension and compression, respectively. The failure bands (for tension L_t and for compression L_d) are defined as projections of the finite element dimensions on the failure planes.

The element orientation effect is reduced, by further increasing of the failure band for skew meshes, by the following formulas [Cervenka et al., 1995].

$$L_t' = \gamma \cdot L_t \tag{4.3}$$

$$L_d' = \gamma \cdot L_d \tag{4.4}$$

$$\gamma = 1 + (\gamma^{max} - 1) \cdot \frac{\theta}{45} \qquad \theta \in \langle 0;45 \rangle \tag{4.5}$$

An angle θ is the angle between the direction of the normal to the failure plane and the element side. In case of general quadrilateral element, it is an average angle. The above formula is a linear interpolation between the factor $\gamma = 1.0$ for the direction parallel with element sides, and $\gamma = \gamma^{max}$, for the direction inclined at 45^0, the recommended value of $\gamma^{max} = 1.5$.

The crack width is calculated as a total crack opening displacement within the crack band.

$$w = \varepsilon_{cr} \cdot L_t' = \varepsilon_{cr} \cdot \gamma \cdot L_t \tag{4.6}$$

where ε_{cr} is the crack opening strain, which is equal to the strain normal to the crack direction in the cracked state after the complete stress release, L_t is tension failure band and γ is a factor depending on the crack direction with respect to the element side orientation.

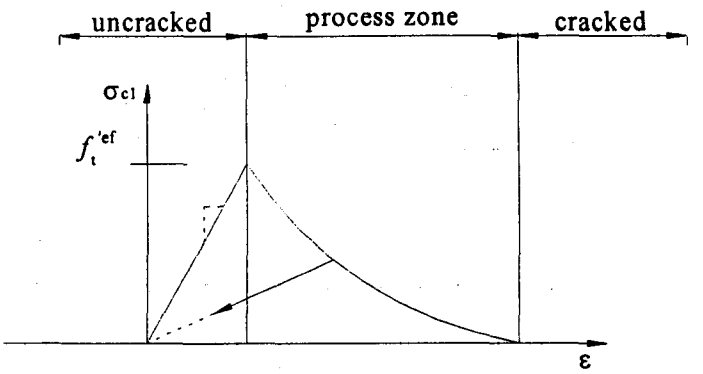

Figure 4.9 Stages of Crack Opening

4.3 Material Modeling – SBETA Material Model

The material properties of reinforcement concrete element are modeled based on the SBETA material model which is defined in the program ATENA. Both properties of concrete and steel bars are studied in this section. This material model is also used in the bond-slip analysis.

The name of material SEBETA means the abbreviation for the analysis of reinforced concrete in German language – StahlBETonAnalyse. The material model SBETA includes the following effects of concrete behavior.

(1) None-linear behavior in the compression including hardening and softening,

(2) Fracture of concrete in tension based on the nonlinear fracture mechanics

(3) Biaxial strength failure criterion

(4) Reduction of compression strength after cracking

(5) Tension stiffening effect

(6) Reduction of the shear stiffness after cracking (variable shear retention)

(7) Two crack model: fixed crack discretion and rotate crack direction

4.3.1 Stress-Strain Relations for Concrete

4.3.1.1 Equivalent Uniaxial Law

The nonlinear behavior of concrete in biaxial stress state is described by means of so called effective stress, σ_c^{ef}, and the equivalent uniaxial strain, ε^{eq} [Chen and Salrrb, 1982]. In this section the stress-strain relationships of concrete in the uniaxial condition is discussed.

The purpose of the introduction of effective stress and equivalent uniaxial strain is to eliminate the Poisson's effect in the plane stress state. The effective stress in most cases is a principal stress. It can be expressed as:

$$\varepsilon^{eq} = \frac{\sigma_{ci}}{E_{ci}} \tag{4.7}$$

where σ_{ci} is the stress in a unaxial test and E_{ci} is the modulus associated with the direction i. Within this assumption, the nonlinearity representing damage is caused only by the governing stress, σ_{ci}.

The complete equivalent uniaxial stress-strain diagram for concrete is shown in Figure 4.10. Unloading is a linear function to the origin. Thus, the relation between stress σ_c^{ef} and strain ε^{eq} is not unique and depends on the load history. A change from loading to unloading occurs, when the increment of the effective strain changes the sign. If subsequent reloading occurs the linear unloading path is followed until the last loading point, U, is reached again, then, the loading function is resumed.

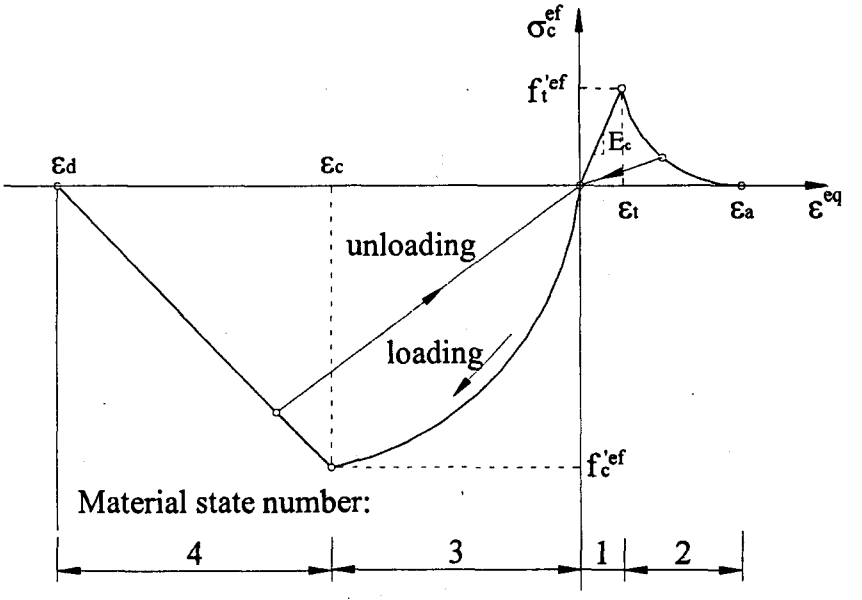

Figure 4.10 Uniaxial Stress-strain Law for Concrete

4.3.1.2 Stress-Strain Relations in Tension Condition

The behavior of concrete in tension without crack is assumed linear elastic. E_c is the initial elastic modulus of concrete, $f_t^{'ef}$ is the effective tensile strength derived from the biaxial failure function as shown below:

$$\sigma_c^{ef} = E_c \varepsilon^{eq}, 0 \le \sigma_c \le f_t^{'ef} \tag{4.8}$$

After crack opens in the concrete, strain-softening phenomenon is considered. Five softening models are available in SEBETA material model:

(1) Exponential cracking opening law

The function of crack opening was derived experimentally by Hordijk (1991).

$$\frac{\sigma}{f_t^{'ef}} = \{1 + (c_1 \frac{w}{w_c})^3\} \exp(-c_2 \frac{w}{w_c}) - \frac{w}{w_c}(1 + c_1^3) \exp(-c_2) \tag{4.9}$$

where w is the crack opening, w_c is the crack opening at the complete release of stress, σ is the normal stress in the crack (crack cohesion). It is that:

$$w_c = 5.14\frac{G_f}{f_t'^{ef}} \tag{4.10}$$

Values of constants are c_1=3, c_2=6.93. G_f is the fracture energy needed to create a unit area of stress-free crack, $f_t'^{ef}$ is the effective tensile strength derived from a fracture function. The crack opening displacement w is derived from strains according to the crack band theory in Eq. 4.6.

(2) Linear crack opening law

$$\frac{\sigma_c^{ef}}{f_t'^{ef}} = \frac{f_t'}{w_c}(w_c - w) \tag{4.11}$$

$$w_c = \frac{2G_f}{f_t'} \tag{4.12}$$

(3) Linear softening based on local strain

It is the descending branch of the stress-strain diagram defined by the c_3 corresponding to zero stress (complete release of stress).

(4) SFRC based on fracture energy

$$\text{Parameters: } c_1 = \frac{f_1}{f_t'^{ef}}, c_2 = \frac{f_2}{f_t'^{ef}}, w_c = \frac{2G_f}{f_1 + f_2} \tag{4.13}$$

(5) SFRC based on strain

$$\text{Parameters: } c_1 = \frac{f_1}{f_t'^{ef}}, c_2 = \frac{f_2}{f_t'^{ef}} \tag{4.14}$$

Parameters c_1 and c_2 are relative positions of stress levels, and c_3 is the end strain. In this research exponential crack opening law is used.

4.3.1.3 Stress-Strain Relations in Compression Condition

The stress-strain law in compression adopted in ATENA is CEB-FIP Model Code 90, Figure 4.11. It can be expressed as that:

$$\sigma_c^{ef} = f_c'^{ef} \frac{kx - x^2}{1 + (k-2)x}, x = \frac{\varepsilon}{\varepsilon_c}, k = \frac{E_o}{E_c} \tag{4.15}$$

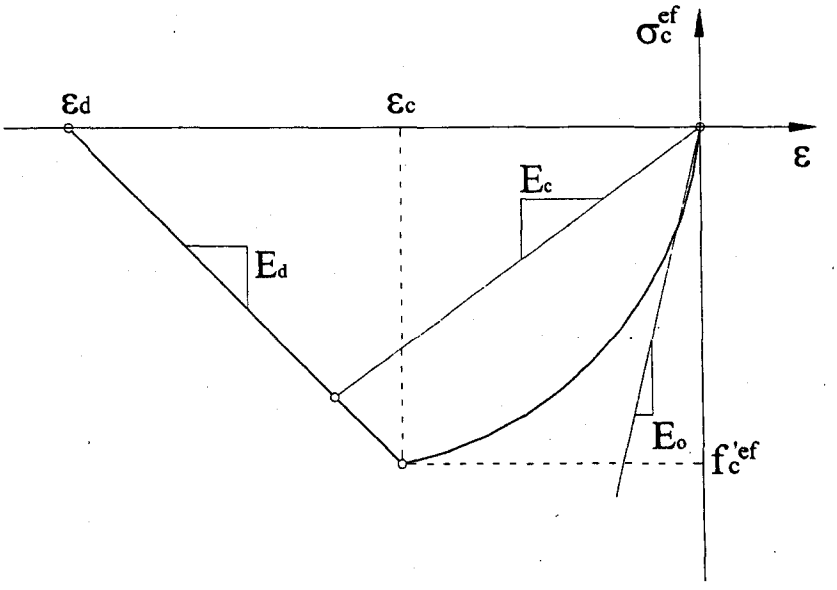

Figure 4.11 Compressive Stress-strain Diagram

where σ_c^{ef} : concrete compressive stress

$f_c^{'ef}$: Concrete effective compressive strength

x: normalized strain

ε : strain

ε_c :strain at peak stress $f_c^{'ef}$

k: shape parameter, k=1, linear

k=2, parabola.

E_o : initial elastic modulus

E_c : secant elastic modulus at peak stress, $E_c = \frac{f_c^{'ef}}{\varepsilon_c}$

The softening law in compression is linearly descending. Two models of strain softening in compression are available in ATENA: one based on dissipated energy, and other based on the local strain softening. In this research the later model is used. The stress-strain relation is shown in Figure 4.11, it assumes that compression failure is localized in a plane normal to the direction of compressive principal stress. All post-peak compressive displacements and energy dissipation are localized in this plane and are independent on the size of the structure. This hypothesis is supported by experiments conducted by Van Mier (1986). Two points define the slop of the softening part of the stress-strain: a peak of the diagram at the maximal stress and a limit compressive strain, ε_d, at the zero stress. This strain is calculated from a plastic displacement, w_d, and band size, $L_d^{'}$, according to the following expression:

$$\varepsilon_d = \varepsilon_c + \frac{w_d}{L_d^{'}} \tag{4.16}$$

w_d is equal to 0.5 mm for normal concrete. The advantage of this formulation is reduced depending on finite element mesh.

4.3.1.4 Biaxial Stress Failure Criterion of Concrete

The biaxial stress failure criterion used in ATENA is according to Kupfer et al. (1969) as shown in Figure 4.12. In the biaxial stress state, the strength of concrete is predicted under the assumption of a proportion stress path.

For the compressive failure, in the biaxial compressive stress state the failure function is:

$$f_c^{'ef} = \frac{1+3.65a}{(1+a)^2} f_c^{'} \tag{4.17}$$

$$a = \frac{\sigma_{c1}}{\sigma_{c2}} \tag{4.18}$$

where σ_{c1}, σ_{c2} are the principal stress in concrete and $f_c^{'}$ is the uniaxial cylinder strength. In the tension-compression state, the failure function continues linearly from the point $\sigma_{c1} = 0, \sigma_{c2} = f_c^{'}$ into the tension-compression region with the linear decreasing strength:

$$f_c^{'ef} = f_c^{'} r_{ec} \tag{4.19}$$

where r_{ec} is the reduction factor of the compressive strength in the principal direction 2 due to the tensile stress in the principle direction 1. It is determined by:

$$r_{ec} = (1+5.3278)\frac{\sigma_{c1}}{f_c^{'}} \text{ and } 1.0 \geq r_{ec} \geq 0.9.$$

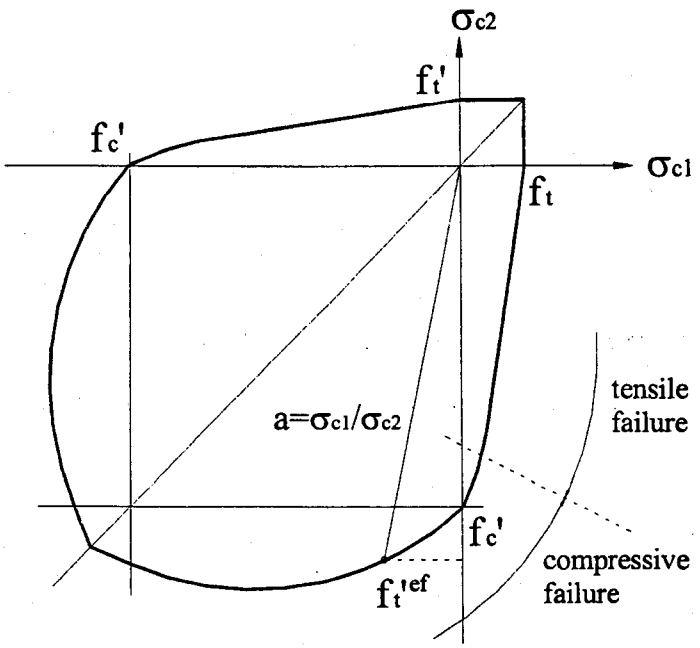

Figure 4.12 Biaxial Failure Function for Concrete

For the tensile failure, in the tension-tension state, the tensile strength is constant and equal to the unaxial tensile strength $f_t^{'}$. In the tension-compression state, the tensile strength is reduced by the relation:

$$f_t^{'ef} = f_t^{'} r_{et} \tag{4.20}$$

where r_{et} is the reduction factor of the tensile strength in the direction due to the compressive stress in the direction 2. The reduction function has one of the following forms (Figure 4.13).

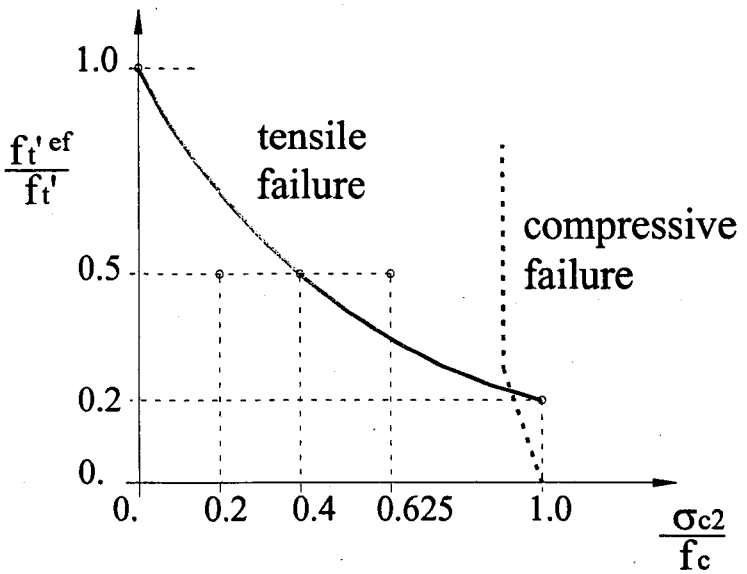

Figure 4.13 Tension-compression Failure Function for Concrete

$$r_{et} = (1 - 0.8)\frac{\sigma_{c2}}{f_c'} \tag{4.21}$$

$$\text{or} \quad r_{et} = \frac{A + (A-1)B}{AB}, B = Kx + A, x = \frac{\sigma_{c2}}{f_c'} \tag{4.22}$$

The relation in Eq. (4.21) is the linear decrease of the tensile strength and Eq. (4.22) is the hyperbolic decrease. In this research the point and parameters specified in above equation are:

Point		Parameter	
r	x	A	K
0.5	0.4	0.75	1.125

4.3.2 Shear Stress and stiffness in Cracked Concrete

For the smeared crack model, two options are available: the fixed crack model and the rotated crack model. In both models the crack is formed when the principal stress exceeds the

tensile strength. It is assumed that the cracks are uniformly distributed within the material volume. This is reflected in the constitutive model by an introduction of orthotropy.

In the fixed crack model the crack direction is given by the principal stress direction at the time of the crack initiation and will not change with the further loading. Figure 4.14 shows stress and strain state in fixed crack model. After cracking the weak material axis, m_1, is normal to the crack direction and strong axis, m_2, is parallel with the crack are fixed and will not rotate with principal strain axes ε_1 and ε_2. In the rotated crack model both principal strain and crack coordinate systems rotate with the increase of load as shown in Figure 4.15.

For fixed crack model, as two axes are not coincide, it results in a shear stress on the crack face demonstrated in Figure 4.14. The stress σ_{c1} and σ_{c2} are not principal stresses due to shear stress τ. The shear modulus is reduced with growing strain normal to the crack as shown in Figure 4.16.

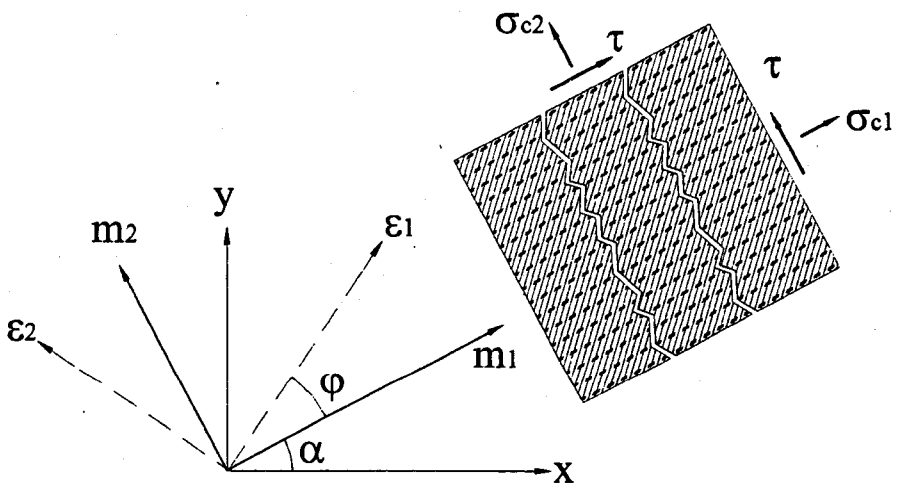

Figure 4.14 Stress and Strain State in Fixed Crack Model

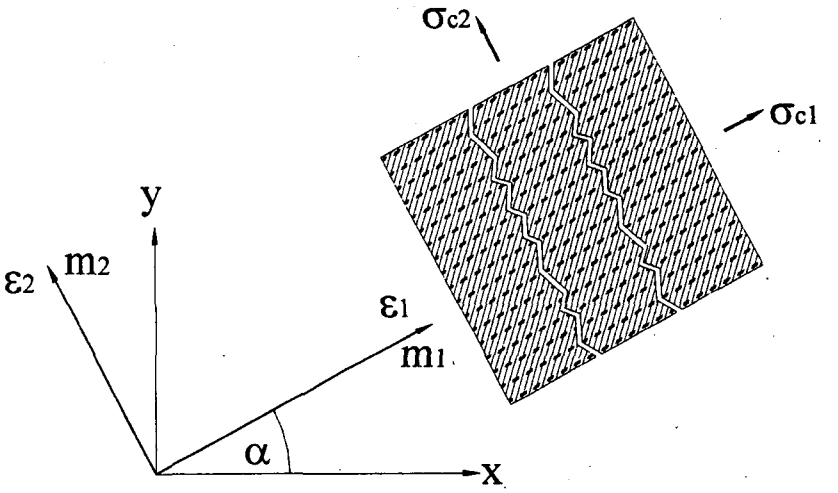

Figure 4.15 Stress and Strain in Rotated Crack Model

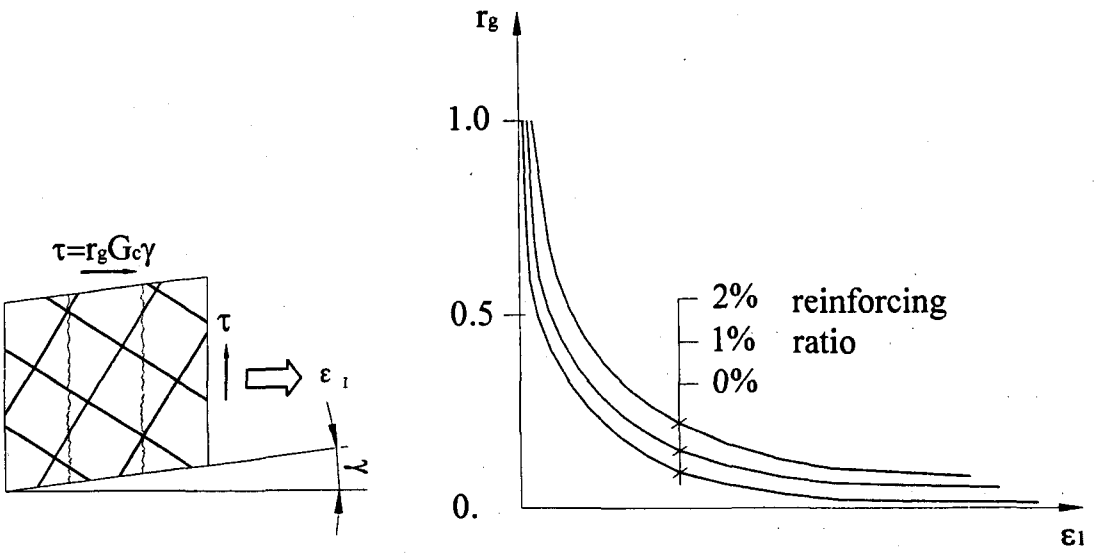

Figure 4.16 Shear Retention Factor

$$G = r_g G_c \tag{4.23}$$

$$r_g = c_3 \frac{-\ln\left(\frac{1000\varepsilon_u}{c_1}\right)}{c_2} G_c \tag{4.24}$$

$$c_1 = 7 + 333(p - 0.005), \quad c_2 = 10 - 167(p - 0.005), \quad 0 \le p \le 0.02 \tag{4.25}$$

$$G_c = \frac{E_c}{2(1+\nu)} \tag{4.26}$$

where r_g is the shear retention factor, G is the reduced shear modulus, G_c is the inertial concrete shear modulus, E_c is the initial elastic modulus and ν is the Poisson's ratio. The strain ε_u is normal to the crack direction (the crack opening strain), c_1 and c_2 are the parameters depending on the reinforcing crossing the crack direction, p is the transformed reinforcing ratio (all reinforcement is transformed on the crack plane) and c_3 is the scaling factor equal to 1 by default. In ATENA the effect of reinforcement ratio is not considered, thus p is assumed to be 0. In addition, the shear stress on the crack plane $\tau_{uv} = G\gamma$ is limited by the tensile strength f_t. The secant and tangent shear modulus of cracked concrete are equal.

For the rotated crack model, in order to ensure the co-axialilty of the principal strain axes with the material axes the tangent shear modulus G_t is calculated according to Crisfield and Wills (1989) as:

$$G_t = \frac{\sigma_{c1} - \sigma_{c2}}{2(\varepsilon_1 + \varepsilon_2)} \tag{4.27}$$

4.3.3 Reinforcement Properties

Two forms can model the reinforcement: discrete and smeared model. The discrete reinforcement is in form of reinforcing bars and is modeled by truss element. The smeared reinforcement is a component of composite material and can be considered either as a single (only one-constituent) material in the element under consideration or as one of the more such constituent.

The smeared reinforcement model is used to evaluate the stress in the cracks. Therefore it also includes a part of stress due to tension stiffening. The tension stiffening effect can be described as a contribution of cracked concrete to tensile stiffness of reinforcing bars. This stiffness is provided by the uncracked concrete or not fully opened crack and is generated by the strain localization process. It was verified by simulation experiments and published in paper [Margoldova et al., 1998]. It can be expressed as:

$$\sigma'_{scr} = \sigma'_{s} + \sigma_{ts} \tag{4.28}$$

Where σ'_{s} is the steel stress between the cracks (the steel stress in smeared reinforcement), σ'_{scr} is the steel stress in crack. For the discrete reinforcement model the $\sigma_{ts} = 0$ thus the steel stress is always equal to $\sigma'_{scr} = \sigma'_{s}$

The reinforcement in both forms, smeared and discrete, is in the uniaxial stress state in material model SBETA. The stress-stain relationship of reinforcement follows the multi-linear laws, which consists of four regions, the linear region (elastic), yield plateau, strain hardening and fracture. The multi-line can be defined by four points 1, 2, 3, 4 as shown in Figure 4.17. For simplicity the fracture is not considered in this research. Thus a trilinear curve was used for modeling stress-strain relationship of the reinforcement, which means that point 4 will equal to point 3.

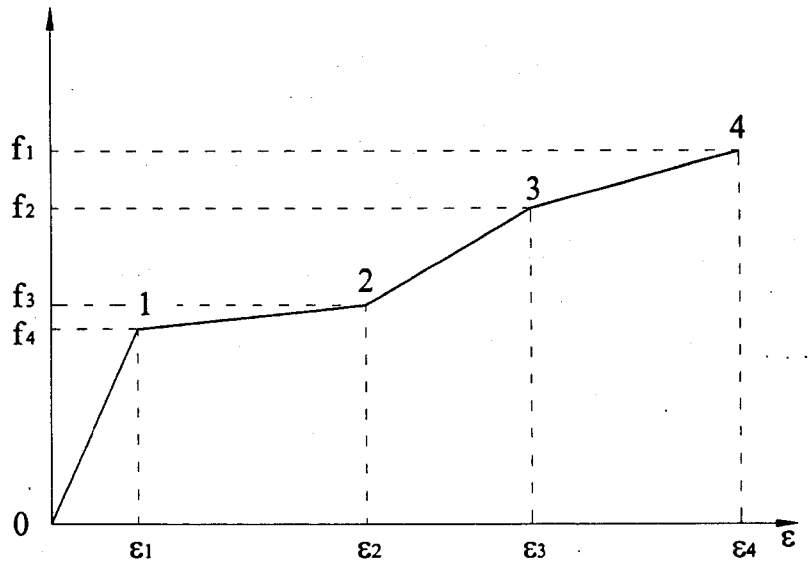

Figure 4.17 The Multi-linear Stress strain Law for Reinforcement

The equations for stress-strain relationship of reinforcement are:

$$f_s = E_s \cdot \varepsilon_s \qquad \text{For } \varepsilon_s < \varepsilon_1 \tag{4.29}$$

$$f_s = f_y \qquad \text{For } \varepsilon_1 < \varepsilon_s < \varepsilon_2 \tag{4.30}$$

$$f_s = f_y + E_{sh}(\varepsilon_s - \varepsilon_{sh}) < f_3 \qquad \text{For } \varepsilon_1 < \varepsilon_s < \varepsilon_2 \tag{4.31}$$

$$E_{sh} = \frac{f_3 - f_2}{\varepsilon_3 - \varepsilon_2} \tag{4.32}$$

where f_y is the yield strength of reinforcement; E_s is the Young's modulus of reinforcement; E_{sh} is the strain-hardening modulus; and ε_{sh} is the strain at the strain hardening.

In the smeared reinforcement model, two additional parameters, the reinforcing ratio p ($p = A_s / A_c$) and the direction angle, β, which is the angle between the local reinforcement

stress $\sigma_{si}^{'}$ and global coordinate, X, must be defined. (Figure 4.18) The spacing s of the smeared reinforcement is assumed infinitely small.

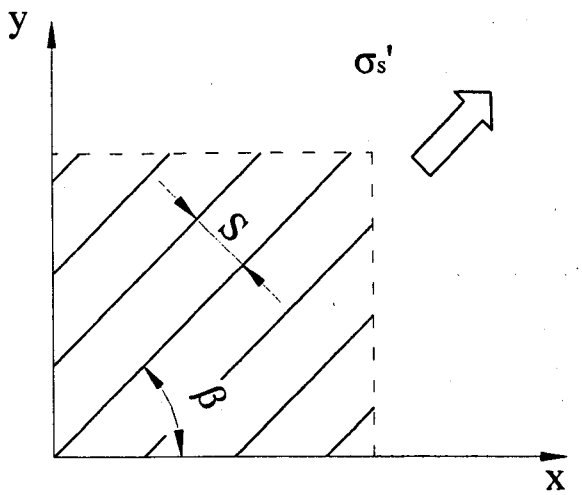

Figure 4.18 Smeared Reinforcement

4.4 Fracture Analysis by Finite Element Method

The formulation of constitutive relations considered in this research is in the plane stress state. A smeared approach is used to model the material properties, such as cracks or distributed reinforcement. This means that material properties defined for a material point are valid within a certain material volume, which in this case is associated with the entire finite element. The constitutive model is based on the stiffness and is described by the equation of equilibrium in a material point that:

$$s = De \tag{4.33}$$

$$s = \{\sigma_x, \sigma_y, \tau_{xy}\}^T, \quad e = \{\varepsilon_x, \varepsilon_y, \gamma_{xy}\}^T \tag{4.34}$$

where D is a material stiffness matrix, s is a stress vector $s = \{\sigma_x, \sigma_y, \tau_{xy}\}^T$, and e is a strain

vector $e = \{\varepsilon_x, \varepsilon_y, \gamma_{xy}\}^T$. The stress and strain vectors are composed of the stress components of the plane stress state σ_x, σ_y, τ_{xy}, as shown in Figure 4.19, and the strain components ε_x, ε_y, γ_{xy}, as shown in Figure 4.20, where γ_{xy} is the engineering shear strain.

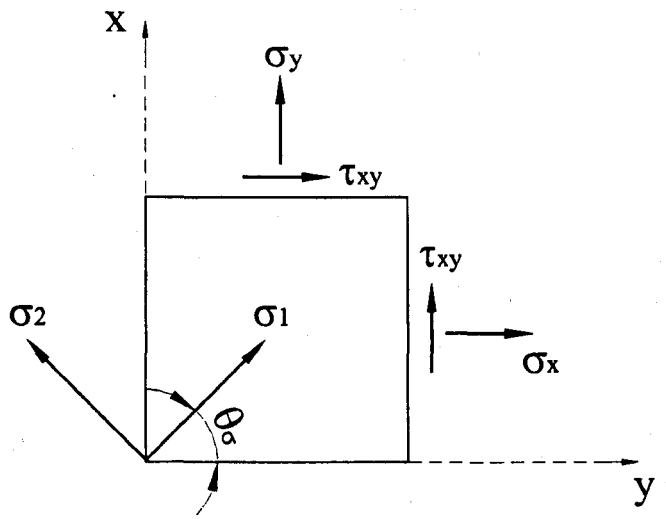

Figure 4.19 Components of Plane Stress State

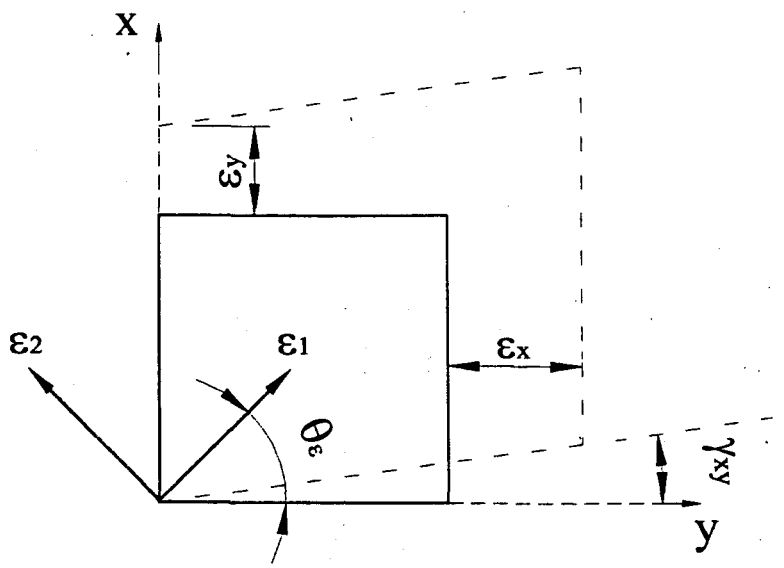

Figure 4.20 Components of Stain State

The stress vector s can be decomposed into the material components due to concrete and reinforcement as:

$$s = s_c + s_s \tag{4.35}$$

The concrete stress s_c is acting on the material area of concrete, which is approximately set equal to the cross section of the composite material $A_c \approx A$ (the area of concrete occupied by reinforcement is not subtracted). The stresses in concrete are obtained using the actual secant component material stiffness matrix

$$s_c = D_c^s e \tag{4.36}$$

D_c^s is the secant material stiffness matrix discussed below for the uncracked or cracked concrete depending on the material state. The reinforcement stress vector s_s is the sum of stresses of all the smeared reinforcement components.

The transformation of the stresses from local coordinate to global coordinate is that:

$$s_g = T_\sigma \cdot s_l \tag{4.37}$$

$$T_\varepsilon = \begin{bmatrix} \cos(\alpha)^2 & \sin(\alpha)^2 & 2\cos(\alpha)\sin(\alpha) \\ \sin(\alpha)^2 & \cos(\alpha)^2 & -2\cos(\alpha)\sin(\alpha) \\ -\cos(\alpha)\sin(\alpha) & \cos(\alpha)\sin(\alpha) & \cos(\alpha)^2 - \sin(\alpha)^2 \end{bmatrix} \tag{4.38}$$

where α is the angle between the local axes and global axes, the position direction is for the counterclockwise rotation.

The transformation of the strains:

$$e_g = T_\varepsilon \cdot e_l \tag{4.39}$$

$$T_\varepsilon = \begin{bmatrix} \cos(\alpha)^2 & \sin(\alpha)^2 & \cos(\alpha)\sin(\alpha) \\ \sin(\alpha)^2 & \cos(\alpha)^2 & -\cos(\alpha)\sin(\alpha) \\ -2\cos(\alpha)\sin(\alpha) & 2\cos(\alpha)\sin(\alpha) & \cos(\alpha)^2 - \sin(\alpha)^2 \end{bmatrix} \tag{4.40}$$

The angles of principal axes of stresses and strains Figure 4.19 and Figure 4.20 are found from the equations:

$$\tan(2\theta_\sigma) = \frac{2\tau_{xy}}{\sigma_x - \sigma_y} \tag{4.41}$$

$$\tan(2\theta_\varepsilon) = \frac{2\gamma_{xy}}{\varepsilon_x - \varepsilon_y} \tag{4.42}$$

where θ_σ is the angle of the first principal stress axis and θ_ε is the angle of the first principal strain axis.

The material stiffness matrix for the uncracked concrete has the form of an elastic matrix of the isotropic material. It is written in the global system x and y.

$$D_c = \frac{E_{ci}}{1-\nu^2}\begin{bmatrix} 1 & \nu & 0 \\ \nu & 1 & 0 \\ 0 & 0 & \frac{1-\nu}{2} \end{bmatrix} \tag{4.43}$$

In the above E is the concrete elastic modulus derived from the equivalent unaxial law. The Poisson's ratio, ν, is constant.

For the cracked concrete the matrix has the form of the elastic matrix for the orthotropic material. The matrix is formulated in a coordinate system m_1, m_2, Figure 4.14 and Figure 4.15, which is coincident with the crack direction. The local coordinate system is referred to the superscript L later. The direction 1 is normal to the crack and the direction 2 is parallel with the crack. The definition of the elastic constants for the orthotropic material in the plane stress state follows from the flexibility relation:

$$\begin{Bmatrix} \varepsilon_1 \\ \varepsilon_2 \\ \gamma \end{Bmatrix} = \begin{bmatrix} \frac{1}{E_1} & \frac{\nu_{21}}{E_2} & 0 \\ -\frac{\nu_{12}}{E_1} & \frac{1}{E_2} & 0 \\ 0 & 0 & \frac{1}{G} \end{bmatrix} \begin{Bmatrix} \sigma_1 \\ \sigma_2 \\ \tau \end{Bmatrix} \tag{4.44}$$

First we eliminate the orthotropic Poisson's ratios for the cracked concrete, because they are commonly not known. For this we use the symmetry relation $\nu_{12}E_2 = \nu_{21}E_1$. Therefore, in Eq. 4.44 there are only three independent elastic constants E_1, E_2, ν_{21}. Assuming that $\nu_{21} = \nu$ is the Poisson's ratio of the uncracked concrete and using the symmetry relation, we obtain:

$$\nu_{12} = \frac{E_1}{E_2}\nu \tag{4.45}$$

The stiffness matrix D_c^L is found as the inverse of the flexibility matrix in Eq. 4.45:

$$D_c^L = H\begin{bmatrix} \xi & \nu\xi & 0 \\ \nu\xi & 1 & 0 \\ 0 & 0 & G \end{bmatrix} \tag{4.46}$$

$$\xi = \frac{E_1}{E_2}, H = E_1(1-\xi v^2) \tag{4.47}$$

In the above relation E_2 must be nonzero. If E_2 is zero and E_1 is nonzero, then an alternative formulation is used with the inverse parameter $\frac{1}{\xi} = \frac{E_1}{E_2}$. In case that both elastic modules are zero, the matrix D_c^L is set equal to the null matrix.

The matrix D_c^L is transformed into the global coordinate system using the transformation matrix T_ε from: $D_c = T_\varepsilon^T D_c^L T_\varepsilon$ (4.48)

The angle α is between the global axis x and the 1st material axis m_1, which is normal to the crack, Figure 4.14. It is noted that the tangent material stiffness matrix is used to construct the element stiffness matrix.

The material stiffness matrix of the i^{th} smeared reinforcement is:

$$D_{si} = p_i E_{si} \begin{bmatrix} \cos(\beta_i)^4 & \cos(\beta_i)^2 \sin(\beta_i)^2 & \cos(\beta_i)^3 \sin(\beta_i) \\ \cos(\beta_i)^2 \sin(\beta_i)^2 & \sin(\beta_i)^4 & \cos(\beta_i)\sin(\beta_i)^3 \\ \cos(\beta_i)^3 \sin(\beta_i) & \cos(\beta_i)\sin(\beta_i)^3 & \cos(\beta_i)^2 \sin(\beta_i)^2 \end{bmatrix} \tag{4.49}$$

The angle β is between the global axis x and the i^{th} reinforcement direction, and E_{si} is the elastic modulus of reinforcement. The reinforcing ratio is $p_i = A_s / A_c$.

The total material stiffness of the reinforced concrete is the sum of material stiffness of concrete and smeared reinforcement:

$$D = D_c + \sum_{i=1}^{n} D_{si} \tag{4.50}$$

The summation is over n smeared reinforcing components. In ATENA the smeared reinforcement is not added on the constitutive level, but it is modeled by a separate layers of elements whose nodes are connected to those of the concrete elements.

4.5 Finite Element Analysis of Bond-Slip

Two basic approaches are used in the analysis of bond-slip model, microscopic and macroscopic analysis. The microscopic analysis is for the stress state in the neighborhood of the reinforcement [Gajer and Dux, 1990; Ingraffea et al., 1984]. The macroscopic analysis is for the global behavior of a member or a structural assemblage [Ngo and Scordels, 1967; Nilson, 1968; Keuser and Mehlhorn, 1987].

In micro-level, the stress transfer mechanism by bond is treated as the local contact in front of the bar ribs. The interface slip is due to crushing of concrete within limited zone in front of ribs, and can be derived from material properties and the configuration of the bars. Through the study of local concrete stress nearby the reinforcement, the initiation and propagation of internal cracks can be analyzed, both longitudinal splitting and cone-shape cracks, and thus the local bond stress versus the local slip relationship can be derived.

In a macro-level a relative slip displacement between reinforcement and concrete is directly modeled by one or two dimensional bond element using constitutive law derived from experimental data or the results of microscopic analysis. The stress state of the concrete nearby the reinforcement is simplified and not as realistic as that analyzed by the microscopic analysis. In current research the analysis is carried out in this level.

This "bond" strength is specified by so called cohesion stress in ATENA. The bond-slip element is denoted as CCBarWithBond. Typical reinforcement bar of this type is depicted in the Figure 4.21. Figure 4.21 shows undeformed and deformed shape of a segment of the bar. The original length, l_o, will change to l due to displacement, u, of the surrounding body and bar slips, δ.

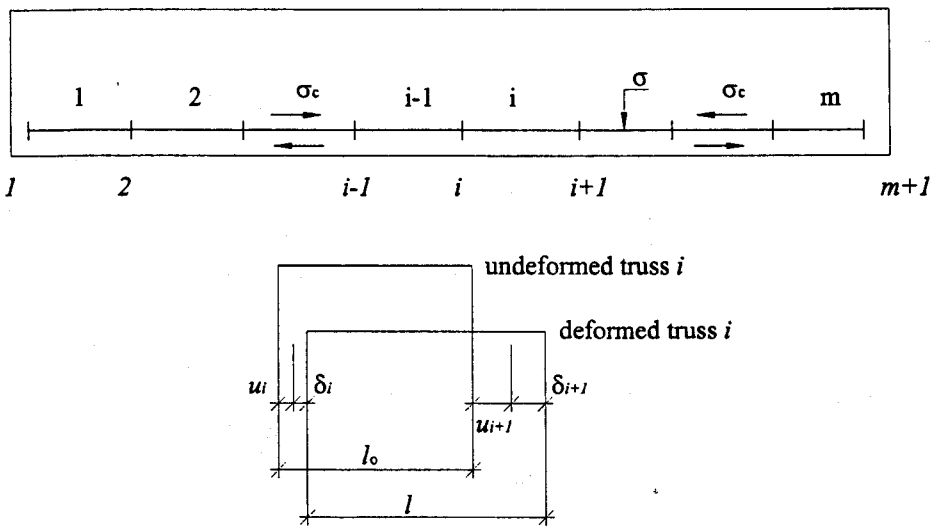

Figure 4.21 Reinforcement Bar with Slips

Normal stress at element i is calculated by:

$$\sigma_i = \frac{(u_{i+1} + \delta_{i+1} - u_i - \delta_i)}{l_i} E \tag{4.51}$$

Its derivative is compared with the cohesion stress. If the cohesion stress between the bar and the surrounding concrete is becoming too high, the bar will slip to reduce this stress. Otherwise, the slips will remain unchanged (or initially equal to zero), which correspond to the case of perfect bond. The cohesion stress can be constant or it can be defined as a

function of δ.

$$\sigma_c = \sigma_c(\delta) \tag{4.52}$$

The equilibrium condition for the reinforcing bar with prescribed bond yields:

$$\frac{\partial \sigma}{\partial x} \leq \sigma_c \frac{p}{A} \tag{4.53}$$

where σ is stress in the bar, x is local coordinate axis in direction of the bar and p and A are the perimeter and cross sectional area of the bar respectively.

Discretized form of Eq. (4.53) for node i reads (the bars are of constant strain type):

$$A(\sigma_i - \sigma_{i-1}) \leq \frac{l_i + l_{i-1}}{2} p\sigma_c \tag{4.54}$$

If the above equation is written for all nodes on the bar, we obtain a set of inequalities. It has to be solved in iterative manner (within each iteration of the main solution loop).

In order to obtain more realistic shape, the resulting cohesion stresses are smoothed prior their output. The smoothing operation for node i is expressed as follows:

$$\tilde{\sigma}_{right} = \frac{\sigma_{i+1} l_{i+1} + \sigma_i l_i}{l_{i+1} + l_i} \tag{4.55}$$

$$\tilde{\sigma}_{left} = \frac{\sigma_i l_i + \sigma_{i-1} l_{i-1}}{l_i + l_{i-1}} \tag{4.56}$$

$$\sigma_c = \frac{(\tilde{\sigma}_{right} - \tilde{\sigma}_{left})A}{pl_i} \tag{4.57}$$

The Eq. 4.51 together with Eq. 4.54 complete the element description. The element can be used to model realistically the cohesion between the reinforcing bars and concrete. Such a model is needed for analysis of pullout tests etc. Although the adopted solution is fairly simple, it provides reasonable results accuracy at low computation cost. A more elaborate model of cohesion between the reinforcing bars and the surrounding concrete can be achieved by using a special interface element that is described in the next chapter.

Chapter 5

Result of Finite Element Analysis

This chapter presents a practical corrosion analysis. The residual capacity of the corroded reinforcement was determined through the evaluation of the increase of steel volume and crack propagation. The final determination of the service life of concrete structures was made based on the above evaluation results. Finally, the volume expansion of corroded reinforcement bars is analyzed, and one example is presented to improve the understanding of such analysis.

A finite element analysis, using ATNEA software, was carried out to help clarify the influence of corrosion and bond behavior. The three different specimens used are corrosion expansion, pull-out, and beam specimen. Details of the three different specimens and their analytical results which investigated aspects of the bond behavior between the concrete and reinforcing steel are also presented. The specimens were considered from first cracking until failure.

5.1 Material Properties

The detailed material modeling for concrete and reinforcement steel is described in Chapter 4. In the three different specimens, the cube strength of concrete, $f_{cu}^{'}$, (nominal strength) is 30MPa. The corresponding parameters of concrete material are summarized in Table. 5.1. While The relative parameters of the uniaxial stress state of the reinforcing steel bars that was used in the three specimens are listed in Table 5.2.

Table 5.1 Properties of Concrete Material

Parameter	Data
Elastic modulus E	3.032×10^4MPa
Poisson ratio μ	0.2
Tensile strength f_t	2.317MPa
Compressive strength f_c	25.50MPa
Type of tension softening	Exponential
Fracture Energy G_f according to Vos (1983)	5.793×10^{-5}MPa
Compressive strain at compressive strength in the uniaxial compressive test ε_c	-1.682×10^{-3}
Reduction of compressive strength due to cracks	0.8
Type of compression softening	Crush band
Critical compressive displacement, w_d	-0.0005mm
Shear retention factor	Variable
Tension stiffening stress σ_n	0
Tension-compression function type	linear

Table 5.2 Properties of Reinforcement Steel

	Specimen I	Specimen II	Specimen III
Diameter (mm)	20	16	16
Yield strength f_y (MPa)	560	560	560
Elastic modulus (MPa)	2×10^5	2×10^5	2×10^5

5.2 Corrosion Analysis

5.2.1 Methods and Procedures

When a certain level of corrosion of reinforcement bars in the concrete elements is reached, structures are out of service which means the service life of structures is ended. Some repairs may be needed or even new structures must be built. In order to evaluate the intensity of the corrosion and its environment factors which effect the service-life of the structural members, two process must be studied. They are:

(1) The process of rust production and build up of corrosion product around the bar

(2) The propagation of cracks through the cover.

The corrosion damage analysis is consisted of several steps. The first one can be analyzed by the volume expansion of rust production with the time. The second can be calculated by width or/and length of crack in the concrete element at a determined time. After studying the intensity of the corrosion and crack, the residual development capacity of reinforcement anchorages can be evaluated by the stress analysis of bond slip in the concrete members. Finally, a decision that the structures are to be repaired or demolished will be made.

Cracking can often be found in the existing concrete structures. The causes of cracking are variable and have been studied extensively. One critical cracking in the concrete structures is due to the corrosion of reinforcement in concrete. When the reinforcement is corroded, corrosion products increase the volume of the reinforcement and hence generate tensile stress around it. Because concrete can endure less tensile stress than compressive stress, tensile cracks will appear. With the propagation of crack in concrete, the reinforcement bars are exposed to the environment as a result they are more venerable to the attack. It may accelerate the corrosion and consequently more new cracks appear. Figure 5.1 shows corrosion-cracking cycle. The detailed crack analysis is discussed in Chapter 4. Here only first process is studied.

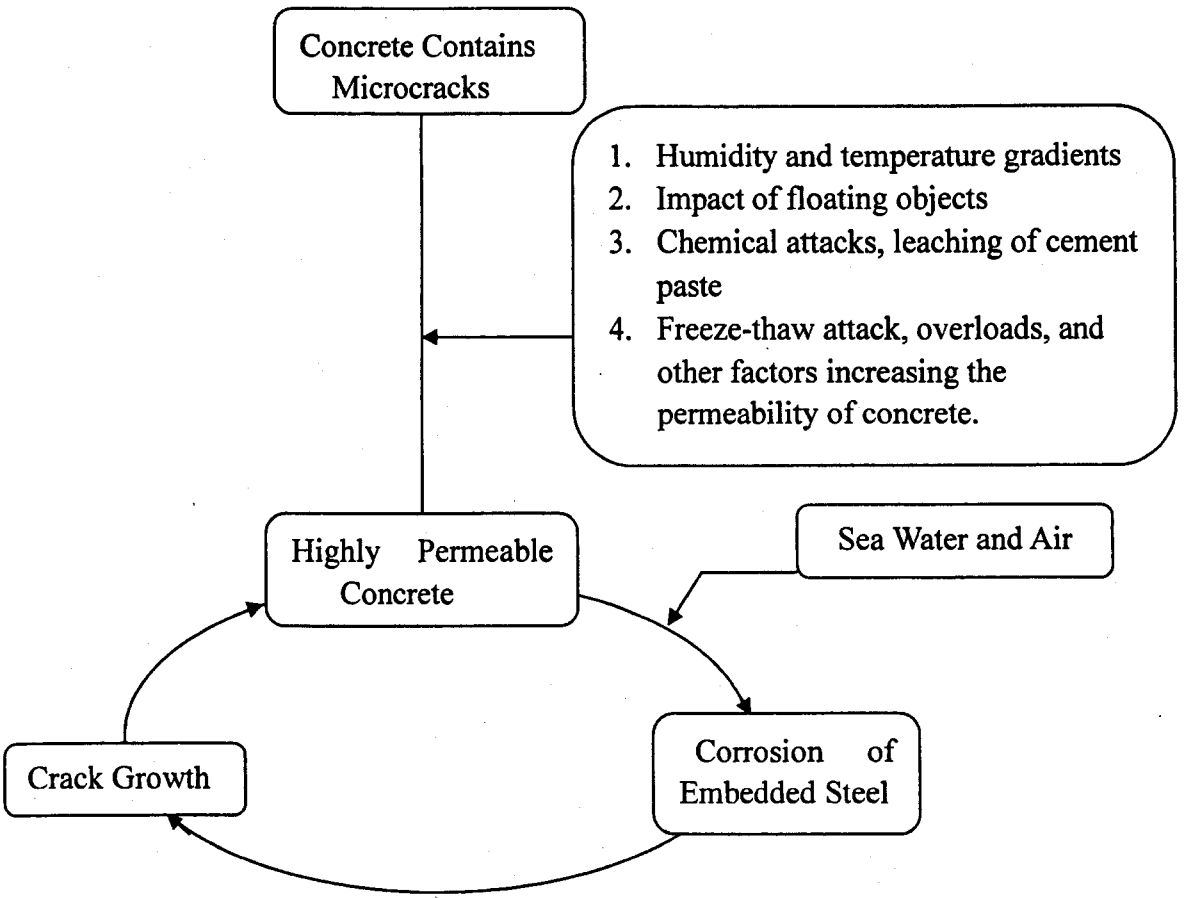

Figure 5.1 Diagrammatic Representation of the Cracking-Corrosion-Cracking Cycles in Concrete [Metha, 1993]

5.2.2 Volume Increase of the Corrosion Products

Depending on the level of oxidation, iron may expand by as much as six times its original volume, shown in Figure 2.5 [Liu and Weyers, 1998]. The actual volume increase depends on the fraction by which the various oxide forms in the corrosion products. Composition of rust cannot be credibly postulated because it depends largely on circumstantial factors such as the chloride concentration, oxygen supply and moisture. In modeling the mechanical effects of corrosion, the general practice is to represent the density of the rust product ρ_r as a fixed fraction of that of the iron consumed for the reaction; i.e., $\rho_r = \rho_s / v_{r/s}$, where ρ_s is the

density of the steel bars, $\nu_{r/s}$ is the steel rust density ratio and usually taken between 2 and 4 [Andrade et al., 1993; Liu and Weyers, 1998].

5.2.3 Mathematical Simulation of Corrosion

In this simulation, a constant rate of rust production is assumed. The mass of iron *Ms* consumed over time is related to the amount of current I_{corr} (A) that flows through the electrochemical corrosion cell (comprising anodic and cathodic bar areas and the pore solution through which ions are conducted). The process is prescribed by Faraday's law as below:

$$dMs/dt = I_{corr} A/(nF) \tag{5.1}$$

where A is the atomic weight of the ion being dissolved (for Fe, A=55.85 g/mol), and F is Faraday's constant F=96500 C/mol. Because little is known on the chemical composition of the product, the valency of the reaction n is empirically usually taken equal to 2, [A value of n =2 assumes that all the corrosion product is $Fe(OH)_2$] it follows that $dMs/dt = 2.893\times10^{-4} I_{corr}$. Integration of dMs/dt over time produces the total mass of iron consumed since initiation of corrosion, we have

$$\Delta M_s = 2.893\times10^{-4} I_{corr}\Delta t(g/m) = 2.893\times10^{-7} I_{corr}\Delta t \quad \text{(kg/m)} \tag{5.2a}$$

$$\Delta V_s = 3.6853\times10^{-11}\pi D_b i_{corr}\Delta t \quad (\text{m}^3/\text{m}) \tag{5.2b}$$

The total mass of rust produced at the anode is $Mr = Ms/\gamma_m$, with γ_m (the ratio of steel mass and rust mass) ranging between 0.523 and 0.622 [Liu and Weyers, 1998; Bazant, 1979]. For constant I_{corr}, Faraday's law implies a linear increase of the mass of rust with time.

To calculate the volume of rust produced at the anode, Andrade et al. (1993) established an empirical relationship between current density i_{corr} and the volume of steel consumed at the anode [i_{corr} is defined as the mean annual corrosion current per unit anodic surface area of steel (μ Acm^2)]. Thus, the reduced diameter $D_{rb}(t)$ of a reinforcing steel bar for a time period (years) $\Delta t = t - t_0$ (t_0 represents corrosion initiation time in years) is

$$D_{rb} = D_b - 0.023 i_{corr} \Delta t \tag{5.3}$$

Assuming that $D_b - D_{rb} << D_b$, the corresponding volume and mass of steel consumed per unit length of anodic bar is

$$\Delta V_s = \frac{0.023}{2} \pi D_b i_{corr} \Delta t \quad (\text{mm}^3/\text{mm}) \tag{5.4a}$$

$$\Delta M_s = 0.0902 \pi D_b i_{corr} \Delta t \times 10^{-3} \quad (\text{g/mm}) \tag{5.4b}$$

which, when converted to consistent units (D_b in meters, i_{corr} in amperes per square meters, and Δt in seconds), leads to

$$\Delta V_s = 3.6466 \times 10^{-11} \pi D_b i_{corr} \Delta t \quad (\text{m}^3/\text{m}) \tag{5.5a}$$

$$\Delta M_s = 2.862 \times 10^{-7} \pi D_b i_{corr} \Delta t \ (\text{kg/m}) \tag{5.5b}$$

Equation (5.5a) and (5.5b) conform with Faraday's law mentioned above with $I_{corr} = i_{corr} \pi d b l$.

Martin-Perez (1998) used early results by Bazant (1979) to describe the rate of production of hydrated red rust [$Fe(OH)_3$] per unit of anodic surface area in the bar, $Jr=dMr/dt$ [Jr (kg/m^2-s)=$5.536\times10^{-7}i_{corr}$, where i_{corr} is in amperes per square meters [Bazant, 1979]. The mass of hydrated red rust formed per unit length of rebar ΔMr is equal to $\pi D_b J_r \Delta t = 5.536\times10^{-7}\pi D_b \Delta t \cdot i_{corr}$ (kg/m), where $\Delta t = t - t_0$ is the duration of ongoing corrosion since initiation (unit is second, s). The mass of steel consumed for reaction per unit length of rebar ΔMs required to produce ΔMr is $\Delta Ms=0.523\Delta Mr$. The volume of steel consumed is obtained from the ratio of mass per density. Thus, conforming again with Faraday's law and Eq.(5.5).

$$\Delta M_s = 2.895\times10^{-7}\pi D_b i_{corr}\Delta t \quad \text{(kg/m)} \tag{5.6a}$$

$$\Delta V_s = 3.68\times10^{-11}\pi D_b i_{corr}\Delta t \quad \text{(m}^3\text{/m)} \tag{5.6b}$$

where i_{corr} is in amperes per square meters, D_b is in meters, and Δt is in seconds.

Assuming uniform corrosion on the bar surface, the bar diameter is reduced, because of iron depletion, to R_{rb}. If the volume reduction of steel per unit length of bar ΔVs is known [estimated from current density by Eqs (5.4) to (5.6)] then

$$R_{rb} = (R_b^{\,2} - \Delta V_s/\pi)^{1/2} \tag{5.7}$$

The oxide layer thickness that builds up around the bar is denoted as t_r. The effective radius of the internal boundary is $R_r = R_{rb} + t_r$. If the volume of oxide generated is $\Delta V_r = \Delta V_s \rho_s/(\rho_r \gamma_m)$, then t_r may be estimated from Figure 5.2.

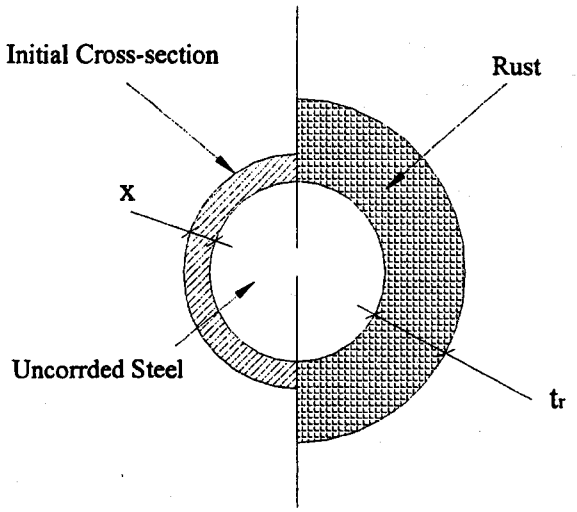

Corrosion penetration: x

Volume rust / volume steel: ν

Oxide layer thickness around the uncorroded bar: t_r

Figure 5.2 Physical Interpretation of the Variables in the Corrosion Model

$$\Delta V_r = \pi(R_r^{\,2} - R_{rb}^{\,2}) = \pi(t_r^{\,2} + 2R_{rb}t_r) = \pi t_r(2R_{rb} + t_r) \tag{5.8}$$

hence,

$$t_r = \sqrt{R_{rb}^{\,2} + \frac{\Delta V_r}{\pi}} - R_{rb} \tag{5.9}$$

Therefore, stress is generated as the inner boundary of the cover layer is forced to undergo the prescribed radial displacement

$$u_{r=R_b} = R_r - R_b \tag{5.10}$$

with the controlling variable being the volume of accumulated rust product on the bar perimeter $\Delta V_r = \alpha \Delta V_s$, where $\alpha = \rho_s / (\rho_r \gamma_m)$. (5.11)

5.2.4 Example

A 20 mm reinforcement bar is in the corrosion process. Determine the steel attack penetration, increase of radiometer of steel volume. Assuming that R_b=10 mm, $\gamma_m = 0.523$ and $\nu_{r/s} = 2$. From Eq. 2.38, we can get

$$\alpha = \frac{\Delta V_r}{\Delta V_s} = \frac{\rho_s}{\rho_r \gamma_m} = \frac{\rho_s}{\frac{\rho_s}{\nu_{r/s}}\gamma_m} = \frac{\nu_{r/s}}{\gamma_m} = \frac{2}{0.523} = 3.824 \quad \text{and} \quad \Delta V_r = 3.824 \Delta V_s$$

$$R_r = R_{rb} + t_r = R_{rb} + (\sqrt{R_{rb}^2 + \frac{\Delta V_r}{\pi}} - R_{rb}) = \sqrt{R_{rb}^2 + \frac{\Delta V_r}{\pi}}$$

$$= \sqrt{(R_b^2 - \frac{\Delta V_s}{\pi}) + \frac{\Delta V_r}{\pi}} = \sqrt{R_b^2 + \frac{2.824}{\pi}\Delta V_s}$$

$$= \sqrt{R_b^2 + \frac{2.824}{\pi} \times 3.6853 \times 10^{-11} \pi D_b i_{corr} \Delta t}$$

$$= \sqrt{R_b^2 + 2.08 \times 10^{-10} R_b i_{corr} \Delta t}$$

Assuming i_{corr}=1 μ A/cm^2=10^{-2} A/m^2.

Inputting in

R_b = 10mm = 10x10^{-3}m and

Δt = 1year = 8 6400s/dx365d = 3.1536x10^{7}s

in $u_r = R_b = R_r$-R_b,

We get the result shown in Table 5.3.

Table 5.3 Corrosion Penetration Calculation Results

Time (years)	i_{corr} (A/m^2)	Corrosion Penetration x (mm)	Radial Displacement at the Hole (mm)
1	10^{-2}	0.0116	0.0327
2	10^{-2}	0.0232	0.0654
3	10^{-2}	0.0349	0.0979
4	10^{-2}	0.0465	0.1303
5	10^{-2}	0.0582	0.1627
6	10^{-2}	0.0698	0.1949
7	10^{-2}	0.0815	0.2270
8	10^{-2}	0.0932	0.2590
9	10^{-2}	0.1050	0.2909
10	10^{-2}	0.1167	0.3228

5.3 Two-Dimensional Corrosion-Cracking Analysis Example (Specimen I)

Chapter 2 investigated the increase in the volume of reinforcement due to the corrosion. As mentioned earlier, such increase in volume results in radial pressure around the surface of concrete and the reinforcing steel. When the corrosion reaches a high level, spalling and cracking will occur in the concrete nearby the reinforcement. In this section, a finite element method will be used to study this crack propagation due to corrosion products expansion. The calculation of corrosion attack penetration and the increase of diameter of the steel bar due to the corrosion is demonstrated in section 5.2.

In the test, a specimen with a concentrically embedded reinforcing bar was 100x100x200 mm, as shown in Figure 5.3. Here, a slice (section A-A) of it was analyzed, corresponding with a plane strain assumption. A smeared crack model was used in this test. The bar is processing corrosion which creates uniform corrosion products around its surface. The corrosion rate is constant during the whole procedure. The load of corrosion is applied by the radial displacement around the surface of concrete and bar. There are 10 steps of analysis in which each of them represents a one-year of corrosion. The applied load history is obtained from section 5.2 and summarized in Table 5.4.

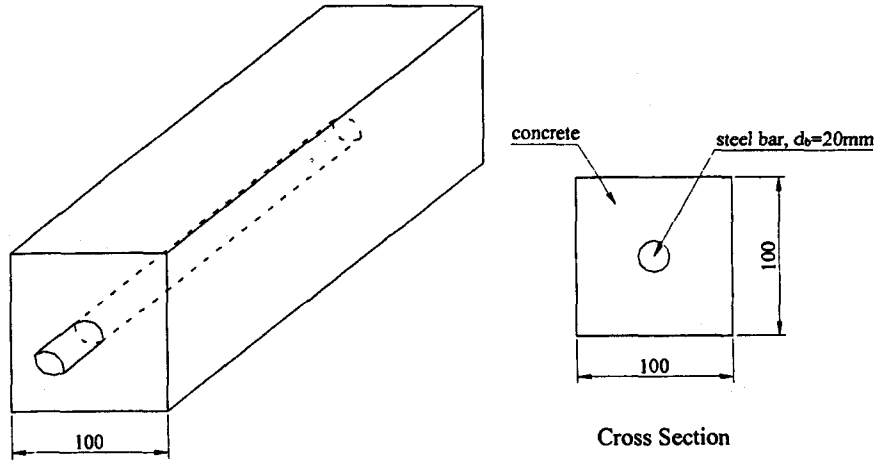

Figure 5.3 Specimen for Corrosion Crack Analysis (Specimen I)

The type of finite element used in the analysis is CCIsoQuad element. The geometry of this kind element is shown in Figure 5.4. The finite element mesh type is quadrilateral, and the element size is 0.01m. Due to the limitation of element numbers in the software, the reinforcement is approximated by a hexagon. But the cracking progress will not have significant difference with that of circular. The boundary condition is to hinge the cross section at the four corners.

Table 5.4 Applied load (Displacement) due to Corrosion and the Crack Width

Time (years)	Radial Displacement (mm)	Accumulate Displacement (mm)	Max. Crack width (mm)
1	0.0327	0.0327	0.1372
2	0.0327	0.0654	0.2419
3	0.0325	0.0979	0.3466
4	0.0324	0.1303	0.4516
5	0.0324	0.1627	0.5594
6	0.0322	0.1949	0.6429
7	0.0321	0.2270	0.7416
8	0.0320	0.2590	0.8045
9	0.0319	0.2909	0.8702
10	0.0319	0.3228	0.9598

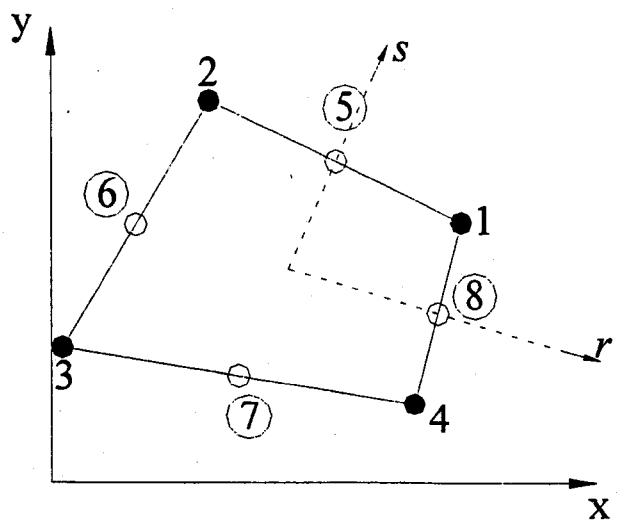

Figure 5.4 Geometry of CCIsoQuad Element

Chapter 5
Corrosion Cracking Analysis
Step 1

Scalars:iso-areas, Basic material, in nodes, Engineering Strain, Eps xx, <-9.519E-04;1.316E-03>[None]
Cracks: in elements, openning: <1.059E-08;9.642E-05>[m], Sigma_n: <1.407E-01;2.287E+00>[MPa], Sigma_T□: <0.000E+00;0.000E+00>

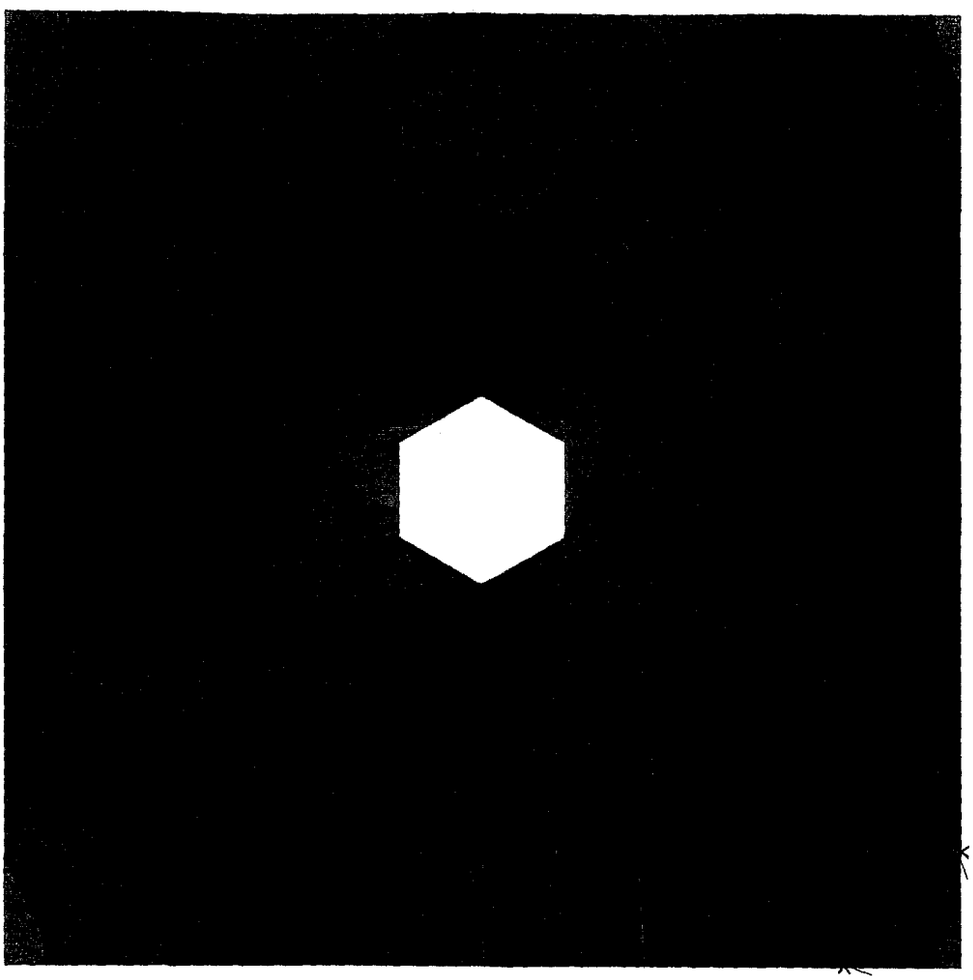

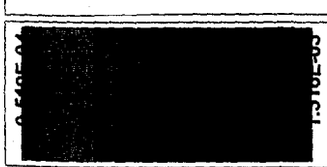

Figure 5.5 Corrosion Crack Analysis -Step 1

Chapter 5
Corrosion Cracking Analysis
Step 2

Scalars:iso-areas, Basic material, in nodes, Engineering Strain, Eps xx, <-1.952E-03;3.799E-03>[None]
Cracks: in elements, openning: <1.062E-07;1.719E-04>[m], Sigma_n: <1.811E-02;2.239E+00>[MPa], Sigma_T□: <-9.748E-01;5.475E-01>

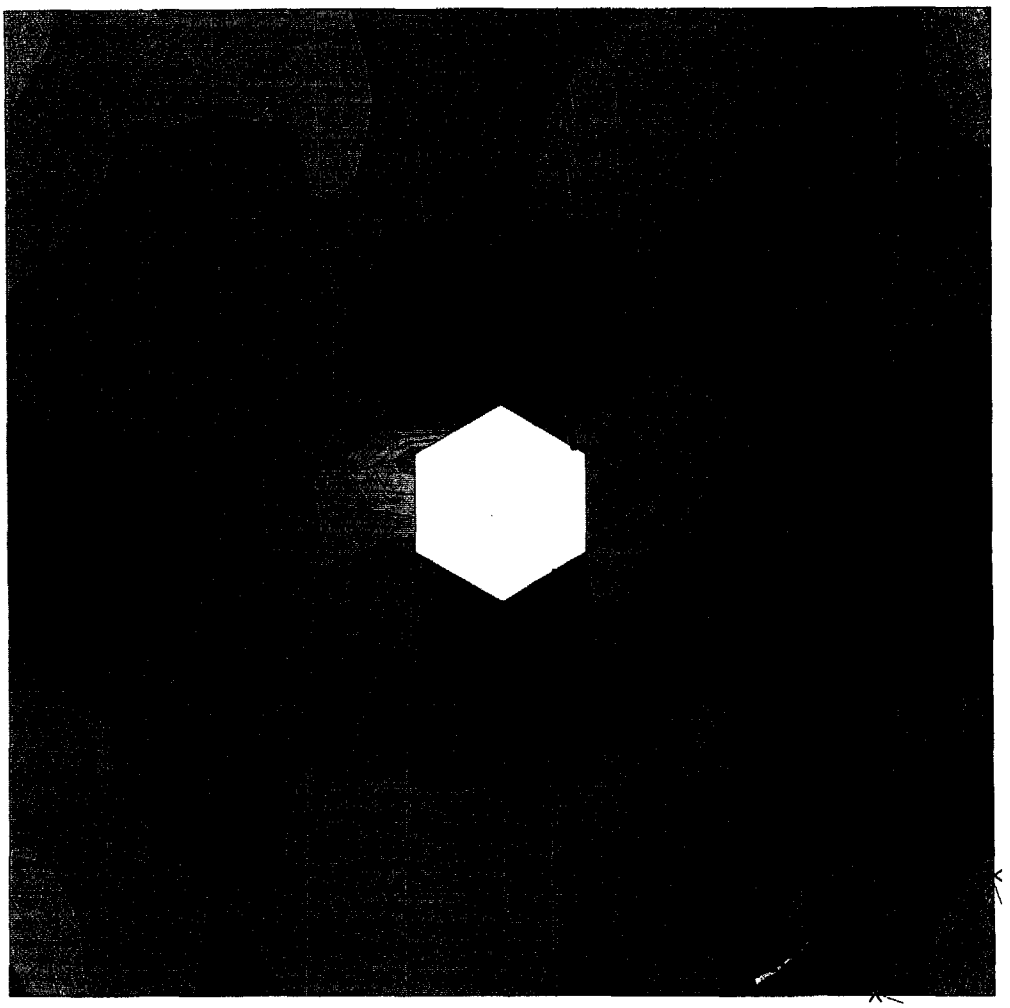

Figure 5.6 Corrosion Crack Analysis -Step 2

Scalars:iso-areas, Basic material, in nodes, Engineering Strain, Eps xx, <-4.785E-03;8.770E-03>[None]
Cracks: in elements, openning: <1.034E-07;3.477E-04>[m], Sigma_n: <0.000E+00;2.237E+00>[MPa], Sigma_T□: <-1.314E+00;1.703E+00

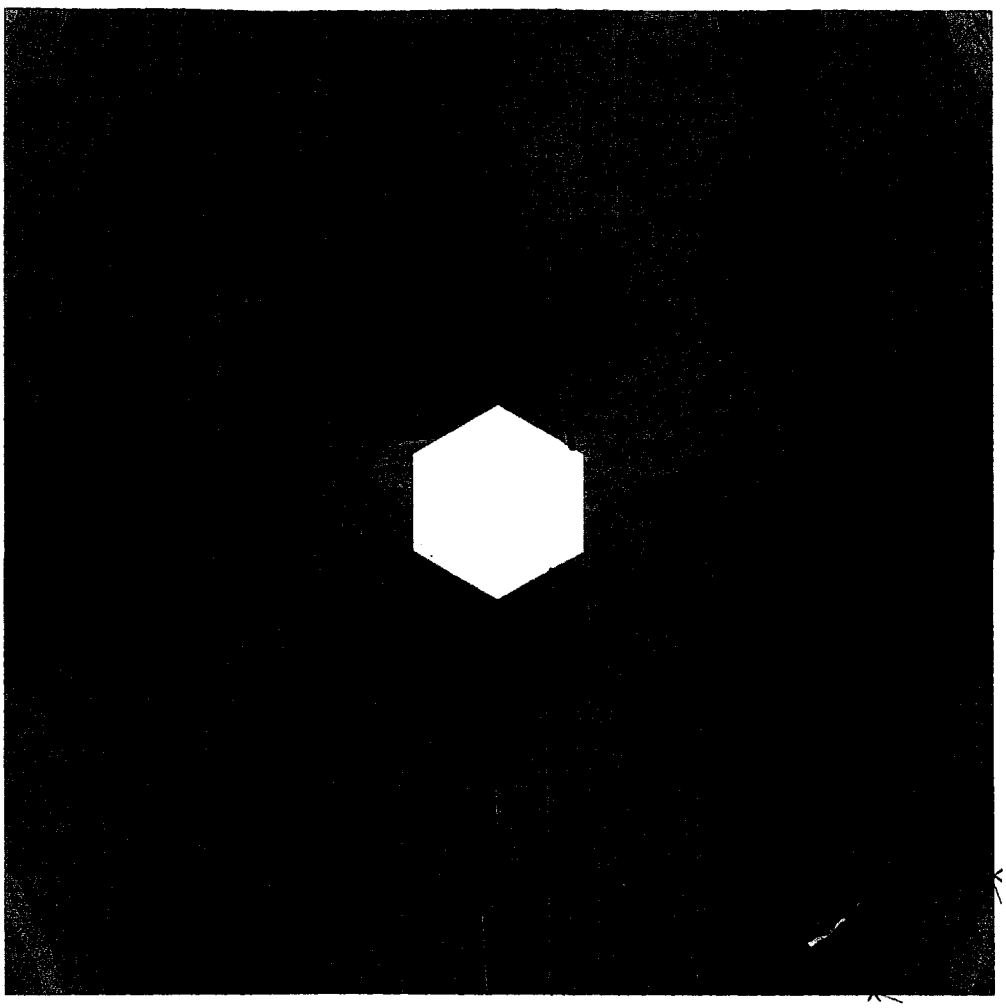

Figure 5.7 Corrosion Crack Analysis -Step 4

Scalars:iso-areas, Basic material, in nodes, Engineering Strain, Eps xx, <-8.782E-03;1.369E-02>[None]
Cracks: in elements, openning: <8.607E-08;5.022E-04>[m], Sigma_n: <-1.261E-01;2.239E+00>[MPa], Sigma_T□: <-1.742E+00;2.317E+0

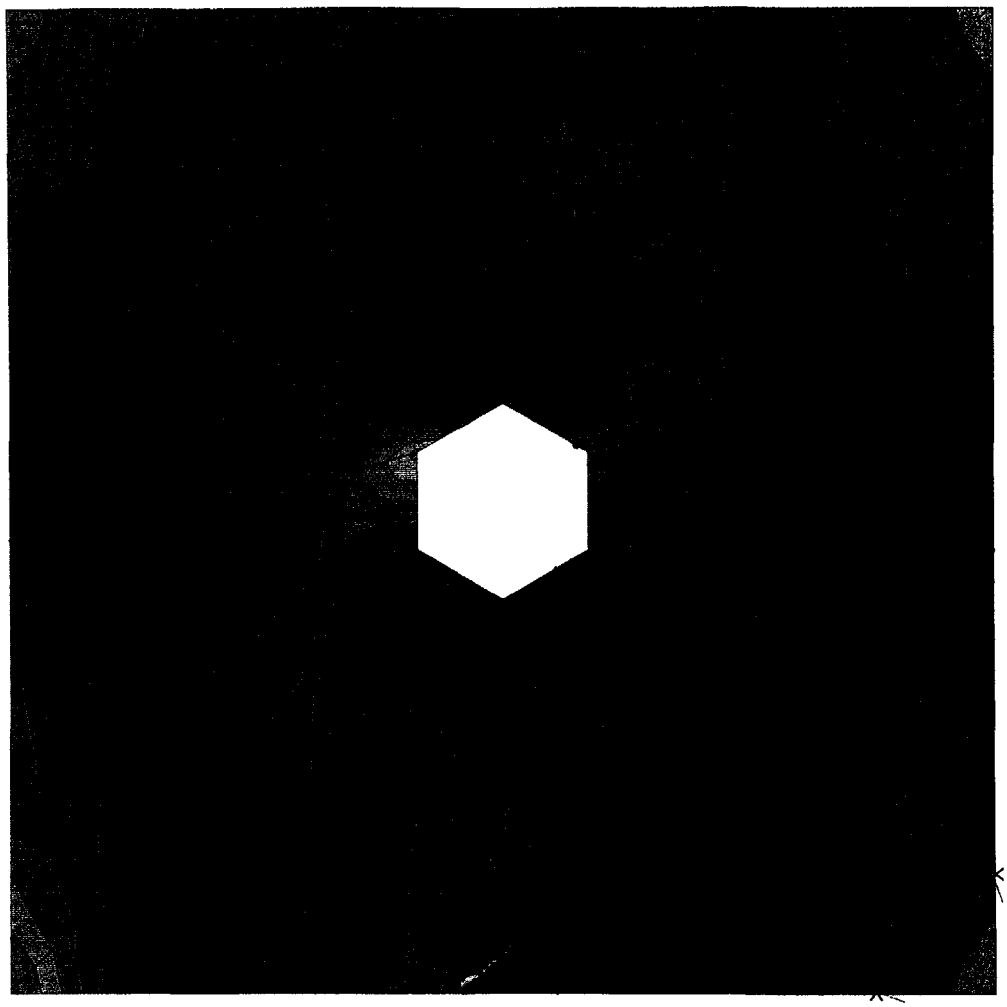

Figure 5.8 Corrosion Crack Analysis -Step 6

Chapter 5
Corrosion Cracking Analysis
Step 8

Scalars:iso-areas, Basic material, in nodes, Engineering Strain, Eps xx, <-1.572E-02;1.988E-02>[None]
Cracks: in elements, openning: <-4.367E-07;6.209E-04>[m], Sigma_n: <-2.141E+00;2.278E+00>[MPa], Sigma_T□: <-1.593E+00;1.452E+

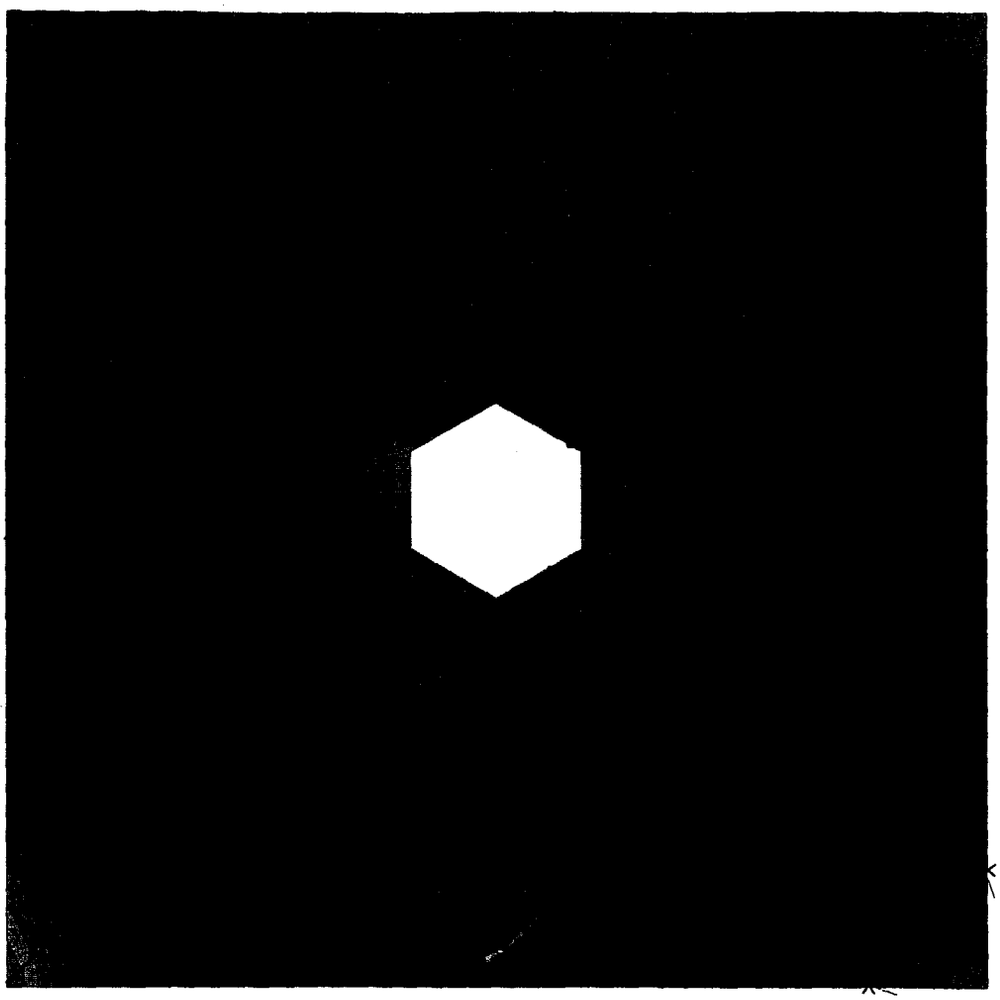

Figure 5.9 Corrosion Crack Analysis -Step 8

Scalars:iso-areas, Basic material, in nodes, Engineering Strain, Eps xx, <-2.860E-02;2.624E-02>[None]
Cracks: in elements, openning: <-7.886E-07;6.727E-04>[m], Sigma_n: <-1.352E+00;2.191E+00>[MPa], Sigma_T□: <-1.994E+00;1.695E+

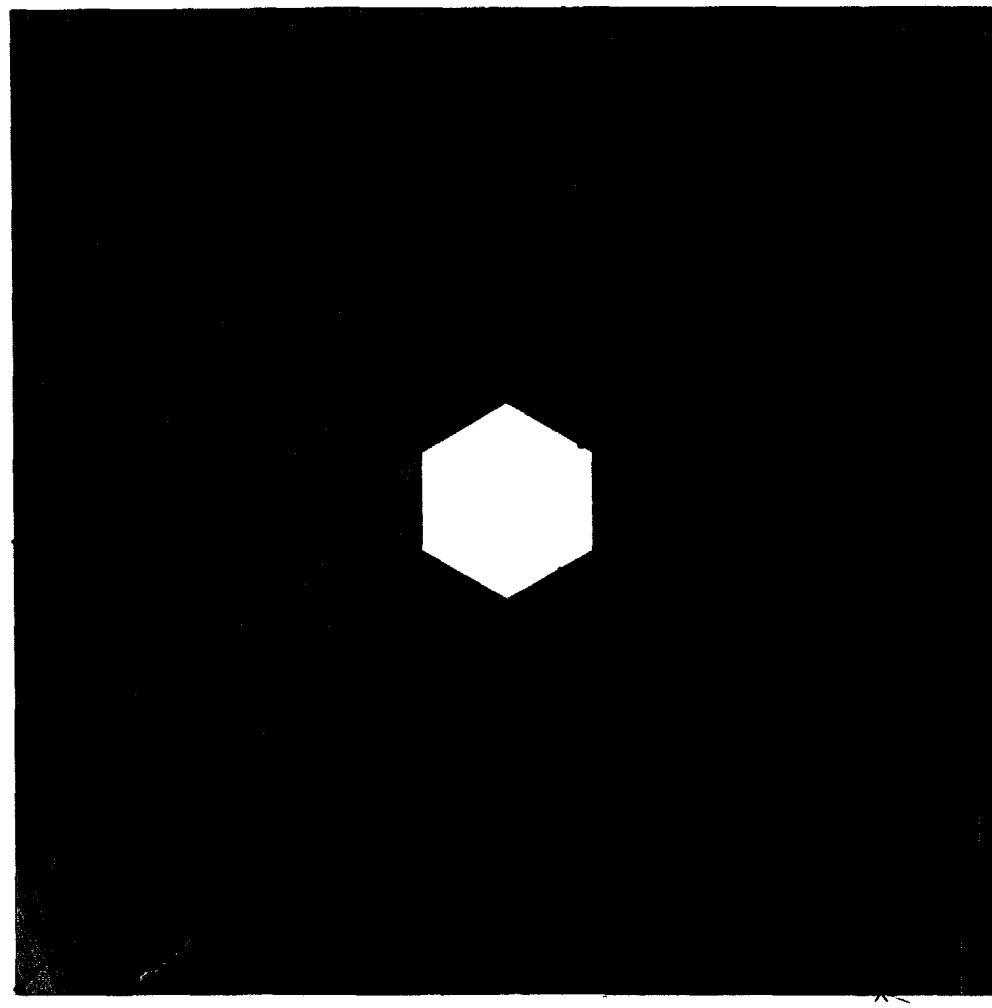

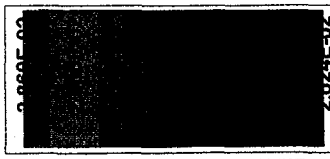

Figure 5.10 Corrosion Crack Analysi-Step 10

Figure 5.5 to Figure 5.10 illustrate the failure progress in the 10 years. The propagation of crack and the stress distribution are also shown in these diagrams. The accumulated maximum crack width at the end of each year is listed in Table. 5.4. It can be seen that the maximum crack width is nearly 1mm after ten years of corrosion in this case. The relationship between corrosion penetration and maximum crack width is shown in Figure 5.11.

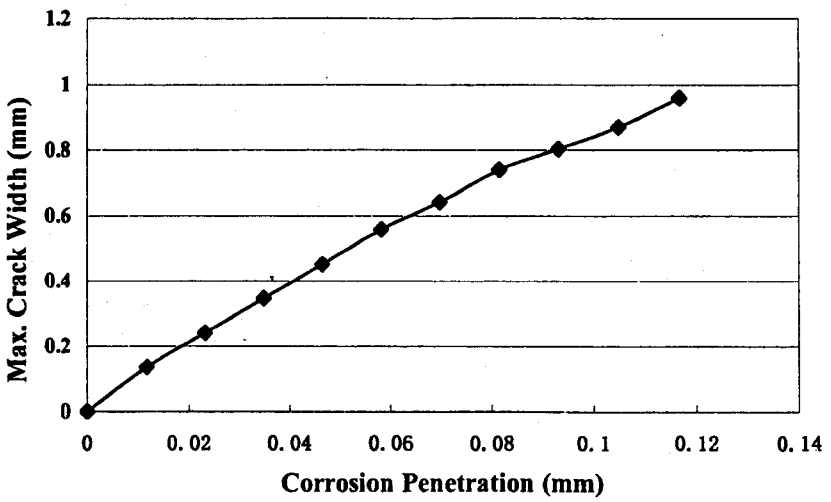

Figure 5.11 Corrosion Penetration Verse Max. Crack Width Response

From the calculation results, we can find that the cracking propagates away from the vicinity of the bar. The first visible crack appears in the elements around the bar at a corrosion level equivalent to radial expansion of 0.03 mm. Basically the location probability of the first crack can be either vertical or horizontal. In this case it is in horizontal direction. It must be noted that some microcracks have existed before any visible crack appeared as shown in the result of analysis Step1. After the first crack is formed, this crack continues to expand wider and wider and eventually extends to the surface of the specimen. During this procedure some

new cracks will continue to appear around the reinforcing bar. The crack extending to the surface, which can be observed by the naked eye, indicates that the intensity of corrosion is high in the reinforced concrete members. At this time the reinforcing bar become more venerable because the harmful material can easily go through the crack, at a much faster rate and as a result the corrosion rate will be accelerated. However, the corrosion products, which cause the radial expansion in the concrete, may decrease because such product can flow out through the crack. As we can observe in the reinforced concrete structures, the rust products frequently appear along the crack after corrosion initiates. That means the width of crack may not be expanded further. This leads to more difficulty in predicting the true cracking progress in the structure. In this research such factors are not considered and further research may be needed.

5.4 Two-Dimensional Bond-Slip Modeling Analysis Example

5.4.1 Example 1 - Tension Test (Specimen II)

A tension test is first modeled by finite element to demonstrate the bond behavior. The size of two-dimensional specimen is shown in Figure 5.12 and the finite element mesh is shown in Figure 5.14.

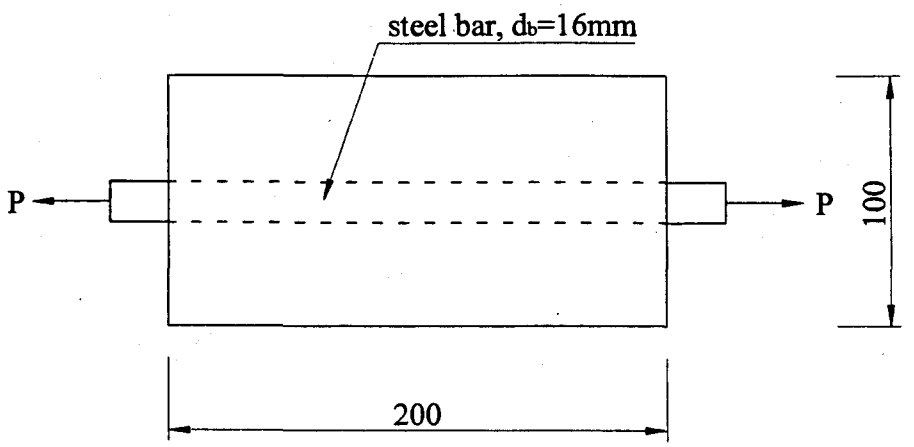

.Figure 5.12 Dimensions of Tension Specimen (Specimen II)

In order to consider the bond slip effect between the concrete and reinforcing bar, an additional material called 'bond for reinforcement' is specified in the finite element analysis. This material considers the bond effect by treating the concrete around the steel bar as a composite material as discussed in Chapter 4. The type of steel bar is ribbed reinforcement and bond quality is defined as in the poor condition. The bond stress to slip model is according to CEB-FIP Model Code 1990 as shown in Figure 3.12. The curve of bond-stress slip relationship used in this study is determined by 7 points and the related parameters are listed in Table 5.5. The bond slip-stress response is shown in Figure 5.13.

Table 5.5 Parameters of Bond Stress and Slip Relationship Used in This Study

Number of Point	Slip (mm)	Bond Stress (MPa)
1	0	2.0917
2	0.25	2.7484
3	0.5	3.9658
4	1	5.2291
5	3	5.2291
6	15	2.0917
7	∞	2.0917

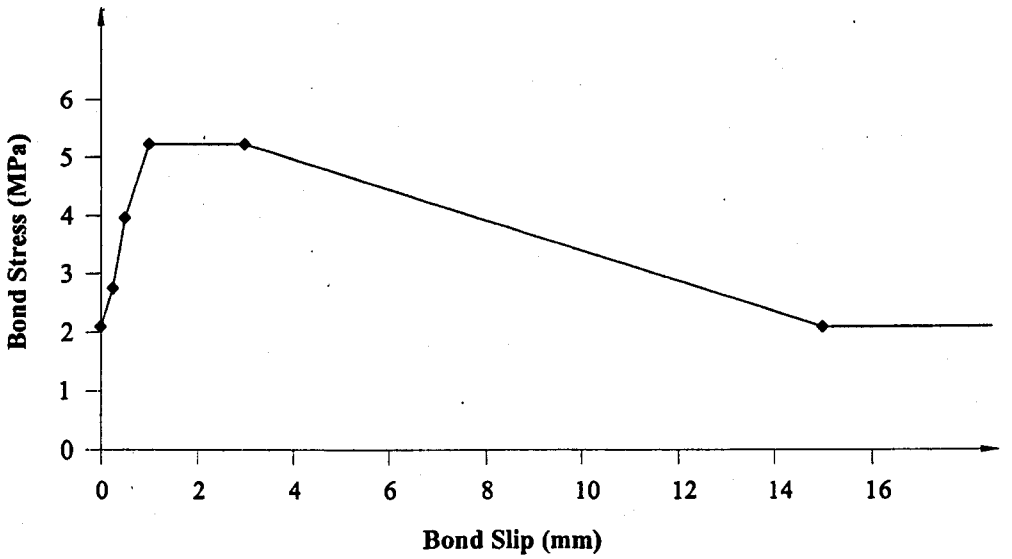

Figure 5.13 Bond Slip-Stress Relationship Used in This Study

The load is applied at the two ends of reinforcing bar. The slip will occur when the stress exceeds a certain level. The increment of load at each load step is 1 kN. The total analysis steps are 10. The specimen is restrained at the middle of its length to prevent the horizontal and vertical movement, but the cross-section can still be free to contract. The calculation results are shown in Figures 5.14 to 5.19. Table 5.5 shows the development of bond stress at the two ends of the specimen. The variation of steel stress along the bar for the tension simulation is shown in Figure 5.20 under P = 1 kN.

From the analysis results, the bond stress was found to be increasing rapidly at the end of the specimen after the tension load was applied. The first group of cracks is also formed in this area after the tension stress exceeded the limitation. Because the concrete is not a homogenous material, the cracks may develop more quickly at one end. Then the bond stress at one end continually increases, while the stress at the other end may either decrease or increase as shown in Table 5.6. The value of bond stress in the crack is equal to zero and reaches the peak in the vicinity of the crack. It agrees with the experimental results as shown

in Figure in Chapter 3. With the increase of tension forces, more cracks appear around this area and some stress redistribution occurs. Finally, the bond stress develops in the whole reinforcement as a result of the change of stress along all the length of the bar. The tension stress is also developed in the concrete by the bond effect. Eventually the cracks are evenly distributed within the specimen. The bond stress is redistributed with the development of cracks. As can be observed in the diagrams, the bond stress redistribution is a very complex progress and unpredictable and the crack propagation in the inhomogeneous concrete material can make it more difficult.

Table 5.6 The Bond Stress at Two Ends of Tension Specimen

Step	Bond Stress (MPa)	
	Left	Right
1	1.8979	-1.899
2	2.093	-1.178
3	2.094	-1.877
4	2.111	2,141
5	2.164	2.248
6	2.244	2.503
7	2.355	3.783
8	2.524	-1.590
9	3.150	-3.390
10	4.092	-5.190

5.4.2 Example 2 - Simply Supported Beam (Specimen III)

Finite element analysis of a simply supported beam, which has also been investigated experimentally by other researchers in the past research, is presented in this section. Due to

Chapter 5
Tension Test Analysis
Step 1

Reinforcements: Bond Stress, Force, <-9.544E-02;9.537E-02>[MN/m]

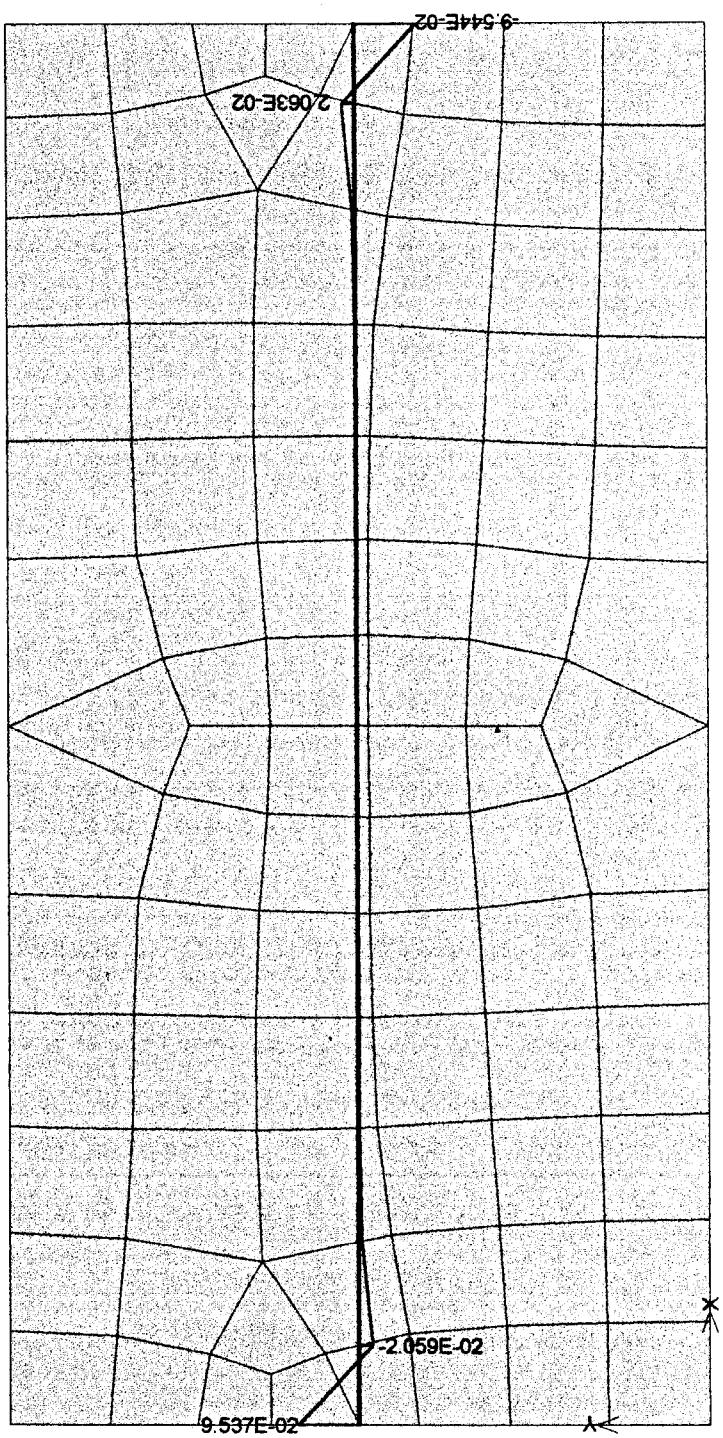

Figure 5.14 Tesion Test- Step 1 (Bond Stress)

Cracks: in elements, openning: <6.244E-07;9.984E-07>[m], Sigma_n: <2.158E+00;2.218E+00>[MPa], Sigma_T□: <0.000E+00;0.000E+00
Reinforcements: Bond Stress, Force, <-9.437E-02;1.052E-01>[MN/m]

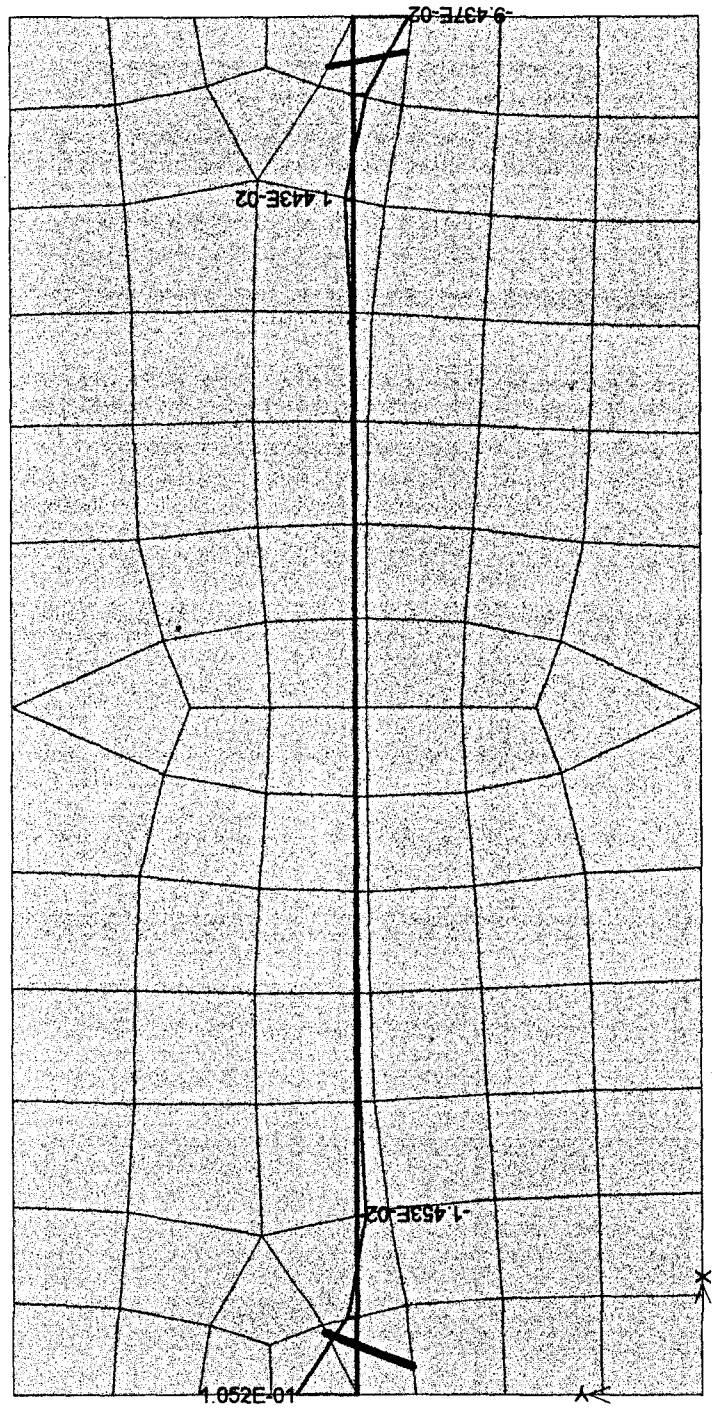

Figure 5.15 Tension Test - Step 3 (Bond Stress and Crack)

Chapter 5
Tension Test Analysis
Step 5

Cracks: in elements, openning: <8.440E-08;7.984E-05>[m], Sigma_n: <3.268E-01;2.301E+00>[MPa], Sigma_T□: <-4.364E-01;1.744E-01>
Reinforcements: Bond Stress, Force, <-1.052E-01;1.130E-01>[MN/m]

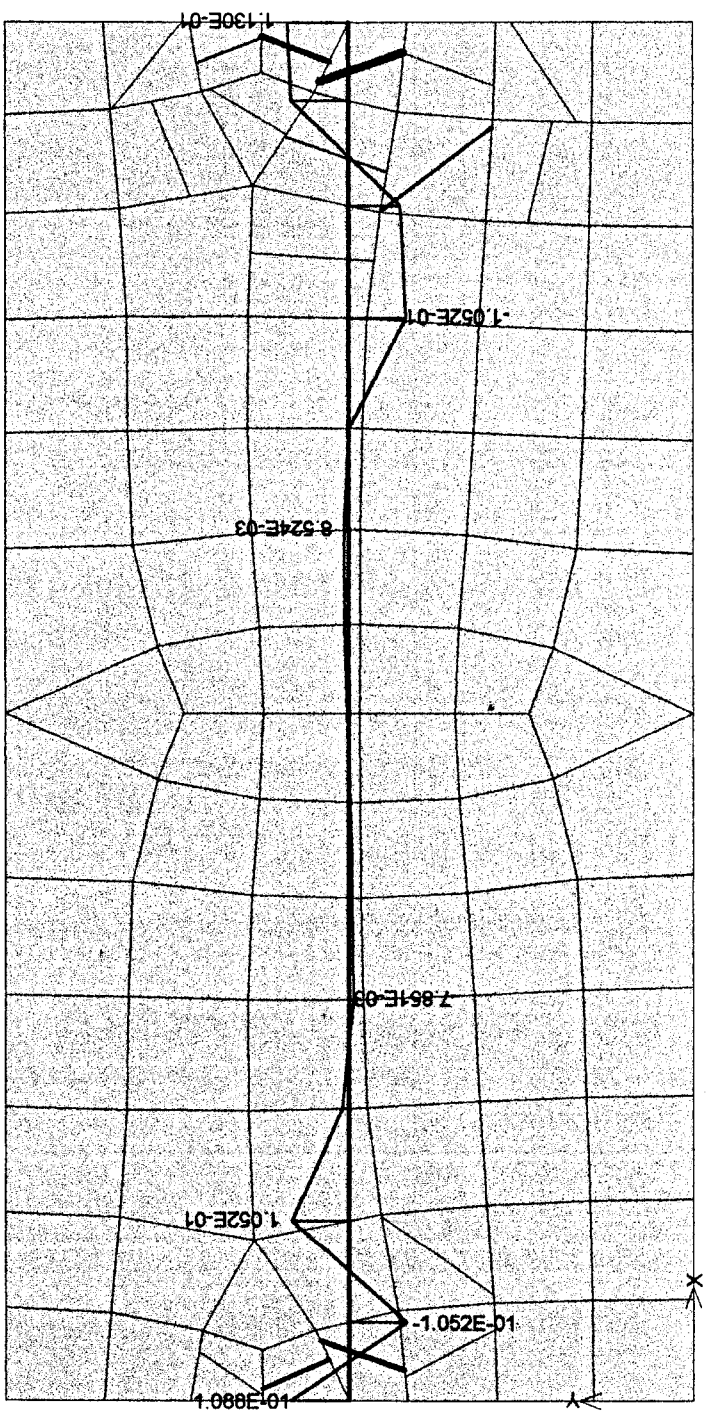

Figure 5.16 Tension Test - Step 5 (Bond Stress and Crack)

Cracks: in elements, openning: <4.551E-07;2.848E-04>[m], Sigma_n: <-1.581E+00;2.213E+00>[MPa], Sigma_T□: <-7.455E-01;8.562E-01
Reinforcements: Bond Stress, Force, <-1.238E-01;1.901E-01>[MN/m]

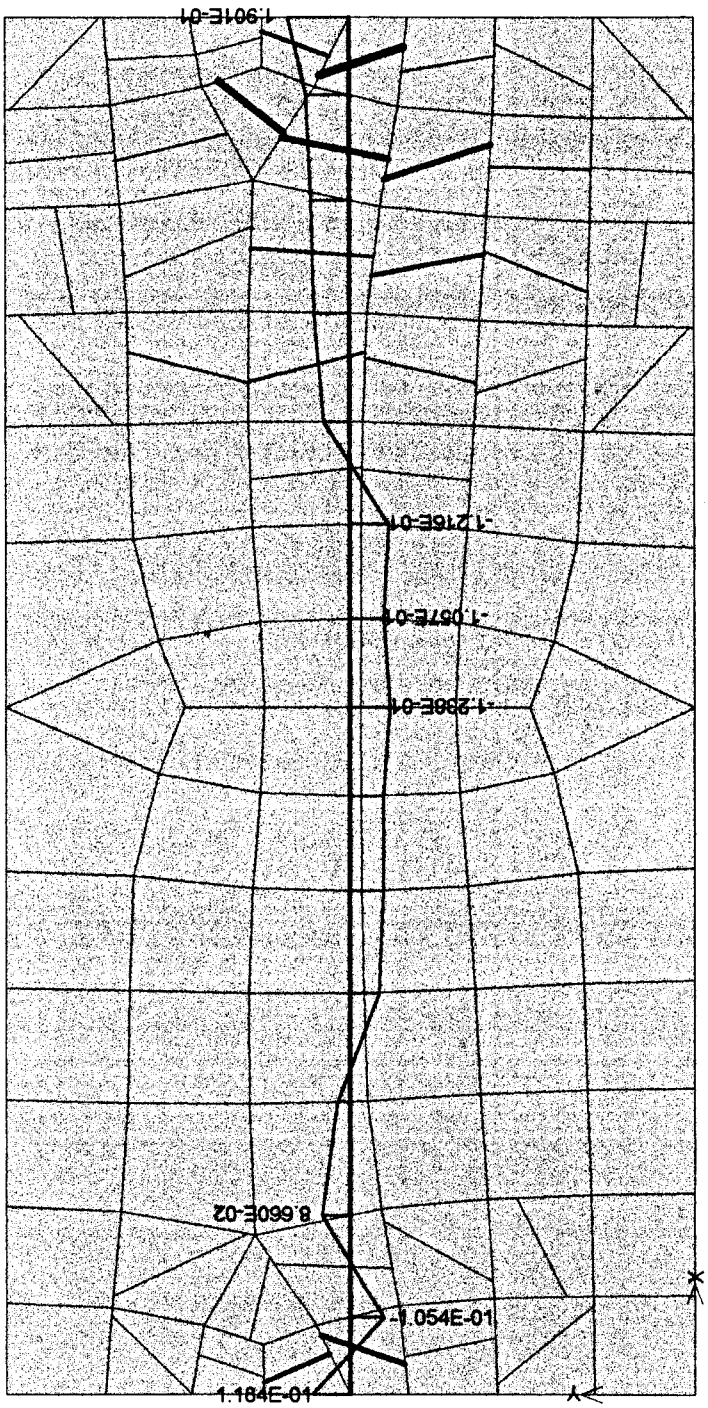

Figure 5.17 Tension Test - Step 7 (Bold Stress and Crack)

Chapter 5
Tension Test Analysis
Step 9

Cracks: in elements, openning: <1.494E-07;5.326E-04>[m], Sigma_n: <-9.793E-01;2.290E+00>[MPa], Sigma_T□: <-9.620E-01;5.462E-01
Reinforcements: Bond Stress, Force, <-2.139E-01;1.583E-01>[MN/m]

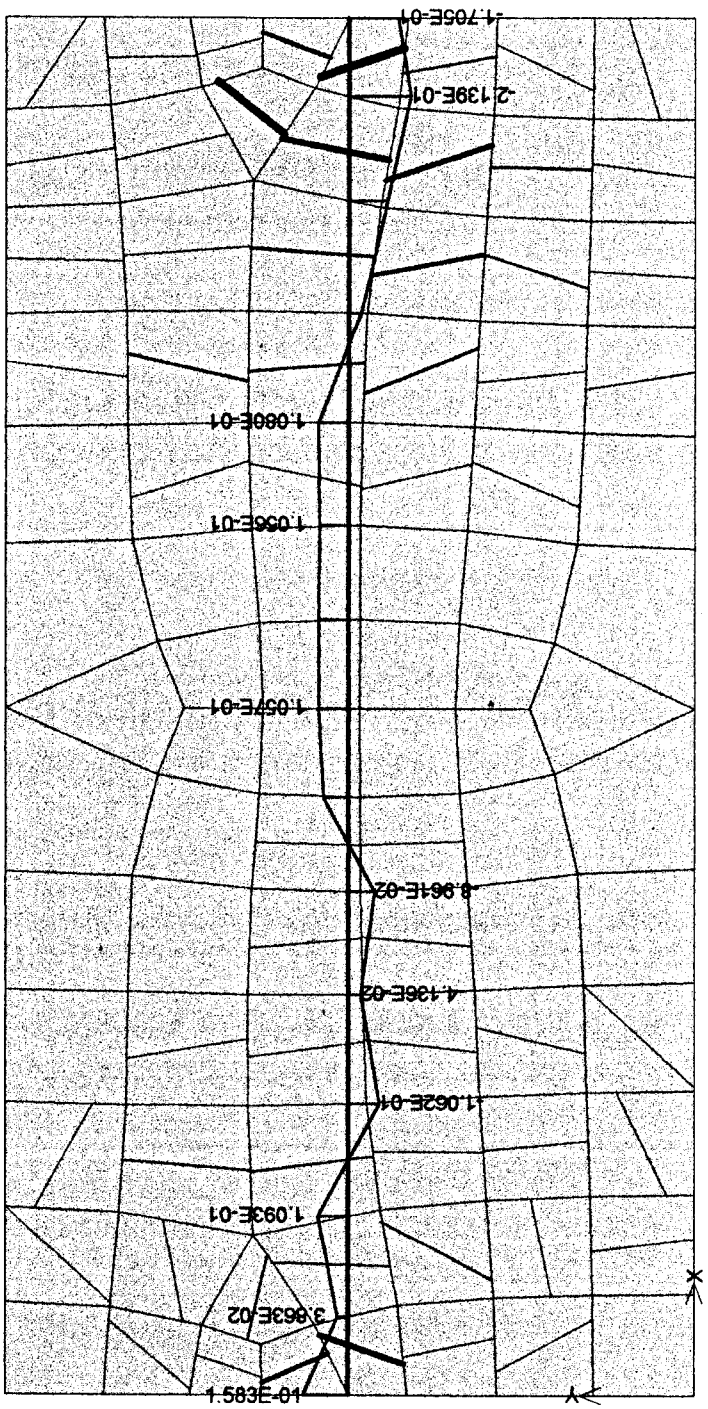

Figure 5.18 Tension Test - Step 9 (Bond Stress and Crack)

Cracks: in elements, openning: <1.286E-07;6.414E-04>[m], Sigma_n: <-9.906E-01;2.127E+00>[MPa], Sigma_T□: <-6.240E-01;5.983E-01
Reinforcements: Bond Stress, Force, <-2.609E-01;2.057E-01>[MN/m]

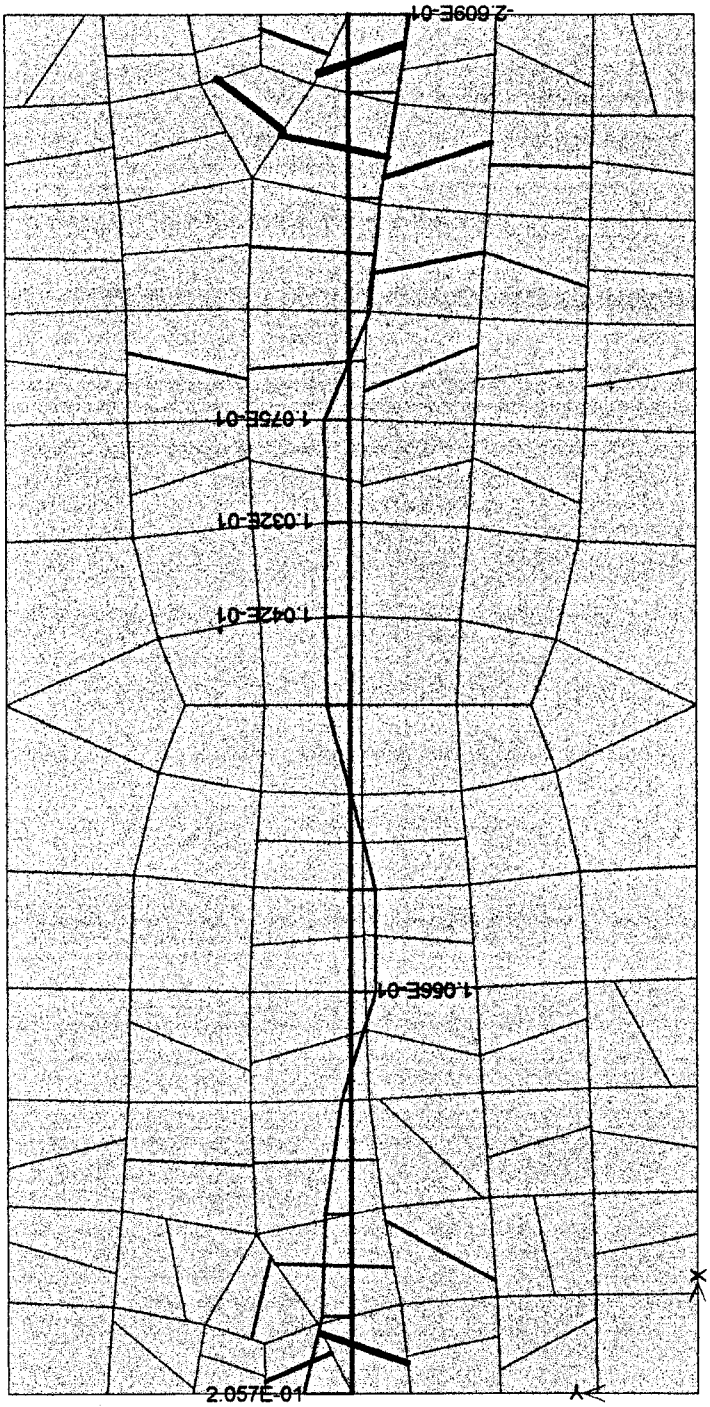

Figure 5.19 Tension Test - Step 10 (Bond Stress and Crack)

Reinforcements: Principal Stress, Max., <6.527E-01;2.705E+00>[MPa]

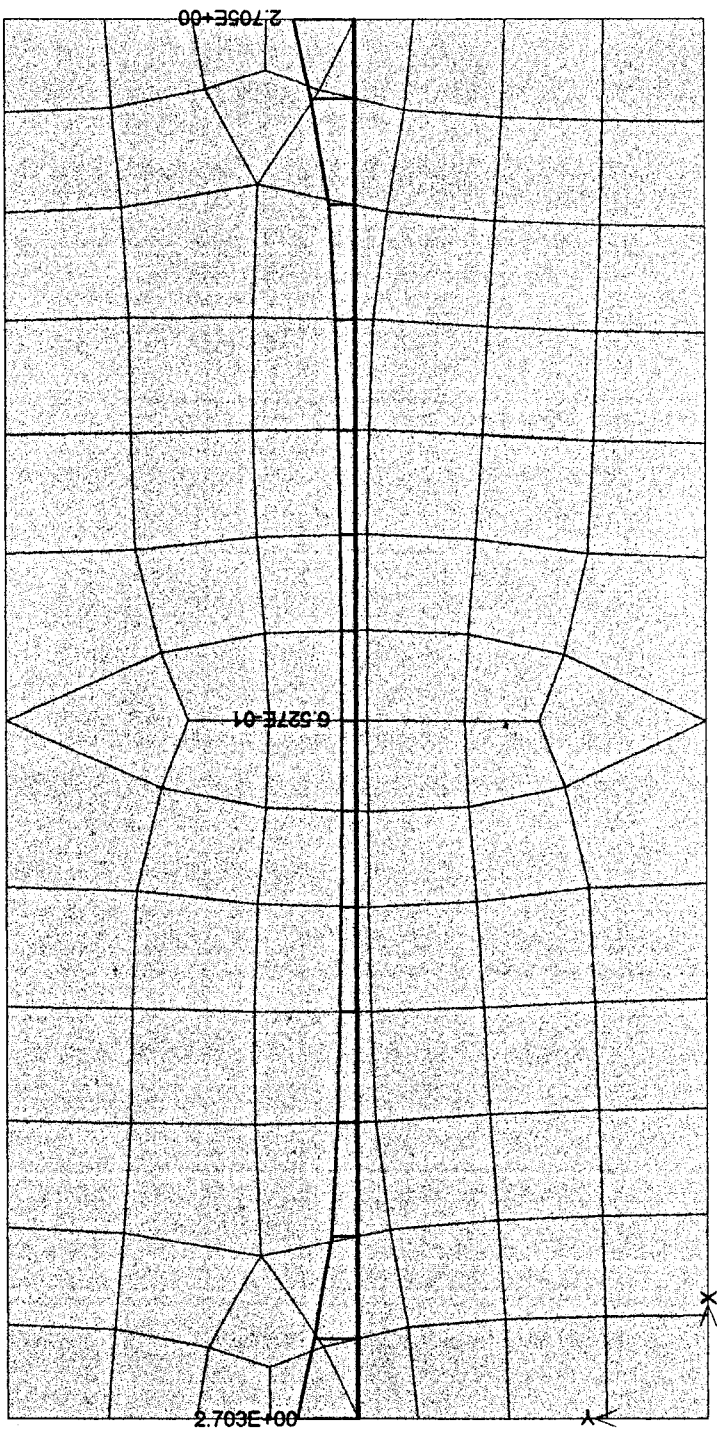

Figure 5.20 Tension Test - Step 1 (Stress Distribution of Reinforcement)

the limitation of element number and requirement of accuracy in calculation, the size of the beam is not very big as shown in Figure 5.21 and the mesh size is shown in Figure 5.22.

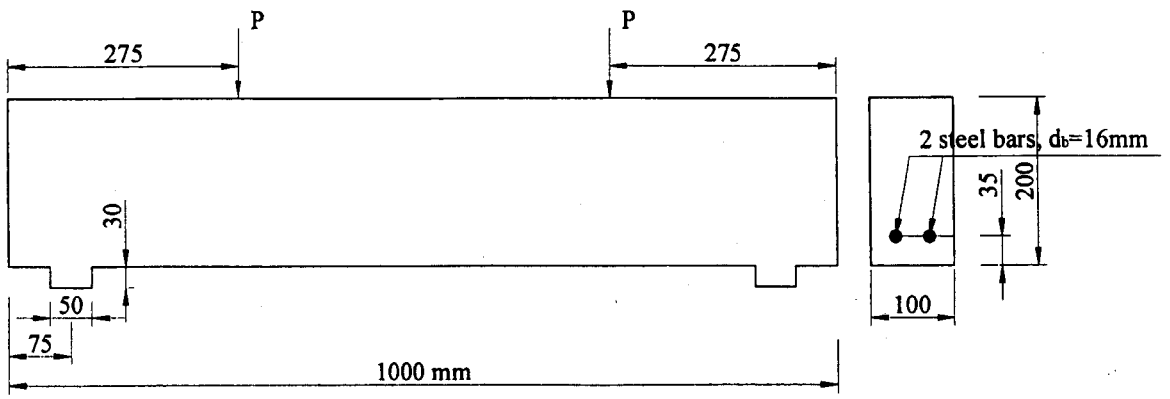

Figure 5.21 Dimensions of Simply Supported Beam (Specimen III)

Both the concrete and reinforcement material properties are the same as those used in the previous analysis. The bond slip is modeled by 'bond for reinforcement' material as discussed in Example 1. The type of steel bar is ribbed reinforcement and bond quality is specified as in good condition.

Two vertical concentrated loads are applied at the top of beam. The increment of load at each step is 0.5kN. The total analysis steps are 10. The supports are two steel plates with 50 mm width and 30 mm thickness. The boundary condition is: the left support is a pin support and the right support is roller. The calculation results are shown in Figures 5.23 to 5.33.

The displacements at the middle of the span and the resisting forces in the left support are obtained by setting two monitor points in the calculation. The one in the support A can give resisting force after each load step. The forces are balanced by the applied loads which means the calculation results are correct. Another monitor point is at the bottom of mid-span

recording maximum deformation of the beam after each load step. The calculation results are listed in Table 5.7 and are shown in Figure 5.34

Table 5.7 The Maximum Displacement after Each Load Step

Step	Maximum Crack Wideth(mm)	Maximum Displacement (mm)
1	0	0.04431
2	0	0.08906
3	5.257×10^{-3}	0.1551
4	2.466×10^{-2}	0.2717
5	4.264×10^{-2}	0.4156
6	5.678×10^{-2}	0.5565
7	0.1119	0.7173
8	0.1496	0.8582
9	0.1950	1.006
10	0.2396	1.156

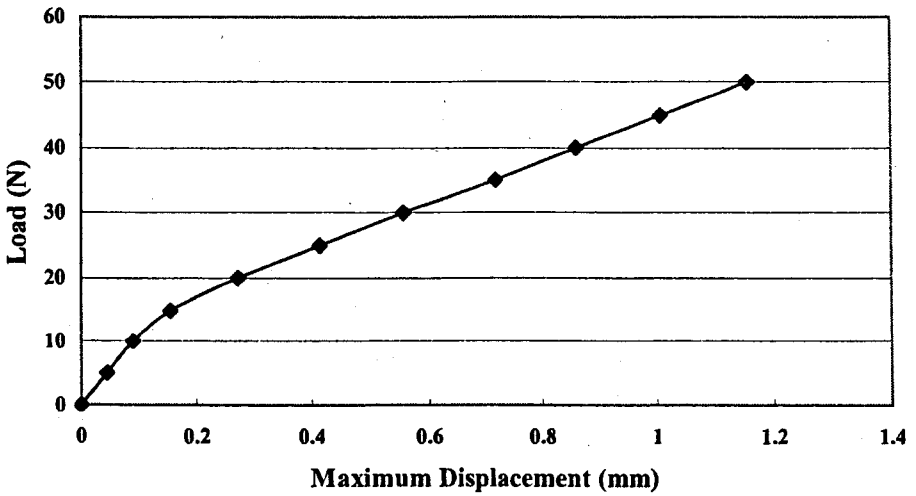

Figure 5.34 Load Deflection Curve

The stress distribution along the height of the cross section is studied, and three cross sections are defined in the analysis. The first one is at the middle of span, the second one is at the point where the external load is applied and the third one is in the support. The calculation results are shown in Figure 5.22 to Figure 5.31. It can be seen that the compression block is reduced with the increase of load and the development of crack.

The propagation of crack is also demonstrated in this example. Initially the flexural cracks appear at the middle of the span in the beam. Then cracks appear near the support due to the large shear stress in this area with an angle equal to 45 degrees. Finally this kind of cracks extends to the top of beam. The beam is finally in the flexural shear failure which is in agreement with the experimental results.

Before cracking occurs, the bond stress exists on the interface between the bars and concrete as a result of the change of stress in the reinforcement. Due to the loading, no bond stresses exist between the concrete and the reinforcing bar in the middle third of the beam. In the outer thirds of the beam, where constant shear force and a corresponding change in moment exist, the steel and the concrete elongate the same amount over any given length. However, due to the difference in the elastic modulus of the two materials, a larger stress change in the steel than in the concrete over a unit length, leading to a bond stress.

After a crack forms in the constant moment region of the beam, the stress condition in the vicinity of the crack is very complex. The tensile stress at the section of crack in the concrete disappeared. This unloading of tensile concrete allows the crack to open at the surface of the beam. This makes certain amount of stress redistributed in the steel. With the increase of load and the propagation of the crack, this kind of redistribution continues until the beam is damaged. These phenomena can be observed in this example.

Chapter 5
Simply Supported Beam Analysis
Step 1

Scalars:cuts, Basic material, in nodes, Stress, Sigma xx, <-1.241E+00;9.905E-01>[MPa]
Reinforcements: Bond Stress, Force, <-1.226E-02;1.223E-02>[MN/m]

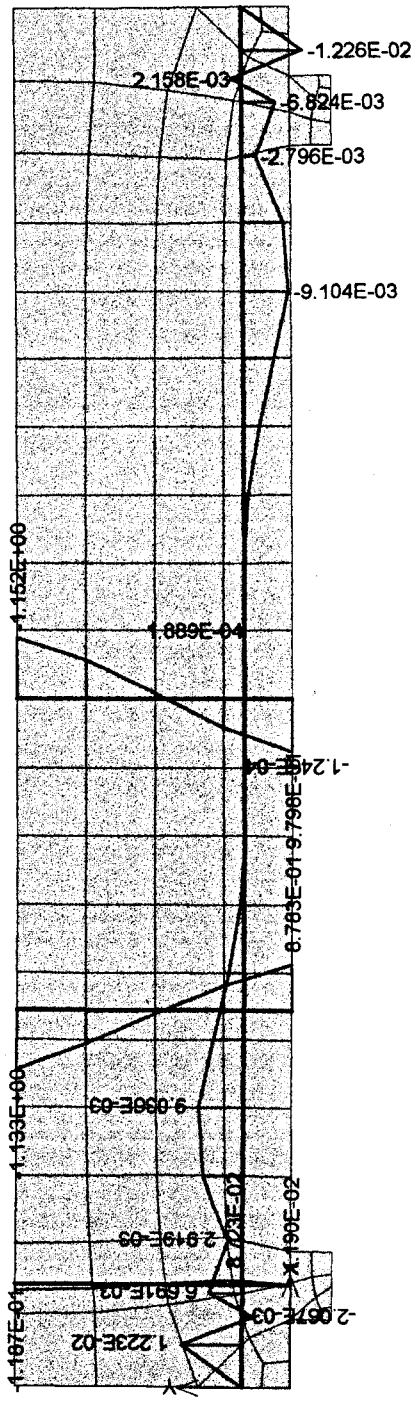

Figure 5.22 Simply Supported Beam - Step 1 (Bond Stree and Concrete Stress of Cuts)

Scalars:cuts, Basic material, in nodes, Stress, Sigma xx, <-2.483E+00;1.986E+00>[MPa]
Reinforcements: Bond Stress, Force, <-2.461E-02;2.455E-02>[MN/m]

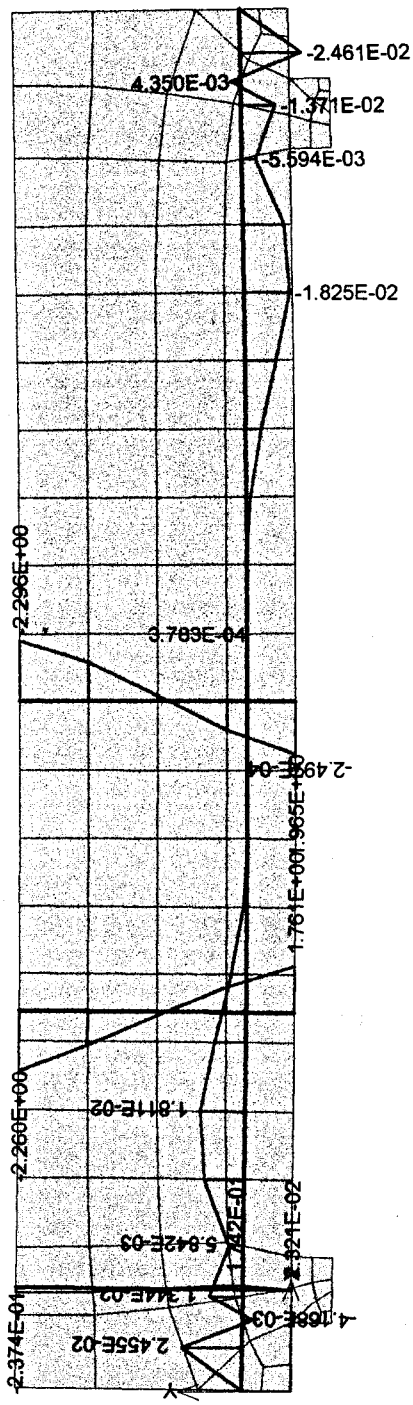

Figure 5.23 Simply Supported Beam - Step 2 (Bond Stree and Concrete Stress of Cuts)

Chapter 5
Simply Supported Beam Analysis
Step 4

Scalars:cuts, Basic material, in nodes, Stress, Sigma xx, <-5.650E+00;2.067E+00>[MPa]
Reinforcements: Bond Stress, Force, <-1.784E-01;1.785E-01>[MN/m]

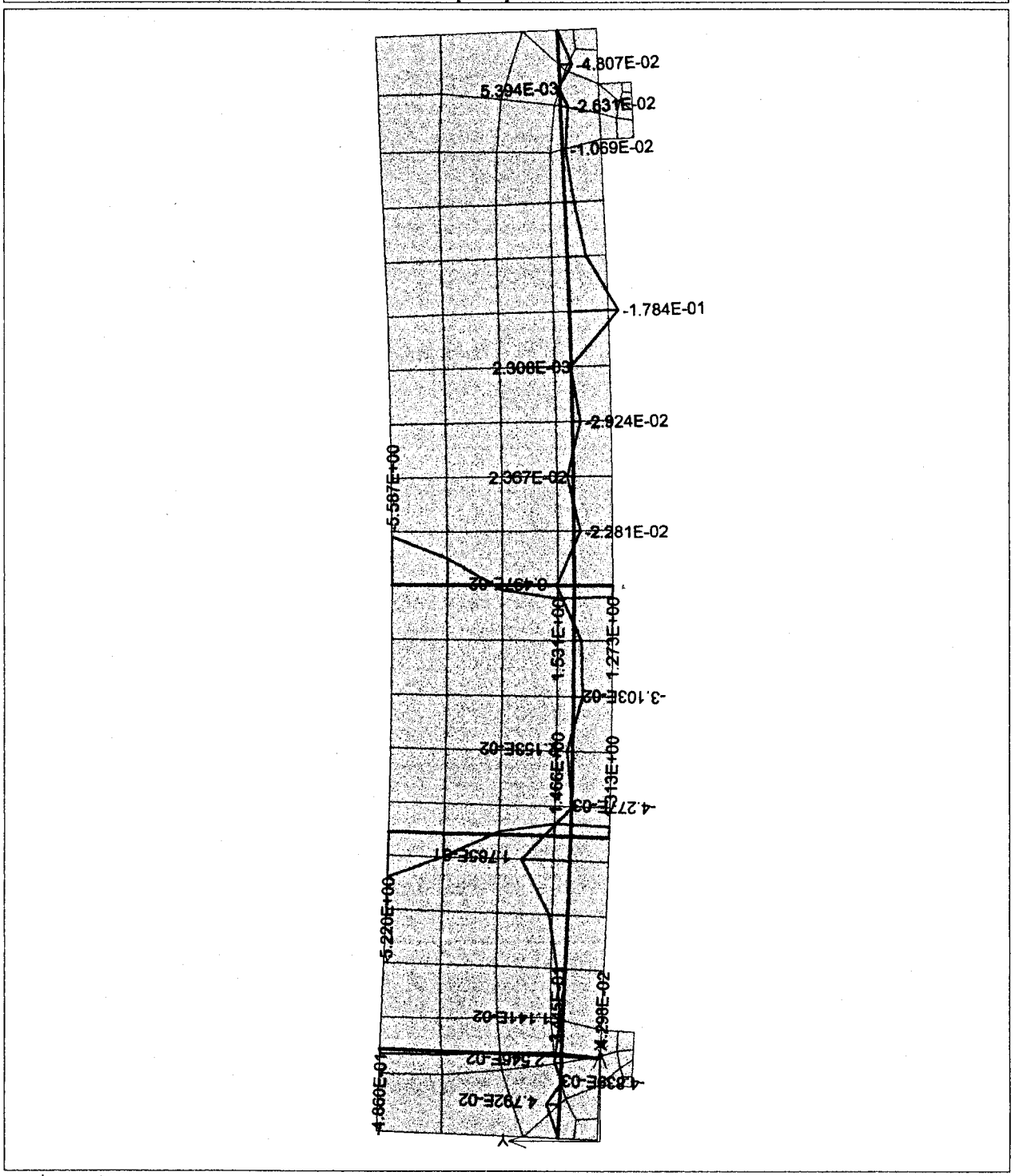

Figure 5.24 Simply Supported Beam - Step 4 (Bond Stree and Concrete Stress of Cuts)

Scalars:cuts, Basic material, in nodes, Stress, Sigma xx, <-9.276E+00;1.647E+00>[MPa]
Reinforcements: Bond Stress, Force, <-2.645E-01;2.658E-01>[MN/m]

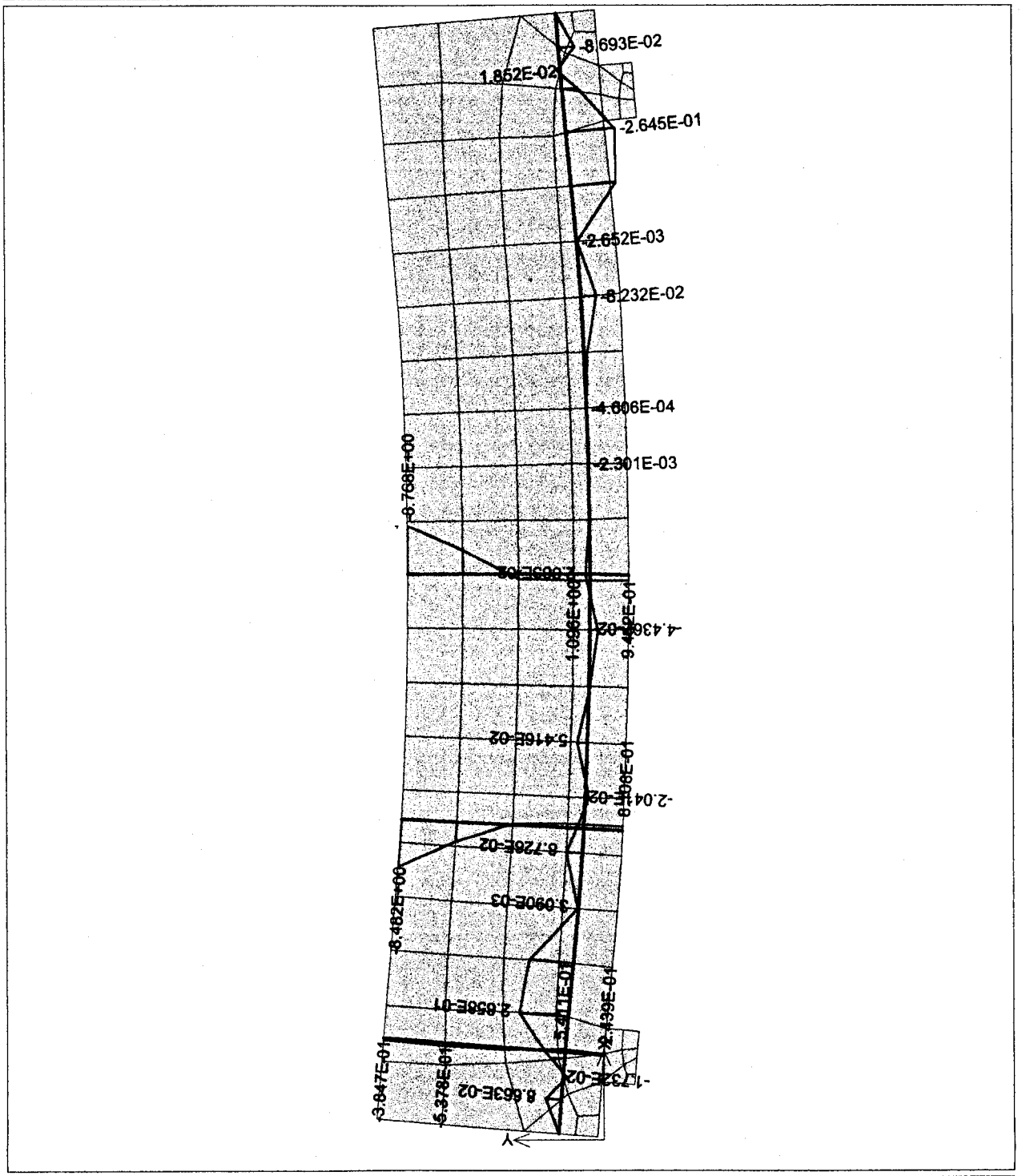

Figure 5.25 Simply Supported Beam - Step 6 (Bond Stree and Concrete Stress of Cuts)

Scalars:cuts, Basic material, in nodes, Stress, Sigma xx, <-1.225E+01;1.468E+00>[MPa]
Reinforcements: Bond Stress, Force, <-4.207E-01;4.207E-01>[MN/m]

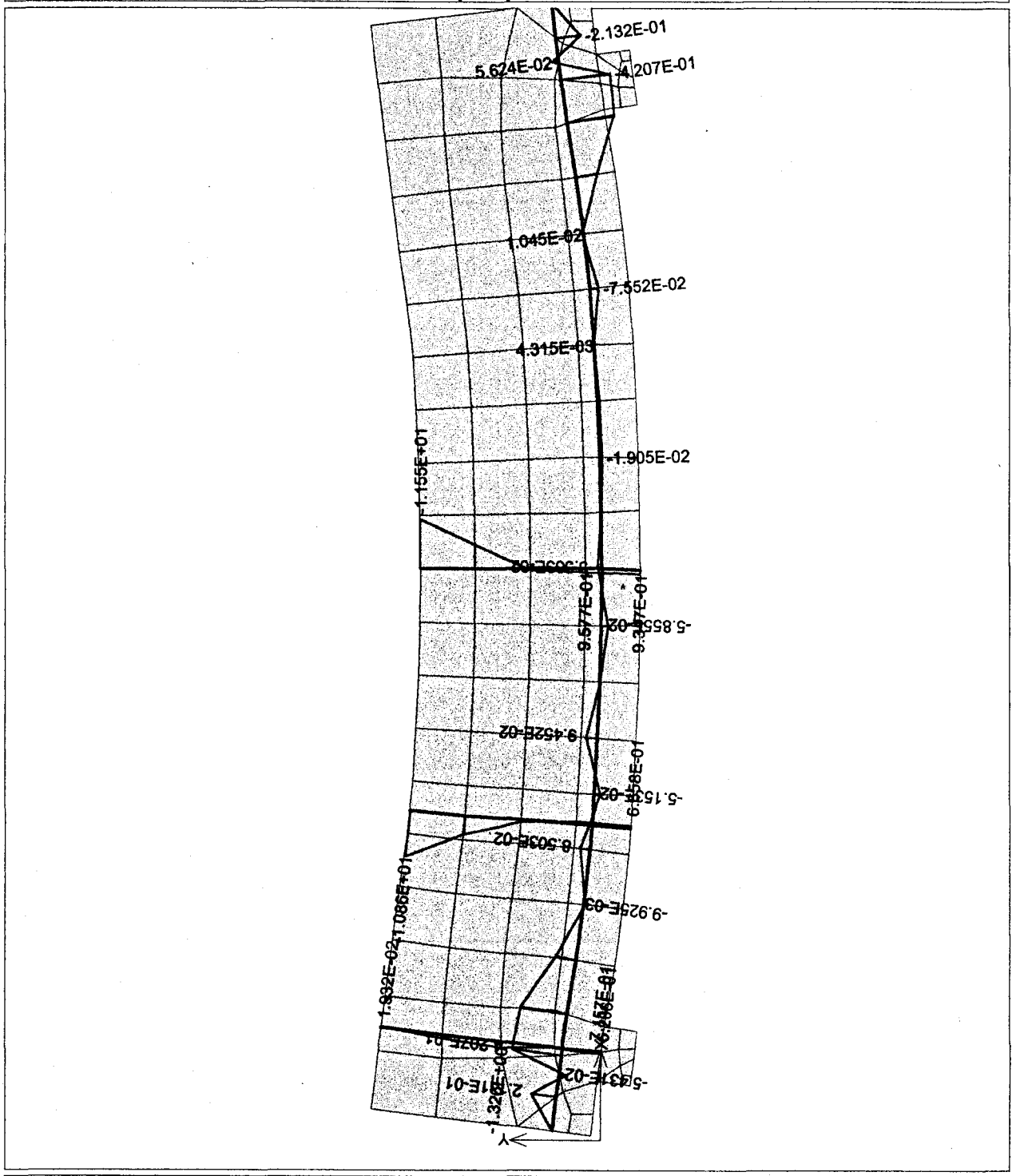

Figure 5.26 Simply Supported Beam - Step 8 (Bond Stree and Concrete Stress of Cuts)

Scalars:cuts, Basic material, in nodes, Stress, Sigma xx, <-1.525E+01;1.954E+00>[MPa]
Reinforcements: Bond Stress, Force, <-4.244E-01;4.244E-01>[MN/m]

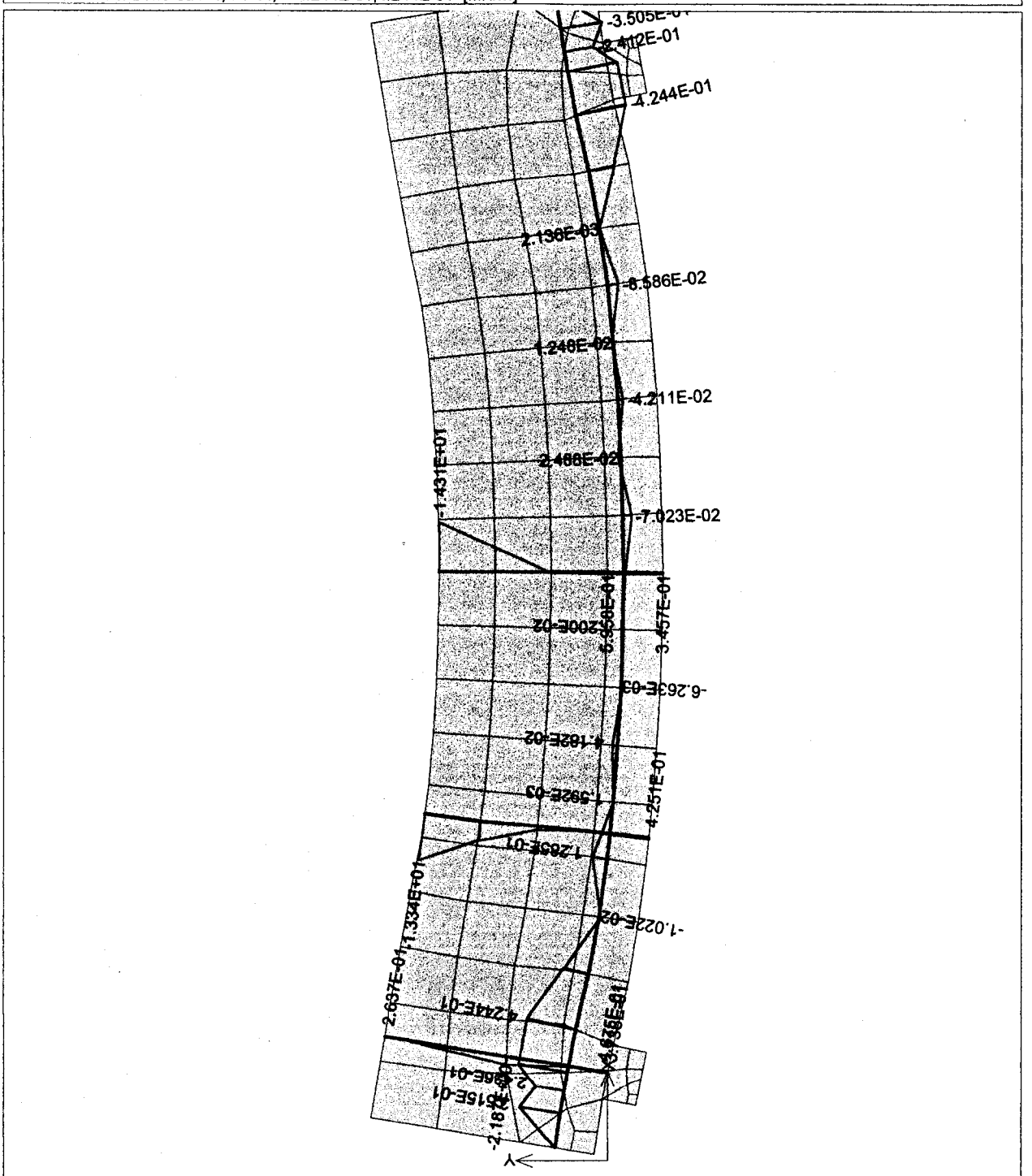

Figure 5.27 Simply Supported Beam - Step 10 (Bond Stree and Concrete Stress of Cuts)

Scalars:iso-areas + cuts, Basic material, in nodes, Principal Stress, Max., <-1.241E+00;9.905E-01>[MPa]

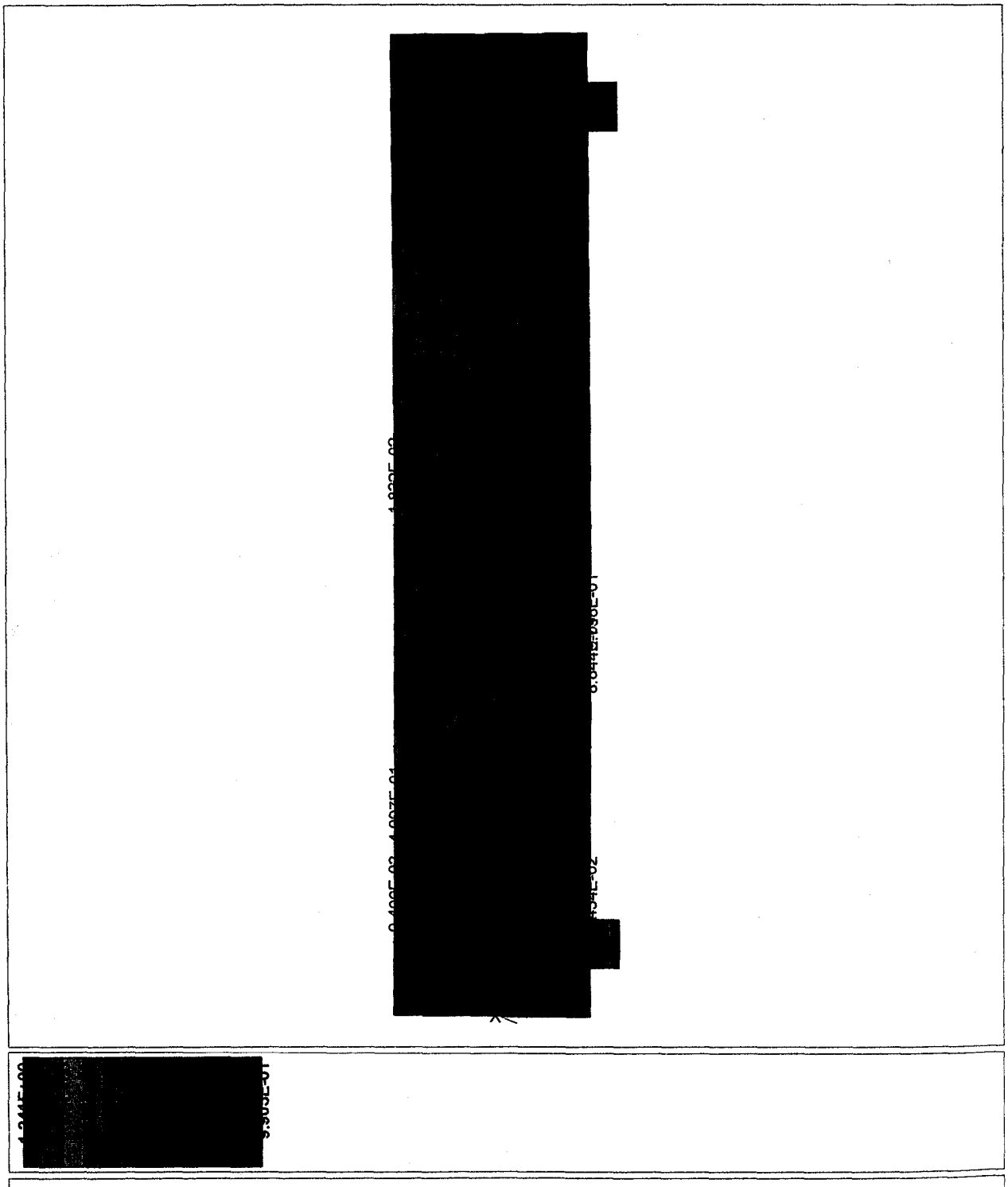

Figure 5.28 Simply Supported Beam - Step 1 (Engineering Stress with Cuts)

Scalars:iso-areas + cuts, Basic material, in nodes, Principal Stress, Max., <-3.727E+00;2.010E+00>[MPa]
Cracks: in elements, openning: <2.536E-06;3.539E-06>[m], Sigma_n: <1.875E+00;1.997E+00>[MPa], Sigma_T□: <0.000E+00;0.000E+00

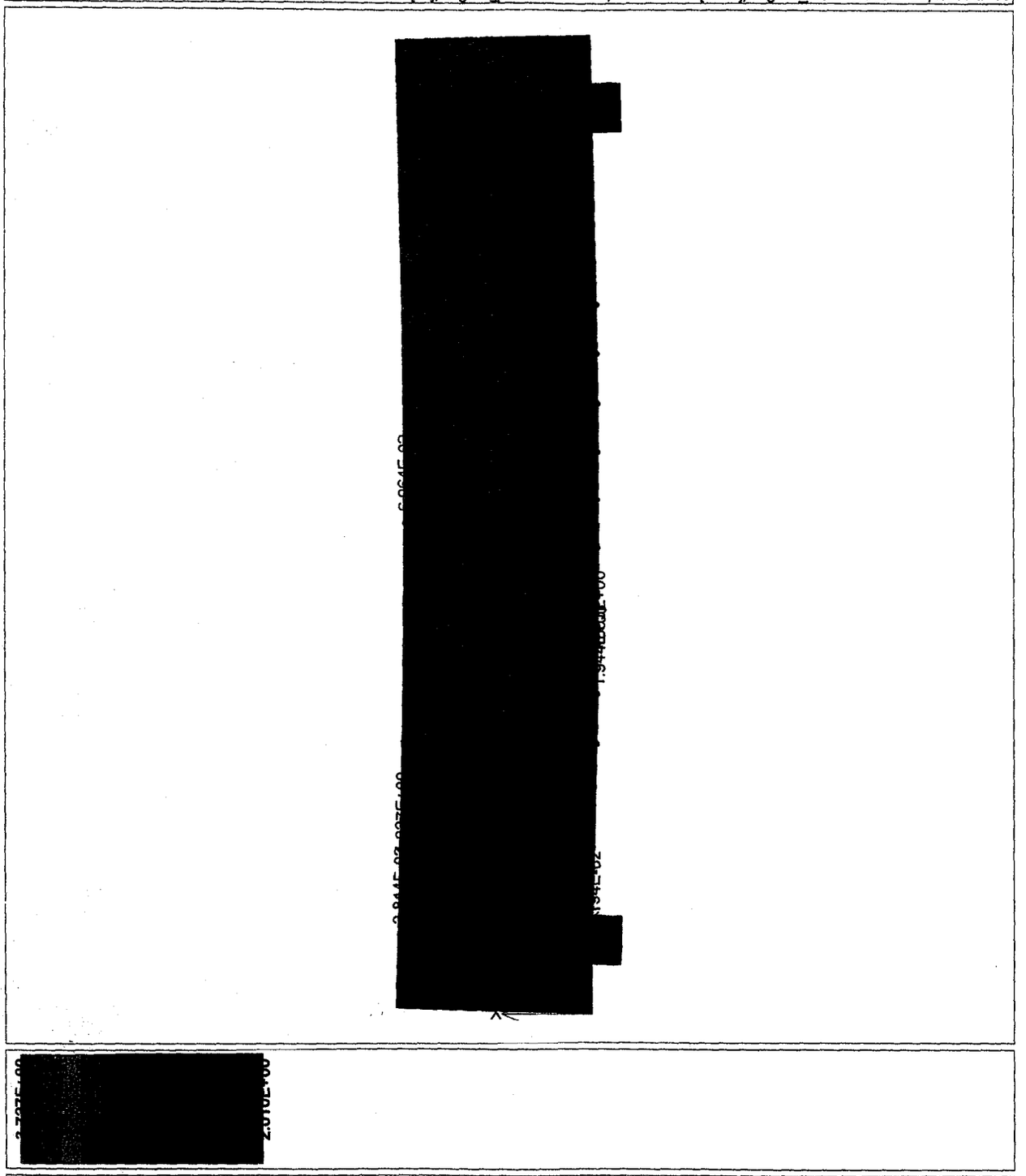

Figure 5.29 Simply Supported Beam - Step 3 (Engineering Stress with Cuts and Cracks)

Scalars:iso-areas + cuts, Basic material, in nodes, Principal Stress, Max., <-4.971E+00;2.097E+00>[MPa]
Cracks: in elements, openning: <1.582E-06;1.631E-05>[m], Sigma_n: <1.093E+00;2.103E+00>[MPa], Sigma_T□: <-1.811E-01;1.386E-01>

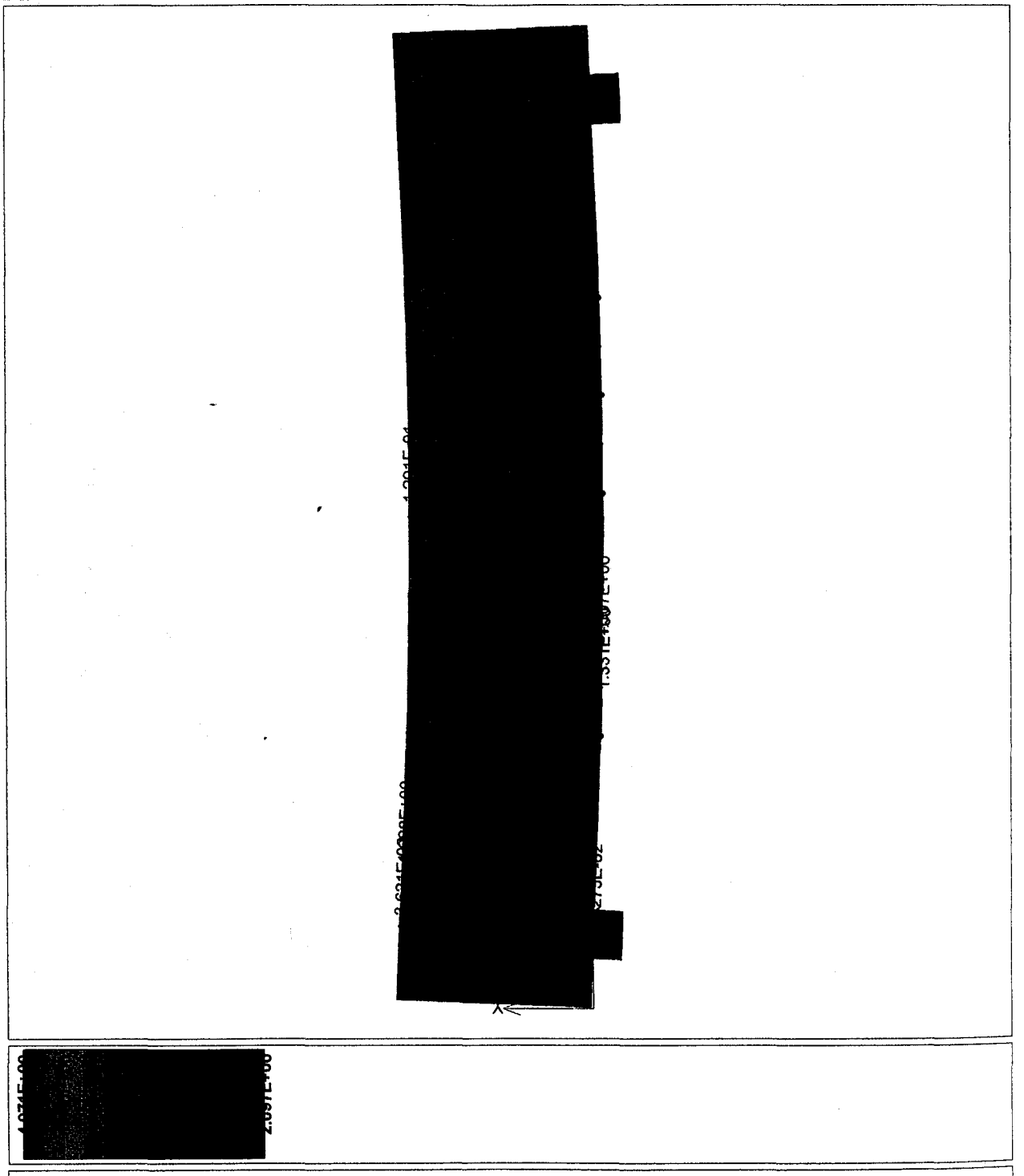

Figure 5.30 Simply Supported Beam - Step 4 (Engineering Stress with Cuts and Cracks)

Chapter 5
Simply Supported Beam Analysis
Step 6

Scalars:iso-areas + cuts, Basic material, in nodes, Principal Stress, Max., <-7.573E+00;2.320E+00>[MPa]
Cracks: in elements, openning: <1.532E-07;5.031E-05>[m], Sigma_n: <3.789E-01;2.297E+00>[MPa], Sigma_T□: <-4.882E-01;4.995E-01>

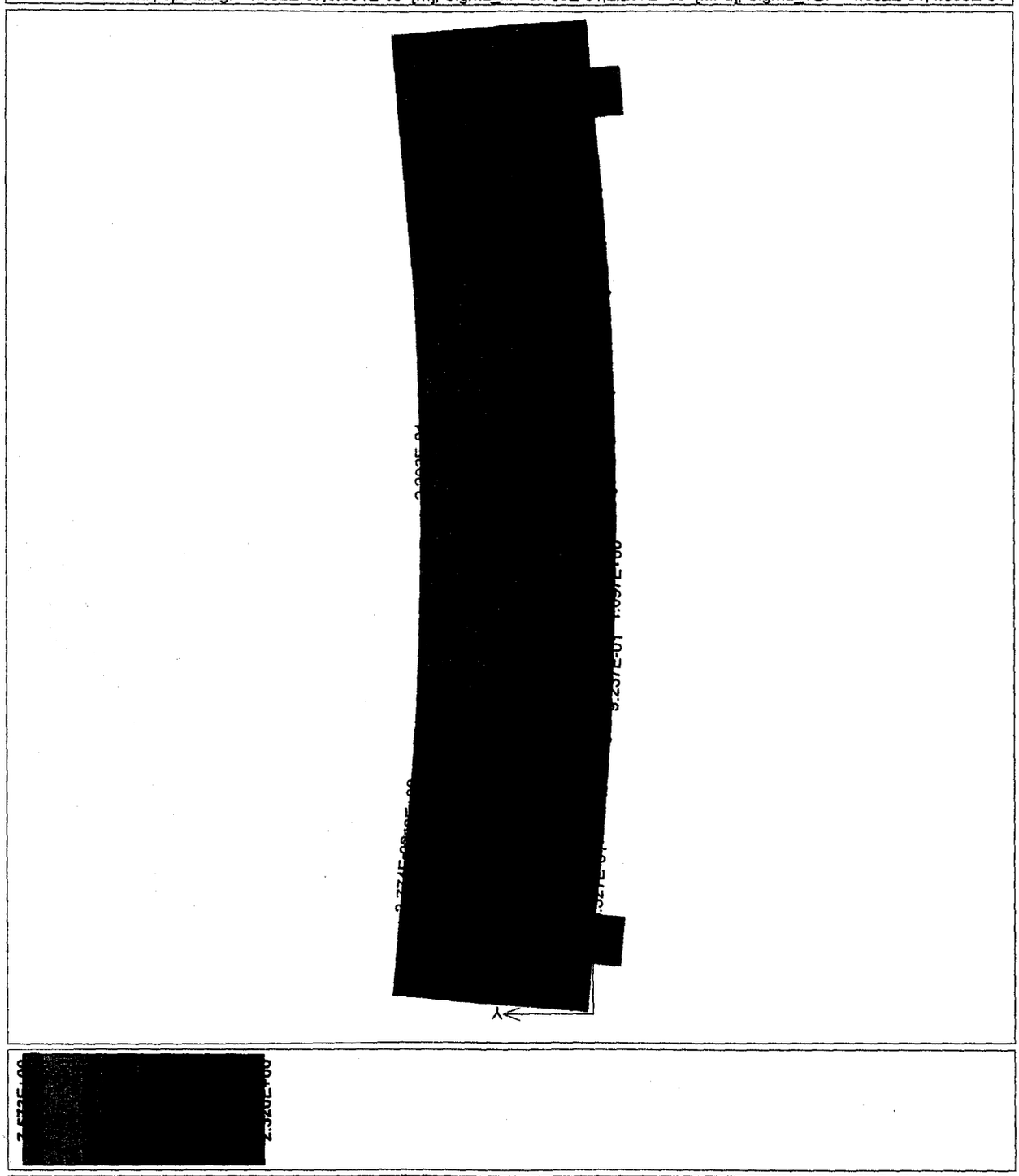

Figure 5.31 Simply Supported Beam - Step 6 (Engineering Stress with Cuts and Cracks)

Scalars:iso-areas + cuts, Basic material, in nodes, Principal Stress, Max., <-1.035E+01;2.931E+00>[MPa]
Cracks: in elements, openning: <8.085E-07;1.259E-04>[m], Sigma_n: <3.438E-02;2.203E+00>[MPa], Sigma_T□: <-1.058E+00;1.064E+00

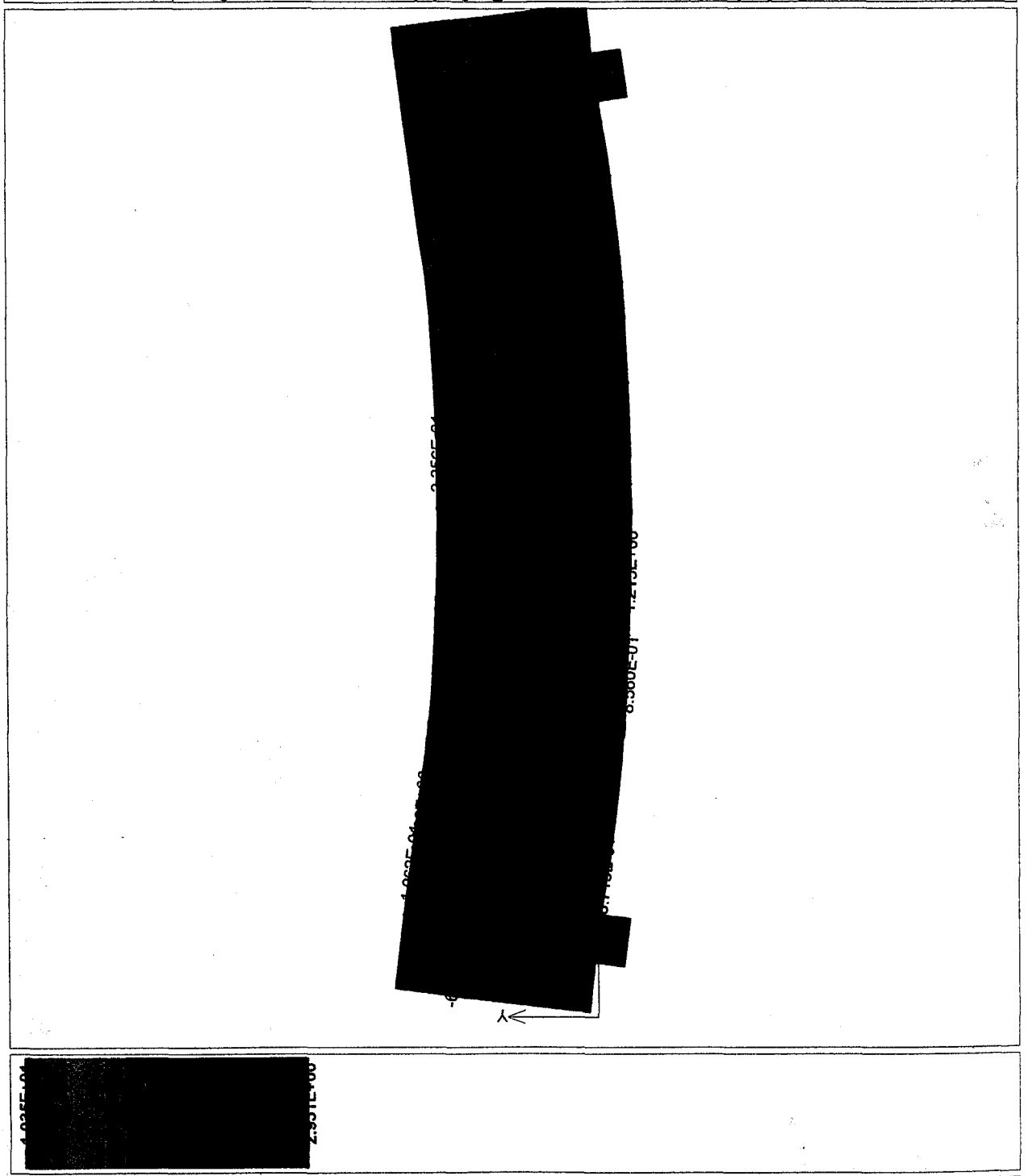

Figure 5.32 Simply Supported Beam - Step 8 (Engineering Stress with Cuts and Cracks)

Chapter 5
Simply Supported Beam Analysis
Step 10

Scalars:iso-areas + cuts, Basic material, in nodes, Principal Stress, Max., <-1.298E+01;3.848E+00>[MPa]
Cracks: in elements, openning: <1.742E-06;1.984E-04>[m], Sigma_n: <0.000E+00;2.104E+00>[MPa], Sigma_T□: <-1.320E+00;1.307E+00

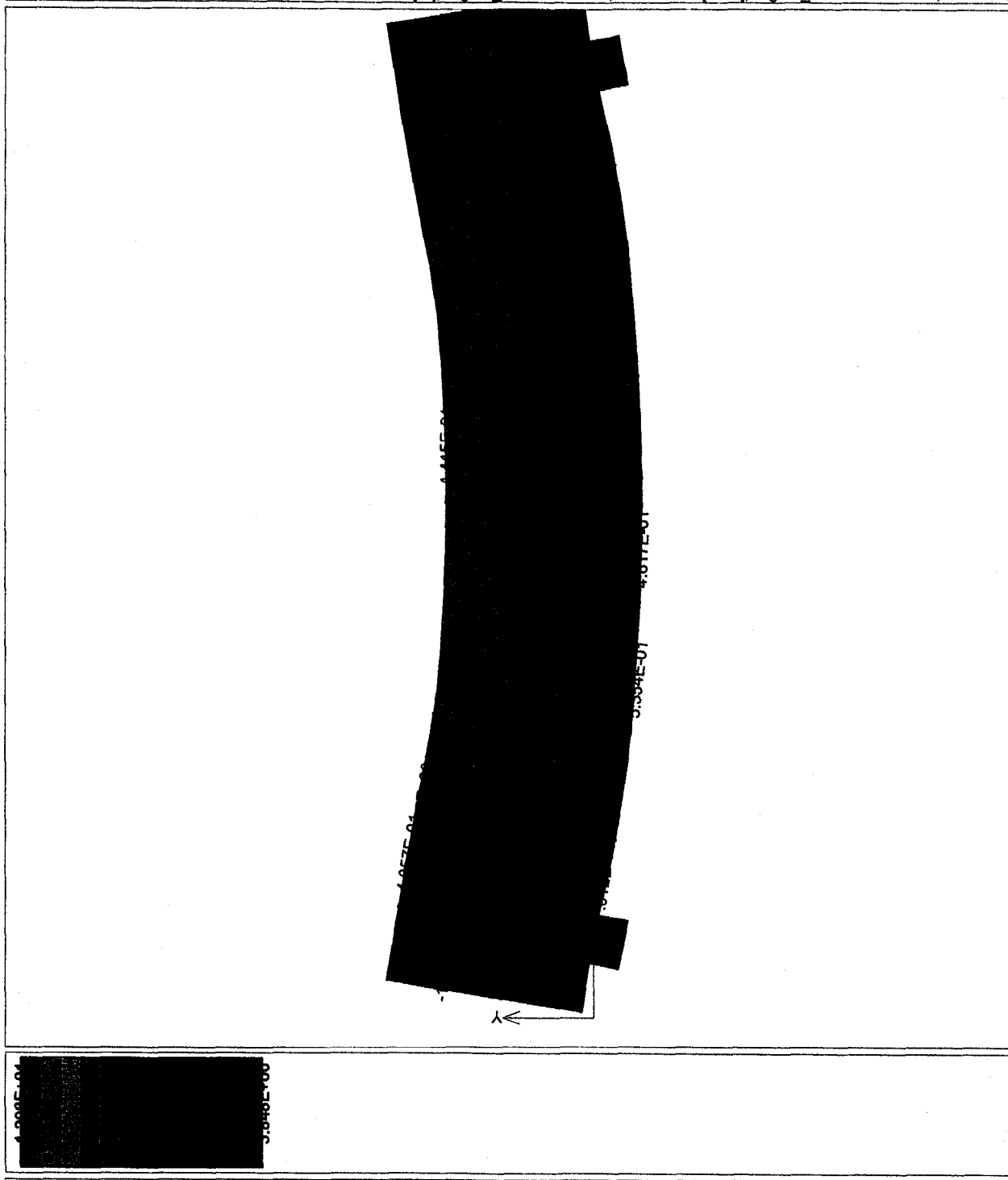

Figure 5.33 Simply Supported Beam - Step 10 (Engineering Stress with Cuts and Cracks)

Chapter 6
Conclusion and Future Direction

6.1 Conclusion

The mechanical behavior of corrosion was studied in this research. The electrochemical process of corrosion is discussed in details. It is believed that the rust behaves like a granular material, which led to the change of the mechanical behavior of bond between the concrete and the reinforcing bars, together with the volume increase of the corrosive products compared with the virgin steel. The corrosion attack penetration has been given as a function of the time as input in the analyses. The load of corrosion applied inside the structural members can be modeled by the displacement around the circumferential surface between the reinforcing bars and concrete. The reduction of capability of the structures is determined from the corrosion level in the service years. Thereby, it would be possible to analyze a structure to investigate its lifetime, and to see what effect of environments would have on for example the deformations and the load-bearing capacity of a structure.

The bond between steel reinforcement and concrete is the critical feature of reinforced concrete structure. It enables the use of concrete, which has low-tension stresses, as a structural material. Consequently, the attention was centralized to develop certain bond slip models in the structural analysis of reinforced concrete structures. This study has been taken to understand the mechanisms of bond-slip and predict analytically the bond-slip behavior from these mechanisms. A finite element modeling method based on nonlinear fracture was presented. The "tension-softening" concept was introduced for the purpose of modeling of bond-slip. In this approach, bond-slip and cracking in concrete are treated in a coherent manner, using basic material properties as input to the analysis.

It is clear that in finite element modeling of the reinforced concrete structures, the internal stresses in the concrete, the formation and stability of concrete cracks, and the distribution

of the stress in the steel reinforcement are profoundly influenced by the proper modeling of concrete and steel material, especially for the concrete. In developing useful finite element models, it is essential to provide not only the constitutive relationships to describe the behavior of concrete and steel material, but also to develop and incorporate analogous relationships for the interface between the two. The nonlinear finite element fracture analysis shows that nonlinear fracture mechanics can be effectively applied to investigate concrete fracture. In this research, three finite element analyses in terms of corrosion, tension and simply supported beam are carried out. It was concluded that with the increase of load and the propagation of the crack, stress redistributed in the steel continues until the specimen is damaged. Comparisons between the analyses of crack propagation and stress redistribution obtained using the finite element analysis was in good agreement with tests fond in the literature.

6.2 Current Needs and Future Directions

A large number of uncertainties are associated with the modeling of corrosion damage in concrete. These include: a) difficulties related to the determination of the onset and the rate of corrosion; b) the randomness of the geometry of the corrosion buildup on the surface of the reinforcing bars; c) the dependence of corrosion damage on other stresses and load histories. In view of these uncertainties, the future research work may present approximate techniques that could be used to estimate the progression of corrosion-induced damage in the concrete.

The effect of the corrosion is modeled as a volume increase of the corrosive products compared with the original diameter of steel bar in this research. In fact, corrosion of reinforcing bars also decreases the friction between the reinforcement and the concrete. However, in the tests of bond mechanism of corroded reinforcement in past research, only the bond stress and the slip have been measured. The normal stress in the bond mechanism, or the effect of the normal stress, has not been measured. Therefore, it is very difficult to evaluate the friction between the reinforcement and the concrete affected by

corrosion of the bars. Further research is needed to study this problem.

As the information is still not enough on the mechanical behavior of the corrosive products, it results in the difficulties in the analytical modeling of this phenomenon. As presented by Petre-Lazar and Gerard (2000), there might be a possibility for the rust to fill up the pores close to the reinforcing bars before starting to apply stresses in the structures. It means that properties of the concrete, such as porosity, will influence the mechanical behavior of the corrosive products. Also the properties of the concrete might influence what type of corrosive products that will form, and thereby the mechanical behavior of it. Further efforts may be made on using a combination of test results and analysis method to investigate such bond behavior.

In this research, we use finite element method to analyze the cracking and bond slip problem. There are several deficiencies and unknowns in the current model applied in engineering practice, the future research may also include improvement of this part of work. Although linear elastic models will still be widely used in the determination of behavior under normal loads and may continue to represent the vast majority of applications, it believes that more and more commonplace for practicing engineers rely on nonlinear methods for assessing structural behavior. Moreover, computer-based methods will principally play an important role in the new analysis. A key ingredient of new generation of structural analysis software will be the accurate modeling of all aspects of structural response, including bond and slippage under load and corrosion. It is the objective for the code writing organizations to provide a unified consensus approach for bond modeling in these applications to ensure accuracy and safety in the analysis.

REFERENCES

ACI Committee 224, (1986), "Cracking of Concrete Members in Direct Tension," *ACI Journal*, Vol. 78, No. 1, pp. 3-19.

ACI Committee 408, (1966), "Bond Stress-The State of the Art," *ACI Journal*, Vol. 63, No. 11, pp. 1161-1188.

Almusallam, A.A., Al-Gahtanl, A.S., Aziz, A.R., and Rasheeduzzafar, (1996), "Effect of Reinforcement Corrosion on Bond Strength," *Construction and Building Materials*, Vol. 10, No. 2, pp. 123-129.

Alonso, C., Andrade, C., Rodriguez, J., and Diez, J.M., (1998), "Factors Controlling Cracking of Concrete Affected by Reinforced Corrosion," *Materials and Structures*, Vol. 31, No. 211, pp. 435-441.

Al-Sulaimani, G.J., Kaleemullah, M., Basunbul, I.A., and Rasheeduzzafar, (1990), "Influence of Corrosion and Cracking on Bond Behavior and Strength of Reinforced Concrete Members," *ACI Structural Journal*, Vol. 87, No. 2, pp. 220-231.

Amleh, L., (2000), *Bond Deterioration of Reinforcing Steel in Concrete due to Corrosion*, Ph.D, Thesis, McGill University, Montreal, QC, Canada..

Amleh, L., and Mirza, S.M., (1999), "Corrosion Influence on Bond between Steel and Concrete," *ACI Structural Journal*, Vol. 96, No. 3, pp. 415-423.

Andrade, C., Alonso, C., and Molina, F.J., (1993), "Cover Cracking as A Function of Bar Corrosion: Part I-Experimental Test," *Materials and Structures*, Vol. 26, No. 162, pp. 453-464.

Andrade, C., and Alonso, C., (1996), "Progress on Design and Residual Life Calculation with Regard to Rebar Corrosion of Reinforced Concrete," ASTM STP 1276, *Techniques to Asses the Corrosion Activity of Steel Reinforced Concrete Structures*, Edited by N.S. Berke, E. Escalante , C.K Nmai, D. Whiting, Philadelphia.

ASCE, (1982), State-of-the-Art Report on "Finite Element Analysis of Reinforced Concrete", Chapter 3 "Modeling of Reinforcement and Representation of Bond," Task Committee "FE Analysis of R/C Structures," Chairman Arthur H. Nilson, pp.149-203.

Auyeung, Y., Balaguru, P., and Chung, L., (2000), "Bond Behavior of Corroded Reinforcement Bars," *ACI Materials Journal*, Vol. 97, No. 2, pp. 214-220.

Baldwin, M. I., and Clark, L. A., (1995), "The assessment of Reinforcing Bars with Inadequate Anchorage," *Magazine of Concrete Research*, Vol. 47, No. 171, pp. 95-102.

Barneyback, R.S., and Diamand, S., (1981), "Expression and Analysis of Pore Fluids from Harden Cement Pastes and Mortars," *Cement Concrete Research*, Vol. 11, pp. 279-285.

Bazant, Z.P., (1976), "Instability, Ductility and Size Effect in Strain-Softening Concrete," *Journal of Engineering Mechanics Division, ASCE,* Vol. 102, No. EM2, pp. 331-344.

Bazant, Z.P., (1979), "Physical Model for Steel Corrosion in Sea Structures-Theory," *Journal of the Structure Division,* Vol. 105, No. 6, pp. 1137-1153.

Bazant, Z.P., (1979), "Physical Model for Steel Corrosion in Sea Structures-Application," *Journal of the Structure Division,* Vol. 105, No. 6, pp. 1155-1166

Bazant, Z.P., (1983), "Crack Band Theory for Fracture of Concrete," *Materials and Structures*, Vol. 16, No. 93, pp. 155-177.

Bazant, Z.P., (1984), "Size Effect in Blunt Fracture: Concrete, Rock, Metal," *Journal of Engineering Mechanics, ASCE*, Vol. 110, No. 4, pp. 518-535.

Bazant, Z.P., and Cedolin, L., (1980), "Fracture Mechanics of Reinforced Concrete," *Journal of the Engineering Mechanics Division*, Vol. 106, No. EM6, Paper No. 15917, pp. 1287-1306.

Bazant, Z.P., and Gambarova, P., (1980), "Rough Cracks in Reinforced Concrete," *Journal of the Structural Division, ASCE*, Vol. 106, No. ST4, Paper No. 15330, pp. 819-842.

Bazant, Z.P., and Jirasek, M., (1994), "Damage Nonlocality Due to Microcrack Interactions: Statistical Determination of Crack Influence Function," *Fracture and Damage in Quasibrittle Structures*, Edited by Z P Bazant, Z Bittnar, M Jirasek and J Mazars, 1st ed., London: E & FN Spon.

Bazant, Z.P., and Lin, F.B., (1988), "Nonlocal Smeared Cracking Model for Concrete Fracture," *Journal of Structural Engineering*, Vol. 114, No. 11, pp. 2493-2510.

Bazant, Z.P., and Oh, B.H., (1983), "Crack Band Theory for Fracture of Concrete," *Materials and Structures*, RILEM, Vol. 16, No. 93, pp. 155-177.

Bazant, Z.P., and Ozbolt, J., (1990), "Nonlocal Microplane Model for Fracture, Damage, and Size Effect in Structures," *Journal of Engineering Mechanics, ASCE*, Vol. 116, No. 11, pp. 2485-2505.

Bazant, Z.P., and Pijaudier-Cabot, G., (1988), "Nonlocal Continuum Damage, Localization Instability and Convergence," *Journal of Applied Mechanics, ASME*, Vol. 55, No. 2, pp. 287-293.

Bazant, Z.P., F. ASCE, and Cedolin, L., (1983), "Finite Element Modeling of Crack Band Propagation," *Journal of Structural Engineering ASCE*, Vol. 109, No. , pp. 69-92.

Bentur, A.; Diamond, S.; and Berke, N.S., (1998), *Steel Corrosion in Concrete*, E & FNSPON.

Berman, H.A., (1975), "Sodium Chloride, Corrosion of reinforcing Steel, and the pH of Calcium Hydroxides Solution," *ACI Journal*, Oct., pp. 3-16.

Bittencourt, T.; Ingraffea, A.R.; and Llorca, J., (1992), "Simulation of Arbitrary, Cohesive Crack Propagation," *Fracture Mechanics of Concrete Structures*, Edited by Z. Bazant, Elsevier, London, pp. 339-350.

Borst, R. de, (1980), "Application of Advanced Solution Techniques to Concrete Cracking and Non-associated Plasticity," *Numerical Methods for Non-linear Problems*, C. Tayler et al., eds., Vol. 2, Prrieridge Press, Swwansea, pp. 314-332.

Bresler, B., and Bertero, V.V., (1968), "Behavior of Reinforced Concrete Under Repeated Load," *Journal of Structural Division, ASCE*, Vol. 94, No. 6, pp. 1567-1590.

Cabrera, J.G., (1996), "Deterioration of Concrete Due to Reinforcement Steel Corrosion," *Cement and Concrete Composites*, Vol. 18, Issue 1, pp. 47-59.

Cabrera, J.G., and Ghodussi, P., (1992), "Effect of Reinforcement Corrosion on the Strength of the Steel/Concrete Bond," *Proceeding International Conference on Bond in Concrete-form Research to Practice*, Riga, Latvia, pp. 10.11-10.24.

Cady, P.D., and Weyers, R.E., (1983). "Chloride penetration and the deterioration of concrete bridge decks." *Cement, Concrete and Aggregates*, Vol. 5, No. 2, pp. 81-87.

Cao, J., and Chung, D.D.L., (2001), "Degradation of the Bond Between Concrete and Steel Under Cyclic Shear Loading, Monitored by Contact Electrical Resistance Measurement," *Cement and Concrete Research*, Vol. 31, No. 4, pp. 669-671.

Capozucca, R., (1995), "Damage to Reinforced Concrete Due to Reinforcement Corrosion," *Construction and Building Materials*, Vol. 9, No. 5, pp. 295-303.

Carpinteri, A., (1989), "Size-Scale Effects on the Brittleness of Concrete Structures: Dimensional Analysis and Snap-Back Instability," *Fracture Mechanics: Application to Concrete,* Edited by V.C. Li and Z.P. Bazant, ACI SP-118, American Concrete Institute, Detroit, pp. 197-235.

CEB-FIP, (2000), *Bond of Reinforcement in Concrete: State-of-Art Report/Prepares by Task Group Bond Models (former CEB Task Group 2.5)*, Lausanne, Switzerland: International Federation for Structural Concrete.

CEB. (1985), "Draft CEB Guide to Durable Concrete Structures," *Bulletin d'Information*, No.166.

Cervenka, V., Pukl, R., Ozbolt, J., and Eligehausen, R., (1995), "Mesh Sensitivity Effects in Smeared Finite Element Analysis of Concrete Fracture," *Proceeding of FRAMCOS2*, Zurich, Aedificatio.

Chen, W.F., and Saleeb, A.F., (1982), *Constitutive Equations fro Engineering Materials*, John Willey & Sons, ISBN0-471-09149-9.

Coronelli, D., (2002), "Corrosion Cracking and Bond Strength Modeling for Corroded Bars in Reinforced Concrete," *ACI Structural Journal*, Vol. 99, No. 3, pp. 267-276.

Crisfield, M.A., Wills, J., (1989), "The Analysis of Reinforced Concrete Panels Using Different Concrete Models," *Journal of Engineering Mechanics, ASCE*, Vol. 115, No. 3, March, pp. 579-597.

Dagher, H. J., and Kulendran, S., (1992), "Finite Element Modeling of Corrosion Damage in Concrete Structurres," *ACI Structural Journal*, Vol. 89, No. 6, pp. 699-708.

Darwin, D., and Graham, E.K., (1993), "Effect of Deformation Height and Spacing on Bond Strength of Reinforcing Bars," *ACI Structural Journal,* Vol. 90, No. 6, pp. 646-657.

Dias, W.P.S., (2000), "Reduction of Concrete Sorptivity with Age through Carbonation," *Cement and Concrete Research*, Vol. 30, pp. 1255-1261.

Eligehausen, R., Popov, E.P., and Bertero, V.V., (1983), "Local Bond Stress-Slip Relationships of Deformed Bars Under Generalized Excitations," Report No. UCB/EERC 83-23, University of California, Berkeley, USA.

Esfahani, M.R., and Rangan, B.V., (2000), "Influence of Transverse Reinforcement on Bond Strength of Tensile Splices," *Cement and Concrete Composites*, pp.159-163.

Evans, U.R. (1960), *The Corrosion and Oxidation of Metals*. Arnold & Co., London.

Gajer, G., and Dux, P.F., (1990), "Crack Band Based Model for FEM Analysis of Concrete Structures," *Journal of Structural Engineering*, Vol. 116, No. 6, pp.1696-1714.

Ghandehari, M., Zulli, M., and Shah, S.P., (2000), "Influence of Corrosion on Bond Degradation in Reinforced Concrete," *Proceedings EM2000, Fourteenth Engineering Mechanics Conference, ASCE*, Austin, Texas.

Giuriani, E., (1982), "On the Effective Axial Stiffness of a Bar in Cracked Concrete," *Bond in Concrete*, Edited by P. Bartos (Applied Science, London), pp. 107-126.

Giuriani, E., Plizzari, G., and Schumm, C., (1991), "Role of Stirrups and Residual Tensile Strength of Cracked Concrete on Bond," *Journal of Structural Engineering ASCE*, Vol. 117, No. 1, pp.1-17.

Gjorv, O.E., and Vennesland, O., (1979), "Diffusion of Chloride Ions from Seawater into Concrete," *Cement and Concrete Research*, Vol. 9, No. 2, pp. 229-238.

Glass, G.K.; Page, C.L.; and Short, N.R., (1991), "Factors Affecting the Corrosion Rate of Steel in Carbonation Motars," *Corrosion Science*, Vol. 32, pp.1283-1294.

Gopalaratnam, V.S., and Ye, B.S., (1991), "Numerical Characterization of Nonlinear Fracture Process in Concrete," *Engineering Fracture Mechanics*, Vol. 40, No. 6, pp. 991-1006.

Goto, Y., (1971), "Crack Formed in Concrete around Deformed Tension Bars," *ACI Journal*, Vol. 68, No. 4, pp. 244-251.

Hamad, B.S., (1995), "Comparative Bond Strength of Coated and Uncoated Bars with Different Rib Geometries," *ACI Material Journal*, Vol. 92, No. 6, pp. 579-590.

Hansen, E.J., and Saouma, E., (1999), "Numerical Simulation of Reinforced Concrete Deterioration—Part I: Chloride Diffusion," *ACI Material Journal*, Vol. 96, No. 2, pp. 173-180.

Hansen, E.J., and Saouma, E., (1999), "Numerical Simulation of Reinforced Concrete Deterioration—Part II: Steel Corrosion and Concrete Cracking," *ACI Materials Journal*, Vol. 96, No. 3, pp. 331-338.

Heidersbach, R., (1986), "Chapter3—Corrosion," *Attorney's Guide to Corrosion*, I. Kuperstein and N. Salters, Eds., Matthew Bender, New York.

Hillerborg, A.; Modeer, M.; and Petersson, P.E., (1976), "Analysis of Crack Formation and Crack Growth in Concrete by Means of Fracture Mechanics and Finite Element," *Cement and Concrete Research*, Vol. 6, pp. 773-782.

Hime, W.; and Erlin, B. (1987), "Some Chemical and Physical Aspects of Phenomena Associated With Chloride-Induced Corrosion," *Corrosion, Concrete, and Chloride-Steel Corrosion in Concrete: Causes and Restraints*, SP-102, A C I, Detroit, pp. 1-12.

Hordijk, D.A., (1991), *Local Approach to Fatigue of Concrete,* Doctor Dissertation, Delft University of Technology, The Netherlands.

Ingraffea, A.R., (1977), "Discrete Fracture Propagation in Rock: Laboratory Tests and Finite Element Analysis," ph.D. Dissertation, University of Colorado, Boulder.

Ingraffea, A.R.; Gerstle, W.H.; Gergely, P., and Saouma, V., (1984), "Fracture Mechanics of Bond in Reinforced Concrete," *Journal of the Structural Division, ASCE*, Vol. 110, No. 4, pp. 871-890.

Isecke, B., (1982), *Materials Performance*, Vol. 21, No. 12, pp. 36,

Jones, D.A., (1992), *Principles and Prevention of Corrosion,* Macmillan Publishing Company, New York, NY.

Keuser, M., and Mehlhorn, G., (1987), "Finite Element Models for Bond Problems," *ASCE Journal of Structural Engineering*, Vol. 113, No. 10, pp. 2160-2173.

Krance, S.C., and Sagues, A.A., (2001), "Detailed Modeling of Corrosion Macrocells on Steel Reinforcing in Concrete," *Corrosion Science*, Vol. 43, Issue 7, pp.1355-1372.

Kupfer, H., Hilsdore, H.K., Rusch, H., (1969), "Behavior of Concrete Under Biaxial Stress," *ACI Journal*, Vol. 66, No. 8, Aug., pp. 656-666.

Leber, I., and Blakey, F.A., (1956), "Some Effects of Carbon Dioxide on Motars and Concrete," *Journal of American Concrete Institute*, Vol. 53, pp. 295-308.

Leonhardt, F., (1964), *Prestressed Concrete: Design and Construction*, 2nd Edition, Wilhelm Ernst & Sohn.

Liu, Y., and Weyers, R.E., (1998), "Modeling the Time-to-Corrosion Cracking in Chloride Contaminated Reinforced Concrete Structures," *ACI Material Journal*, Vol. 95, No. 6, pp.675-681.

Lundgren, K., (2002),"Modeling the Effect of Corrosion on Bond in Reinforced Concrete," *Magazine of Concrete Research*, Vol. 54, No. 3, pp. 165-173.

Lundgren, K., and Gylltoft, K., (2000), "A Model for the Bond between Concrete and Reinforcement," *Magazine of Concrete Research*, Vol. 52, No. 1, pp. 53-63.

Lounis, Z., and Mirza, M.S. (2001). "Reliability-based service life prediction of deteriorating concrete structures." *Proc. 3rd Int. Conf. on Concrete under Severe Conditions*, Vol. 1, pp. 965-972.

Lutz, L.A., and Gergely, P., (1967), "Mechanics of Bond and Slip of Deformed Bars in Concrete," *Proceeding of the American Concrete Institute*, Vol. 64, No. 11, pp. 711-721.

Lutz, L.A., Gergely, P., and Einter, G., (1966), "The Mechanics of Bond and Slip of Deformed Reinforcing Bars in Concrete, "*Structural Engineering Report No. 324*, Cornell University.

Maeda, M., (1995), "Effect of Confinement on Bond Splitting Behavior in Reinforced Concrete Beams," *Structural Engineering International of the IABSE*, Vol. 5, pp. 166-171.

Mangat, P.S., and Elgarf, M.S., (1999), "Bond Characteristics of Corroding Reinforcement in Concrete Beams," *Materials and Structures*, Vol. 32, No. 216, pp. 89-97.

Margoldova, J., Cervenka, V., and Pukl, R., (1998), "Applied Brittle Analysis," *Concrete Engineering International*, November/December.

Marti, P., (1998), "How to Treat Shear in Structural Concrete," *ACI Structure Journal*, Vol. 96, No. 3, pp. 408-414.

Martin-Perez, B., (1998), *Service Life Modeling of R.C. Highway Structures Exposed to Chlorides,* ph.D. Thesis, Department of Civil Engineering, University of Toronto, Toronto, Ontario.

Martin-Perez, B., and Pantazopoulou, S.J., (2001), "Effect of Bon, Aggregate Interlock and Dowel Action on the Shear Strength Degradation of Reinforced Concrete," *Engineering Structures*, Vol. 23, Issue 2, pp. 214-227.

Metha, P.K., and Gerwick, B.C., (1982), "Cracking-Corrosion Interaction in Concrete Exposed to Marine Environment," *Concrete International*, Vol. 4 No. 10, pp. 45-51.

Metha, P.K., and Montiero, P.J.M., (1992), Concrete Structure-Properties and Materials, Prentice-Hall Inc. Englewood Cliffs, N.J.

Metha. P.K., (1993), *Concrete: Structure, Properties, and Materials*. Prentice-Hall, Inc., Englewood Cliffs, N.J.: Prentice Hall.

Mindess, S., and Diamond, S., (1980), "A Preliminary Sem Study of Crack Propagation in Mortar," *Cement and Concrete Research*, Vol. 10, pp. 509-519.

Ministry of Housing, Ontario Building Branch, (1988), *Report of the Advisory Committee on the Deterioration, Repair and Maintenance of Parking Garages.*

Mirza, S.M., and Houde, J., (1979), "Study of Bond Stress-Slip Relationships in Reinforced Concrete," *ACI Journal*, Vol. 79, No. 1, pp. 47-71.

Mo, Y.L., and Chan, J., (1996), "Bond and Slip of Plain Rebars in Concrete," *Journal of Materials in Civil Engineering ASCE*, Vol. 8, No. 4, pp. 208-211.

Molina, F.J., Alonso, C., and Andrade, C., (1993), "Cover Cracking as A Function of Bar Corrosion: Part II-Numerical Model," *Materials and Structures*, Vol. 26, No. 163, pp. 532-548.

Ngo, D., and Scordelis, A.C., (1967), "Finite Element Analysis of Reinforced Concrete Beams," *Journal of the American Concrete Institute*, Vol. 64, No, 3, pp. 152-163.

Nielsen, A., (1985), "Durability," Beton Bogen (The Concrete Book), Edited by Aa. D. Herholdt, Chr. F.P. Justesen, P. Nepper-Christensen, and A. Nielsen, Aalborg, Portland, pp. 200-243.

Nilson, A.H., (1968), "Nonlinear Analysis of Reinforced Concrete by Finite Element Method," *ACI Journal, Proceedings,* Vol. 65, No. 9, pp. 757-766.

Ouyang, C., and Shah, S.P., (1994), "Fracture Energy Approach for Predicting Cracking of Reinforced Concrete Tensile Members," *ACI Structural Journal*, Vol. 91, No. 1, pp. 69-78.

Page, C.L., and Treadaway, K.W.J., (1982), "Aspects of Electrochemical of Steel in Concrete," *Nature*, Vol. 297, pp. 109-115.

Petre-Lazar, I, and Gerard, B., (2000), "Mechanical Behavior of Corrosion Products Formed at the Steel-Concrete Interface," *Proceedings EM2000, Fourteenth Engineering Mechanics Conference, ASCE*, Austin, Texas.

Petersson, P.E., (1980), "Fracture Energy of Concrete: Method of Determination," *Cement and Concrete Research*, Vol. 10, pp. 78-89.

Petersson, P.E., (1980), "Fracture Energy of Concrete: Practical Performance and Experimental Results," *Cement and Concrete Research*, Vol. 10, 9991-101.

Pourbaix, M., (1976), *Atlas of Electrochemical Equilibrium in Aqueous Solutions.* Pergamon, London.

Powers, T.C., (1958), "Structure and Physical Properties of Hardened Portland Cement Paste," *Journal of American Ceramic Society*, Vol. 61, No.1, pp.1-6.

Prasad, M.V.K.V., and Krishnamoorthy, C.S., (2002), "Computational Model for Discrete Crack Growth in Plain and Reinforced Concrete," *Computer Methods in Applied Mechanics and Engineering*, Vol. 191, Issue 25-26, pp. 2699-2755.

Rashid, Y.R., (1968), "Ultimate Strength Analysis of Presetressed Concrete Pressure Vessels," *Nuclear Engineering and Design,* Vol. 7, pp. 334-344.

Rehm, G., (1961), "On the Fundamentals of Steel-Concrete Bond," Deutscher Ausschuss für Stahlbeton (138), pp. 1-59.

Rehm, G., (1968), "The Basic Principles of the Bond Between Steel and Concrete," Translation No. 134, Cement and Concrete Association, London.

Rhem, G., (1958), "The Fundamental Law of Bond," *Proceedings of Symposium on Bond and Crack Formation in Reinforced Concrete, Stockholm, 1957*, Stockholm: Tekniska Hogskolans Rotaprinttrychkeri.

Roper, H., and Baweja, D., (1991), "Carbonation-Chloride Interactions and Their Influence on Corrosion Rates of Steel in Concrete," *Durability of Concrete,* ACI SP-126, Edited by Malbotra, V.M., pp. 295-315.

Russo, G., and Romano, F., (1992), "Cracking Response of RC Members Subjected to Uniaxial Tension," *Journal of Structural Engineering, ASCE*, Vol. 118, No. 5, pp. 1172-1190.

Sagoe-Grentsil, K.K., and Glasser, T.P., (1989), "Steel in Concrete: Part 1: A Review of the Electrochemical and Thermodynamic Aspects," *Magazine of Concrete Research*, Vol. 41, pp. 205-212.

Salari, M.R., and Spacone, E., (2001), "Finite Element Formulation of One-dimensional Elements with Bond-Slip," *Engineering Structures*, Vol. 23, No. 7, pp. 815-826.

Saouma, V.E., (1981), "Interactive Finite Element Analysis of Reinforced Concrete: A Fracture Mechanics Approach," ph.D. Thesis, Department of Structural Engineering, Cornell University, Ithaca.

Schiessl, P., and Raupach, M.. (1990), "Influence of Concrete Composition and Microclimate on the Critical Chloride Content in Concrete," *Corrosion of Reinforcement in Concrete*, Page, C.L., Threadaway, K.W.J., and Bamgforth, P.B. eds, SCI, Elsevier Applied Science, London, pp. 49-58.

Shima, H., Chou, L.L., and Okamura, H., (1987), "Bond Characteristics in Post-yield Range of Deformed Bars," *Concrete Library of JSCE*, Vol. 10, pp. 113-124.

Stanish, K., (1997), *Corrosion Effects on Bond Strength in Reinforcement in Concrete*, MSc Thesis, Dept. of Civil Engineering, University of Toronto, Toronto, ON, Canada.

Stearn, M., and Geary, A.L. (1957), "Electrochemical Polarization No. 1: Theoretical Analysis of the Shape of Polarization Curve," *Journal of Electrochemical Society*, Vol. 104, pp. 56-63.

Tafel, J.Z., (1904), Physik. Chem., 50, pp. 641.

Tassios, T.P., (1979), "Properties of Bond Between Concrete and Steel Under Load Cycles Idealizing Seismic Action," Proceeding AICAP-CEB Symposium, Rome, CEB Bulletin No. 131, pp. 67-122.

Taylor, H.E.W., (1992), *Cement Chemistry*, San Dirgo: Academic Press.

Tepfers, R.A., (1979), "Cracking of Concrete Cover Along Anchored Deformed Reinforcing Bars," *Magazine of Concrete Research*, Vol. 31, No. 106, pp. 3-12.

Tuutti, K., (1982), *Corrosion of Steel in Concrete*, Swedish Cement and Concrete Research Institute, Stochkolm.

V'eleval, L. et al., (1998), "The Corrosion Performance of Steel and Reinforced Concrete in a Tropical Humid Climate. A Review," *Corrosion Reviews*, Vol. 16, No. 3, pp. 235-284.

Val, D.V., Stewart, M.G., and Melchers, R.E., (1998), "Effect of Reinforcement Corrosion on Reliability of Highway Bridge," *Engineering Structures*, Vol. 20, No. 11, pp. 1010-1019.

Van Mier, J.G.M., (1986), "Multiaxial Strain-softening of Concrete, Part I: Fracture," *Materials and Structures*, RILEM, Vol. 19, No. 111, pp. 179-190.

Verbeck, G.J., (1958), "Carbonation of Hydrated Portland Cement," *Cement and Concrete,* STP-205, American Society for Testing and Materials, pp. 17-36.

Vos, E., (1983), "Influence of Loading Rate and Radial Pressure on Bond in Reinforced Concrete," *Dissertation*, Delft University, pp. 219-220

Wamg. K., and Monteiro, P.J., (1996), "Corrosion Products of Reinforcing Steel and their Effects on the Concrete Deterioration," Third CANMET/ACI International Conference on Performance of Concrete in Marine Environment, P.K. Metha, ed., New Brunswick, Canada, pp. 83-97.

Yener, M., and Li, G.C., (1991), "Progressive Finite Element Fracture Analysis of Pullout Concrete ," *Journal of Structural Engineering ASCE*, Vol. 117, No. 8, pp. 2351-2371.